# POLITECNICO DI TORINO

**Master's Degree in Electronic Engineering**

# Sensorized Knee Sleeve to Monitor Bioimpedance in Patients with Osteoarthritis



**Supervisors**

**Prof. Danilo DEMARCHI**

**Prof. Paolo BONATO**

**Benito PUGLIESE**

**Candidate**

**Mattia GHIBAUDO**

**A.A. 2023-2024**

# Summary

Knee osteoarthritis (OA) is a prevalent degenerative condition that significantly impacts mobility and quality of life. This thesis explores the development of a sensorized knee sleeve which is designed to monitor bioimpedance as an indicator of the underlying physiology of the knee. Its purpose is to explore the potential for early detection of inflammation during physical activity and to enable prompt adjustments to rehabilitation exercises. By providing objective, real-time data, this wearable device aims to overcome the timing and subjective biases inherent in self-reported pain and activity level questionnaires. Rather than serving as a substitute for diagnostic tools like MRI, the knee sleeve seeks to complement current methods by offering a non-invasive, cost-effective and wearable solution to quantify and optimize physical activity levels, which is a critical factor in the management of osteoarthritis rehabilitation.

Bioimpedance measures the electrical properties of biological tissues, with changes in impedance reflecting physiological states such as inflammation and tissue degradation—common in OA. The advantages of bioimpedance include its non-invasive nature, affordability, and capability for continuous monitoring, making it suitable for clinical and portable applications.

An in-depth literature review surveys bioimpedance techniques and applications, focusing on frequency-based impedance variations and their role in tissue assessment. Studies highlight bioimpedance as an effective indicator of OA and edema. Factors influencing bioimpedance measurement, including electrode placement, temperature, and intra-subject variability, are crucial for ensuring repeatability and accuracy. Additionally, existing wearable devices are analyzed, noting gaps such as the lack of integrated IMUs for gait analysis and real-time adaptability, which this project aims to address.

The experimental setup and equipment used in this study included the MAX30009 evaluation kit, with key bioimpedance analysis methods involving frequency selection, electrode placement, and testing parameters to ensure consistent data collection. Initial experiments optimized measurement settings and identified variables like electrode type and positioning that could impact readings. These preliminary findings informed the knee sleeve prototype's development, enhancing

measurement reliability through standardized protocols. Additional tests explored physiological changes, comparing bioimpedance in various conditions, further exploring bioimpedance as a possible metric for detecting OA-related alterations.

The knee sleeve was designed to integrate a custom PCB, battery, and dual IMUs for monitoring gait cycles and detecting leg extension. The layout of the PCB is optimized for signal integrity and noise reduction. A preliminary firmware version was developed to validate functionality and ensure reliable measurement acquisition. This wearable prototype addresses limitations in current solutions by enabling transverse bioimpedance measurements with IMU to detect when the leg is straight and ready for bioimpedance measures. Challenges encountered during PCB development, such as sensor placement optimization and Bluetooth antenna integration, are discussed, providing insights for future iterations.

Data collection began with healthy subjects to establish a normative bioimpedance dataset as a benchmark for comparing OA patients, using the Development Kit. This process involves acquiring detailed measurements and recording observations, with future phases of the study planned to compare pre- and post-shockwave therapy measurements from OA patients. These results will help evaluate bioimpedance's efficacy as an indicator of inflammation reduction, contributing to developing objective, data-driven metrics for OA management.

In conclusion, this thesis underscores the potential of bioimpedance as a non-invasive, scalable method for monitoring OA progression and therapeutic responses. The current device represents a key step toward real-time knee health assessment in clinical and remote settings. Future developments will focus on complete firmware integration and expanded data collection across OA patient, refining data processing algorithms, enhancing measurement accuracy, and validating clinical applicability.

# Table of Contents

# List of Tables

# List of Figures

# Acronyms

**BIS**
Bioimpedance Spectroscopy

**GSR**
Galvanic Skin Response

**BIA**
Bioelectrical Impedance Analysis

**IMU**
Inertial Measurement Unit

**ADC**
Analog-to-Digital Converter

**PCB**
Printed Circuit Board

**BLE**
Bluetooth Low Energy

**MCU**
Microcontroller Unit

**Z**
Impedance

# Chapter 1

# Introduction

## 1.1 Introduction to Bioimpedance

Bioimpedance is a technique used to measure the electrical properties of biological tissues. It is based on the principle that when an alternating electrical current is applied to biological tissues, their resistance (real part) and reactance (imaginary part) can be measured as impedance. These properties can provide useful information about the composition and health status of tissues.

The measurement of bioimpedance has a wide range of applications in medical diagnostics, particularly in body composition analysis and hydration status assessment. The underlying principle of bioimpedance is that biological tissues, such as muscle, fat, and bone, conduct electricity differently due to their varying water and electrolyte content.

In medical research, bioimpedance has gained significant attention for its potential in non-invasive diagnosis and monitoring of chronic diseases such as heart failure, cancer, and osteoarthritis. The simplicity, cost-effectiveness, and real-time nature of bioimpedance make it a promising tool in clinical settings.

In the context of osteoarthritis, bioimpedance can be employed to assess the properties of joint tissues, particularly cartilage and surrounding soft tissues. Osteoarthritis is a degenerative joint disease characterized by the breakdown of cartilage, and changes in the bioimpedance of joint tissues can reflect pathological alterations.

### 1.1.1 Principles of Bioimpedance

Bioimpedance measurement relies on two main components: resistance (R) and reactance (X), which together form the complex impedance. Resistance reflects the opposition to current flow through the intracellular and extracellular fluid, while reactance is related to the capacitive properties of cell membranes. By

measuring both, the impedance offers a comprehensive picture of the tissue's electrical characteristics.

In practice, a small alternating current, typically in the order of microamperes (µA), is introduced into the body through surface electrodes, and the resulting voltage is measured. The impedance is then calculated using Ohm's law, as shown in Equation 1.1:

$$Z = \frac{V}{I} \tag{1.1}$$

Ohm's law for impedance: $Z$ (impedance) is the ratio of voltage ($V$) to current ($I$). The frequencies used for bioimpedance measurements can vary depending on the target tissue and the specific application. As an order of magnitude, low frequencies are below 10 kHz and are primarily used to assess extracellular fluids, while high frequencies, typically above 100 kHz, can penetrate cell membranes to evaluate intracellular compartments.

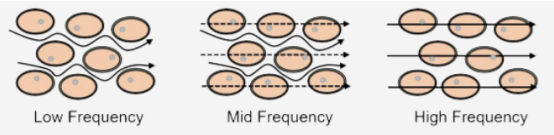


**Figure 1.1:** Current flow in the tissue at based on the frequency - Abasi et al. [1]

### 1.1.2 Clinical Relevance of Bioimpedance in Osteoarthritis

Osteoarthritis is associated with the degradation of cartilage and changes in the surrounding joint tissue, which alters the bioimpedance properties. Specifically, the loss of cartilage and release of synovial fluid, as well as inflammation in the surrounding tissue, can be detected by variations in both resistance and reactance. These impedance changes may correlate with disease severity, making bioimpedance a potentially valuable tool for diagnosis and monitoring.

### 1.1.3 Advantages of Bioimpedance Analysis

The primary advantages of bioimpedance as a diagnostic tool include its non-invasiveness, simplicity, and cost-effectiveness. Unlike imaging techniques such as MRI or X-ray, bioimpedance does not require sophisticated equipment or exposure to radiation. Furthermore, it can provide real-time data, allowing for continuous monitoring of a patient's condition.

In comparison to other diagnostic methods, bioimpedance is also more portable, which makes it suitable for use in a variety of healthcare settings, from hospitals to remote clinics. The equipment required for bioimpedance analysis is relatively

inexpensive, and the procedure can be easily administered by trained healthcare professionals.

### 1.1.4 Limitations of Bioimpedance

While bioimpedance has clear advantages, it also has some limitations. One of the main challenges is the sensitivity of the measurement to electrode placement and skin-electrode contact. Variations in skin properties, such as moisture and temperature, can influence the accuracy of the impedance readings. Additionally, the interpretation of bioimpedance data requires a detailed understanding of the underlying tissue composition and its electrical properties, which may differ from one patient to another.

# Chapter 2

# State of the Art

## 2.1 Introduction

The study of bioimpedance, particularly in relation to the knee, has gained increasing attention due to its potential for non-invasive assessment of various physiological conditions. The field encompasses a wide range of research efforts focusing on understanding the behavior of current flow across tissues at different frequencies, and how these insights can be applied to distinguish between healthy and pathological states, such as osteoarthritis.

In this chapter, we present an in-depth review of the current state of the art in bioimpedance measurements as they pertain to the knee joint. The following sections will delve into key topics that are essential to understanding the complexity of these measurements. First, we will discuss how current flow varies based on frequency and why this phenomenon is critical to bioimpedance analysis. We will then explore how this principle is specifically applied to knee joint assessments and the challenges involved.

Additionally, we will address various factors that can influence the accuracy and reliability of bioimpedance measurements, including electrode placement, tissue heterogeneity, and external conditions. Finally, we will review the outcome measurements commonly used in the literature, such as impedance magnitude and phase angle, and their relevance to clinical applications.

This analysis is based on an exhaustive study of the available literature, highlighting the advancements made thus far and identifying areas that require further exploration.

## 2.2 Current Flow Based on Frequency

Bioelectrical impedance analysis (BIA) and spectroscopy (BIS) provide critical insights into the physiological and molecular composition of tissues, significantly enhancing diagnostic and monitoring capabilities in clinical settings. These techniques leverage the dependency of tissue impedance on electrical frequency, revealing detailed information about tissue health, hydration levels, and cellular integrity.

### 2.2.1 Introduction to Bioimpedance Techniques

The methodological advancements in BIA and BIS have been comprehensively reviewed in recent literature, including a pivotal study by Abasi et al. [1], which discusses the use of BIA/BIS across various frequency domains to monitor mammalian cells and tissues. The study highlights the significance of selecting appropriate frequency ranges to optimize the sensitivity and specificity of impedance measurements for different biological tissues and states.

Another significant contribution to the field is the work by Smith et al. [2], which outlines fundamental advancements and future challenges in bioimpedance. This paper provides a critical overview of the methodologies used to calibrate and apply BIA/BIS across different clinical and research settings, emphasizing the importance of understanding the underlying physical and biological mechanisms that influence impedance measurements.

### 2.2.2 Impedance Behavior Across Frequency Spectrum

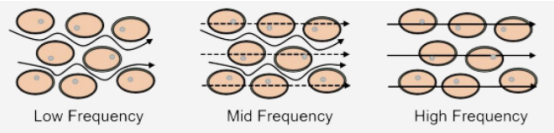


**Figure 2.1:** Current flow in the tissue at based on the frequency - Abasi et al. [1]

#### Low Frequency Domain (10 Hz to 10 kHz)

In the low frequency range, electrical currents primarily flow around the cells, interacting with the extracellular matrix and the interstitial fluids. This frequency domain is highly sensitive to extracellular fluid volume, making it suitable for assessing body hydration and fluid distribution [1]. The impedance measurements at these frequencies are largely influenced by the ionic concentration and mobility in the extracellular space, which can provide insights into extracellular matrix properties, such as conductivity and permittivity.

#### Middle Frequency Domain (10 kHz to 100 kHz)

As the frequency increases, the current begins to interact with the cellular membranes. The middle frequency range allows for the evaluation of membrane integrity and cellular health. According to Smith et al., this range is crucial for understanding the barrier function of cellular membranes and can help in diagnosing conditions that alter cellular permeability [2].

#### High Frequency Domain (100 kHz to 10 MHz)

At higher frequencies, the impedance measurement becomes sensitive to the intracellular components. Currents at these frequencies can penetrate the cellular interior, providing valuable information about the intracellular fluid and organelles, as shown in 2.1 . This range is particularly useful in research settings for differentiating between different cell types and identifying pathological changes at a cellular level [1].

### 2.2.3 Applications and Implications

The application of BIA and BIS across these frequency domains has revolutionized the ability to non-invasively assess tissue properties and function. These methods have shown promising results in monitoring therapy progress, diagnosing diseases, and managing patient care in real-time. The ongoing advancements in bioimpedance technology continue to expand its applications, promising further integration into clinical practice.

### 2.2.4 Application to the Knee: Current Flow and Impedance Measurement

The principles of bioimpedance spectroscopy (BIS) are particularly relevant to the study of knee health, where impedance measurements can provide valuable insights into the structural and compositional changes within the knee joint. The works by Mabrouk et al. [3] and by your team [4] highlight innovative approaches to utilizing BIS in assessing knee conditions such as edema and injury recovery.

Mabrouk et al. introduced a wearable bioimpedance system optimized for longitudinal monitoring of ankle and knee edema [3]. Their study emphasized the capability of BIS to differentiate between impedance properties at various frequencies, which is crucial for identifying fluid accumulations associated with inflammation or injury. Similarly, their methodology can be applied to the knee, where the distribution and type of fluid (interstitial vs. intracellular) significantly influence impedance readings.

In your study, the application of multi-frequency BIS to the knee has allowed for detailed assessments of knee health, particularly in post-operative conditions where monitoring the progression of recovery and the effectiveness of therapeutic interventions is critical. By employing a range of frequencies, your methods enable the differentiation between the extracellular and intracellular fluid dynamics, providing a more comprehensive view of knee health [4].

Both studies utilize the frequency-dependent properties of electrical current flow through biological tissues:

- At lower frequencies, current predominantly passes through the extracellular space, sensitive to changes in extracellular fluid, which increases in conditions like edema.
- At higher frequencies, the current penetrates cell membranes, thus providing information about the intracellular environment and cellular integrity.

These insights are crucial for developing targeted rehabilitation protocols, where the balance between different types of tissues (e.g., muscular vs. adipose) and fluid content can indicate the state of recovery or highlight potential complications. Mabrouk et al. also discussed the challenges of electrode placement variability and introduced a differential measurement technique that minimizes these issues by focusing on the impedance changes with postural variations, which can be directly applied to knee assessments [3].

This approach is particularly beneficial for knee health monitoring, as it allows for dynamic assessments that can correlate changes in bioimpedance with mechanical stress or movement patterns typical in rehabilitation settings. Such dynamic assessments are instrumental in developing personalized therapy regimes that adapt to the progress and specific needs of the patient, further underscored by the data-driven insights from your research [4].

**Conclusion:** The application of BIS in knee health monitoring exemplifies the integration of advanced biomedical engineering techniques with clinical practices to enhance the diagnosis, monitoring, and treatment of knee-related conditions. The use of multi-frequency impedance measurements provides a non-invasive, detailed picture of knee tissue health, making it an invaluable tool in both clinical and research settings.

## 2.3 Confounding factors and repeatability

### 2.3.1 Temperature Effects on Knee Impedance

The impact of temperature on knee bioimpedance is a critical factor in accurate physiological assessments using electrical bioimpedance techniques. The research

conducted by Hersek et al. [5] provides valuable insights into how local changes in temperature can significantly alter bioimpedance measurements of the knee. This study specifically explores the effects of local heating and cooling on knee resistance, which is pivotal in assessing knee joint health outside clinical settings.

#### Temperature Influence on Bioimpedance

Temperature modulates the electrical properties of biological tissues; increasing temperature generally decreases the resistance, whereas cooling increases it. This phenomenon is primarily due to the changes in blood flow and tissue fluidity affecting the electrical paths through the tissues. Hersek et al. demonstrated that local heating of the knee results in a decrease in resistance due to increased blood perfusion, while cooling leads to an increase in resistance, likely due to reduced blood flow and increased tissue stiffness [5].

#### Measurement Challenges

Although significant, the precise temperature of the knee during these impedance measurements remains unknown, and it is unclear if the trends observed under controlled conditions persist in more dynamic, everyday environments. The study highlights a crucial aspect: without knowing the exact knee temperature or its changes over time, interpreting bioimpedance data can lead to inaccuracies in assessing knee health, especially in longitudinal studies or varying ambient conditions.

#### Implications for Bioimpedance Measurement

The findings suggest that incorporating temperature sensors into bioimpedance measurement systems could be essential for ensuring accuracy and reliability, especially in wearable devices intended for continuous health monitoring. Integrating such sensors would allow for the correlation of impedance changes with precise temperature fluctuations, providing a more robust framework for interpreting bioimpedance data in relation to knee health.

### 2.3.2 Electrode Positioning and Its Implications for Knee Impedance Measurements

Electrode positioning significantly influences the sensitivity and specificity of bioimpedance measurements in the assessment of knee osteoarthritis (OA). Insights from recent studies underline the importance of electrode configuration in capturing accurate bioimpedance data related to the severity of OA.

### Sensitivity to OA Severity

Findings suggest that electrode configurations in extension and standing postures provide the highest sensitivity to the degree of osteoarthritis. This insight is pivotal for clinical settings where accurate diagnosis and staging of OA are essential for effective management and intervention [6, 7].

### Intra-subject Variability

Research has shown that standing postures yield less intra-subject variability in impedance measurements compared to configurations where the knee is flexed at 90 degrees [8, 7]. This consistency is crucial for reliable monitoring of OA progression or response to treatment in clinical trials or longitudinal studies.

### Predictive Accuracy of Electrode Configurations

Additionally, the placement of transverse electrodes across the knee has been identified as a significant predictor for knee OA, outperforming longitudinal placements in terms of diagnostic relevance [6, 7]. The placement is shown in 2.2. This finding highlights the importance of aligning the direction of current flow with the anatomical and physiological characteristics of the knee to enhance the predictive accuracy of bioimpedance measurements.

These studies collectively emphasize the critical role of electrode placement in the bioimpedance assessment of the knee, suggesting that tailored electrode configurations can significantly enhance the diagnostic and prognostic capabilities of this non-invasive technique in osteoarthritis.

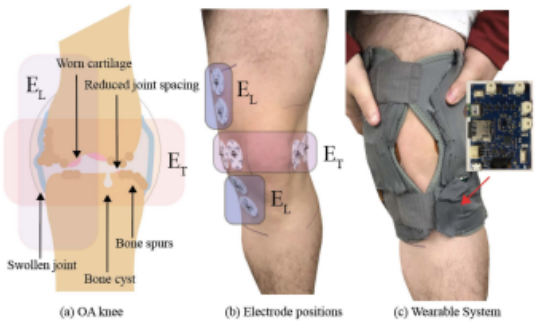


**Figure 2.2:** Electrode positioning trasversal and longitudinal on the knee - Critcher et al. [7]

### 2.3.3 Sex Differences in Knee Bioimpedance Measurements

Sex differences in bioimpedance across the knee are notable, particularly in the context of knee osteoarthritis and injury recovery. Recent findings by Seeley et al. [9] provide crucial insights into how sex influences limb-to-limb bioimpedance differences, with significant implications for clinical assessments and rehabilitation strategies.

#### Influence of Sex on Impedance Variability

The study conducted by Seeley et al. highlighted that females typically exhibit a greater limb-to-limb bioimpedance difference compared to males [9]. This is evidenced by the greater median impedance difference in females (8.04) compared to males (5.41), as illustrated in 2.3 from their study. Such differences are statistically significant and suggest that sex-specific factors, possibly including hormonal influences or differences in body composition, significantly impact bioimpedance measurements.

#### Clinical Implications

These findings underscore the need for sex-specific norms in bioimpedance measurements for more accurate diagnosis and monitoring of conditions such as knee osteoarthritis and swelling post-injury. The larger variability seen in females could influence clinical decisions, especially in determining the severity of knee injuries or the efficacy of recovery strategies.

#### Future Research Directions

Seeley et al. call for further research to understand the underlying mechanisms driving these sex differences in bioimpedance and to explore how these findings can be integrated into personalized treatment plans [9]. Such studies will be crucial in refining bioimpedance as a tool for non-invasively assessing knee health across different patient demographics.

| | Male n=48 median (Q1; Q3) | Female n=25 median (Q1; Q3) | p |
|---|---|---|---|
| BMI | 25.6 (22.5; 29.8) | 24.0 (20.4; 27.0) | p=0.067 |
| KOOS JR | 28 (26; 28) | 28 (26; 28) | p=0.655 |
| AGE | 21 (19; 23.75) | 21 (20; 22) | p=0.873 |
| IMP. DIFFERENCE | 5.41 (1.79; 8.37) | 8.04 (4.44; 16.41) | p=0.015 |

**Figure 2.3:** Demographic Information and Average Impedance Measurements for the Sample Groups - Seeley et al. [9]

### 2.3.4 Exercise-Induced Fatigue and Its Impact on Bioimpedance

Exercise-induced fatigue significantly alters the bioimpedance measurements of skeletal muscle, as observed in various studies. The focus here is on the changes in electrical impedance caused by isotonic and eccentric exercises that induce fatigue in biceps tissue.

#### Isotonic Exercise-Induced Changes

Fatigue protocols involving isotonic exercises, such as those described by Fu and Freeborn [10], demonstrate how exercise intensity influences the bioimpedance values. In their study, subjects underwent a fatiguing protocol using isotonic exercise until task failure. Significant differences were observed in the resistance (R) and reactance (X) values pre- and post-exercise, indicating the physiological changes occurring within the muscle due to fatigue. However, the study found no significant difference in bioimpedance changes between different exercise intensities when the same fatigue criteria were employed [10].

#### Eccentric Exercise-Induced Changes

Similarly, Freeborn et al. [11] investigated the effects of eccentric exercise on bicep tissue bioimpedance. Their findings indicated that localized bioimpedance is sensitive to the microstructural changes in muscle that result from intense eccentric exercises. Significant decreases in both resistance and reactance were noted along with increases in bicep circumference, marking the exercise's impact over a 96-hour observation period. These changes highlight the potential of using EIM (Electrical Impedance Myography) to monitor recovery and the effects of muscle fatigue over time [11]. The main results are shown in 2.4

Both studies underscore the capability of EIM to detect and monitor the acute and longitudinal changes in muscle due to various forms of exercise, illustrating its utility in rehabilitation and sports medicine.

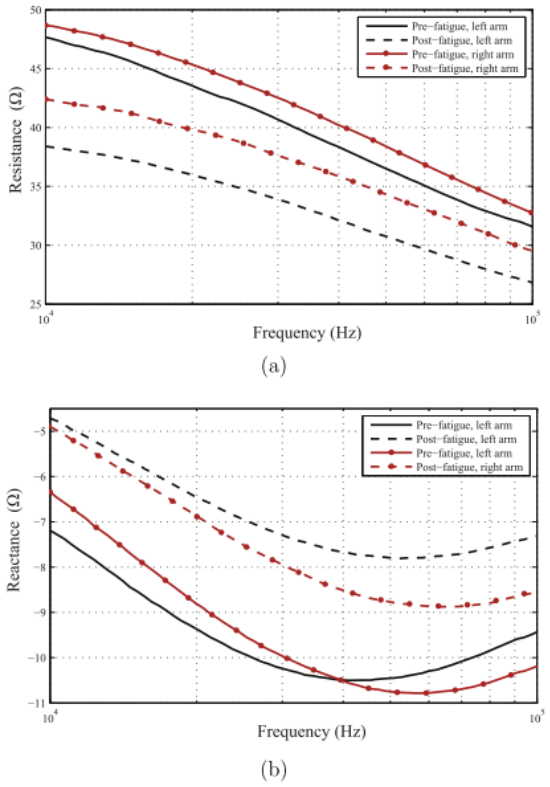


**Figure 2.4:** (a) Resistance and (b)reactance of the left (black) and right(circles) biceps of participant pre (solid) and post (dashed) execution of the fatigue protocol - Freeborn et al.

### 2.3.5 Repeatability of Bioimpedance Measurements

Repeatability is a critical aspect of bioimpedance measurements, particularly when monitoring the health of the knee joint over time. Studies by Seeley et al. [9] and Hersek et al. [5] demonstrate the reliability and consistency of bioimpedance measurements, essential for clinical and research applications.

#### Day-to-Day Variability

According to Seeley et al., bioimpedance measurements exhibit low day-to-day variability, with changes in resistance ($\Delta R$) and reactance ($\Delta X$) being minimal over repeated assessments across three days [9]. This finding supports the use of bioimpedance measurements in longitudinal studies, where consistency in data collection is paramount.

#### Consistency and Reliability

Hersek et al. report high consistency in measurements, with a coefficient of variation (COV) of 1.5% when taken multiple times on a single day. Additionally, the intra-class correlation coefficient (ICC) for measurements taken one week apart is exceptionally high at 97.9%, indicating excellent reliability over time [5].

#### Independence from Circadian Rhythms

Hersek et al. further noted that bioimpedance measurements are not affected by circadian rhythms, suggesting that BioZ measurements can be reliably conducted at any time of day without concern for diurnal variations [5].

These studies collectively underscore the repeatability and reliability of bioimpedance measurements, affirming their utility in clinical settings for monitoring knee health and recovery processes.

## 2.4 Outcome measures

### 2.4.1 Introduction to Outcome Measures

Bioimpedance analysis (BIA) has become an indispensable tool in evaluating joint health, especially in the fields of rehabilitation and orthopedics. By measuring changes in the electrical properties of tissue, BIA provides insights into the physiological and structural integrity of joints. This section explores four critical outcome measures derived from bioimpedance studies: $H_a$ index, Pain assessment, Delta BioZ, and BIKO. Each measure offers unique insights into different aspects of joint health and disease progression:

- $H_a$ **Index:** This index assesses the distribution and mobility of extracellular fluid within the joint, providing a quantifiable measure of fluid dynamics that correlate with inflammation and joint health.
- **Pain:** As a subjective measure, pain assessment through bioimpedance helps correlate electrical impedance changes with patient-reported pain levels, offering a non-invasive way to monitor pain and discomfort associated with joint diseases.
- **Delta BioZ:** This measure reflects the difference in bioimpedance between injured and healthy states of a joint, serving as a benchmark for monitoring injury recovery or disease progression.
- **BIKO (Bioimpedance Knee Output):** Specifically designed to evaluate knee joint health, BIKO quantifies changes in bioimpedance that reflect

joint composition and health, aiding in the diagnosis and monitoring of knee pathologies.

These outcome measures enhance our understanding of joint health, aiding clinicians and researchers in developing targeted treatment strategies and improving patient outcomes. The following subsections will delve deeper into each measure, discussing their applications, benefits, and the research supporting their use.

### 2.4.2 Pain as an Outcome Measure

Pain, a significant subjective indicator of knee health in osteoarthritis (OA) patients, has been extensively explored through bioimpedance measurements. The study by Critcher et al. [7] highlights that specific electrical impedance metrics at certain frequencies correlate with pain probabilities in OA patients. Increases in phase length resistance (PLR) at 128 kHz are associated with an increased likelihood of knee pain, while decreases in phase length reactance (PLX) at 40 kHz also correspond to heightened pain sensations [7], as visible in 2.5. These observations suggest that both resistance and reactance components of bioimpedance serve as reliable indicators of pain levels due to underlying physiological changes such as inflammation or fluid accumulation within the knee joint. Although distinguishing healthy individuals from OA patients based solely on bioimpedance metrics remains challenging, these findings provide a non-invasive method to potentially monitor pain progression or alleviation in response to therapeutic interventions. This capability underscores the need for further research to enhance the diagnostic accuracy of bioimpedance measurements and extend its application in managing OA-related pain effectively.

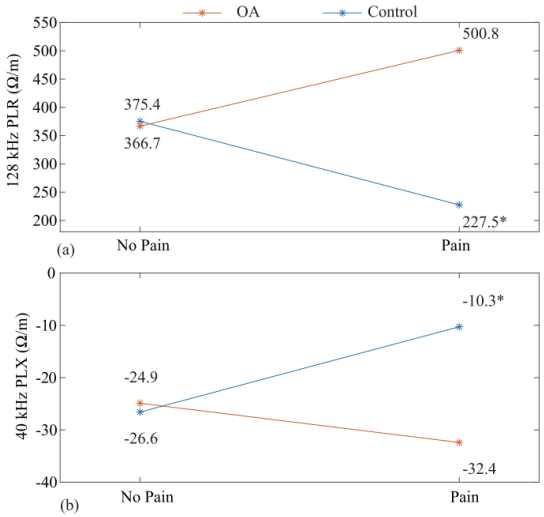


**Figure 2.5:** (a) Moderating effects of group in the association of knee pain with transverse per-length resistance at 128 kHz (b) Moderating effects of group in the association of knee pain with transverse per-length reactance at 40 kHz - Critcher et al.

### 2.4.3 Delta BioZ as an Outcome Measure

Delta BioZ, which represents the difference in bioimpedance between injured and healthy knees, serves as a crucial parameter for assessing knee health and monitoring rehabilitation progress. This section discusses findings from several studies that have investigated delta BioZ across various conditions and frequencies.

#### Benchmarking and Variability

Studies by Seeley et al. [9] and Ye et al. [12] emphasize the utility of comparing the injured knee against the healthy one in the same individual, rather than between individuals. The limb-to-limb bioimpedance differences were generally small (<5%), which supports using the healthy limb as a benchmark for assessing injury [9, 12]. Ye et al. further observed a reduction in bioimpedance by about 5% in injured knees compared to healthy knees, notably around 100 kHz [12], as shown in 2.6.

#### Inflammatory and Osteo-cartilaginous Issues

Hersek et al. [5] and Scandurra et al. [13] provide insights into the implications of different bioimpedance profiles. High delta resistance ($\Delta$ R) with low delta reactance ($\Delta$ X) values typically indicate inflammatory states and edema, while high values in both suggest more severe osteo-cartilaginous issues [5, 13].

### Rehabilitation Monitoring

Scandurra et al. also noted significant changes post-rehabilitation, with delta resistance in injured knees decreasing markedly, underscoring bioimpedance's potential to monitor recovery processes [13], as shown in 2.7 where for the healthy subjects (depicted in blue, N=42), the measurement represents the difference between the left and right knees (L–R). In contrast, for the injured subjects (depicted in red, N=7), it denotes the difference between the injured and healthy knees (I–H). The error bars represent one standard deviation. Part (b) shows the resistance difference versus the reactance difference for the injured subjects (N=7) when the injury is recent (within one month of the measurement, shown in red) and during the recovery phase (four to seven months post-surgery, shown in blue). For these subjects, the displayed difference is I–H. Additionally, the probability density for the data of the healthy subjects (N=42, L–R difference), estimated using a two-dimensional Gaussian kernel density estimation, is illustrated in shades of orange for comparison. The error bars represent one standard deviation.

### Methodological Advancements

The studies collectively highlight the advancements in measurement techniques and methodologies, advocating for more standardized approaches to enhance the reliability of bioimpedance measurements for clinical use.

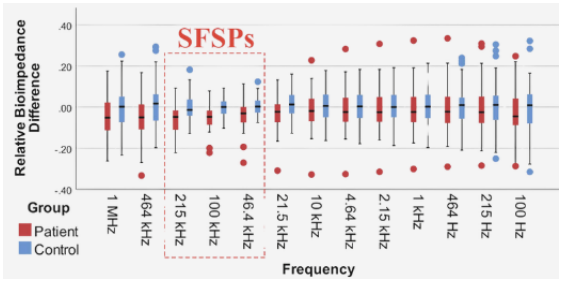


**Figure 2.6:** Box plots of relative bioimpedance differences $\Delta Z_p$ and $\Delta Z_h$ at all frequency nodes. SFSP(s) is an abbreviation of significant frequency sampling point(s) - Ye et al.

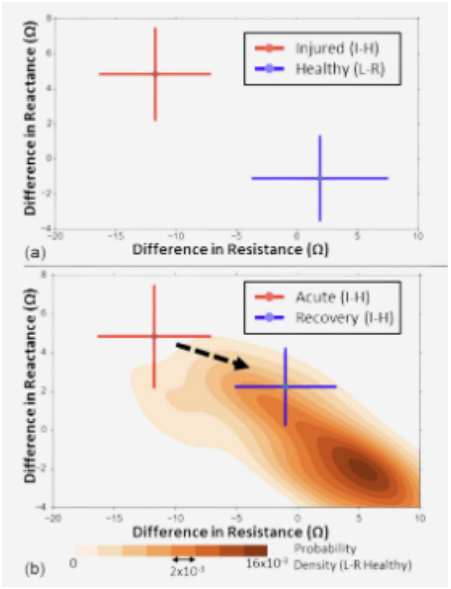


**Figure 2.7:** The difference in resistance versus the difference in reactance for the healthy and injured subjects - Hersek et al.

### 2.4.4 Assessment of Joint Health Using the $H_a$ Index

The $H_a$ index, derived from bioimpedance measurements, offers a nuanced approach to monitoring joint health by quantifying the differences in electrical impedance due to changes in joint positioning. This index is especially valuable in the context of ankle edema and other joint-related conditions where fluid dynamics play a significant role.

#### Definition and Calculation of the $H_a$ Index

The $H_a$ index is defined as the ratio of the change in resistance at lower frequencies to the change at higher frequencies, specifically:

$$H_a = \frac{\Delta R(5\,\text{kHz})_{\text{extension-flexion}}}{\Delta R(100\,\text{kHz})_{\text{extension-flexion}}} \tag{2.1}$$

This formulation captures how extracellular fluid, which is freely mobile within the joint space, redistributes in response to joint movements. A value close to 1.0 typically indicates a healthy joint with normal fluid distribution and mobility. In contrast, deviations from this norm suggest pathological changes, such as those seen in edema or other inflammatory conditions. The results of [3] are shown in the graph 2.8 where we can notice a lower index for the injured subject, and an index close to 1 for the healthy subjects.

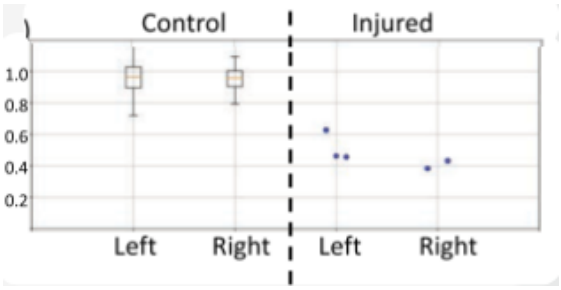


**Figure 2.8:** $H_a$ Index for control and injured subjects - Mabrouk et al.

### Clinical Implications

Mabrouk et al. have demonstrated that the $H_a$ index is effective in assessing the longitudinal effects of treatments on ankle edema, providing a reliable measure of treatment efficacy and fluid dynamics over time [3]. This is particularly relevant in scenarios where continuous monitoring is essential to evaluate the progression or resolution of edema.

### Research Findings

In her thesis, Moise expands on the utility of the $H_a$ index for knee health in juvenile idiopathic arthritis, illustrating how changes in bioimpedance correlate with clinical symptoms and treatment responses [4]. Her findings underscore the index's potential in pediatric rheumatology, offering a non-invasive tool for regular health assessments. Further research is warranted to explore the applicability of the $H_a$ index across different joints and in various pathological conditions beyond those initially studied. Enhancing the sensitivity and specificity of this index through advanced signal processing techniques and integration with other diagnostic modalities could significantly improve its clinical utility. The development of portable bioimpedance devices incorporating the Ha index could also facilitate real-time monitoring of joint health in outpatient settings, improving patient outcomes through timely interventions.

## 2.5 Overview of Current Wearable Devices for Knee Health Assessment

The integration of wearable technologies in knee health assessment has seen notable advancements with various devices offering unique capabilities and specific drawbacks. This section explores five prominent solutions, highlighting their methodologies, strengths, and limitations.

### 2.5.1 Georgia Tech's Solution (Hersek et al.)

The Georgia Tech team, led by Hersek, developed a knee brace with integrated sensors for electrical bioimpedance (EBI) and inertial measurement units (IMUs) to monitor the leg's alignment when straight. However, a significant drawback of this solution is its reliance on longitudinal measurements across the knee, which may not capture transverse bioimpedance changes that are crucial for assessing conditions like osteoarthritis [5]. In 2.9 we can notice the electrode longitudinal placement and the relative measurements, while in 2.10 the graph represent the IMUs accellerometer data, that combined are used to detect when the leg is straight.

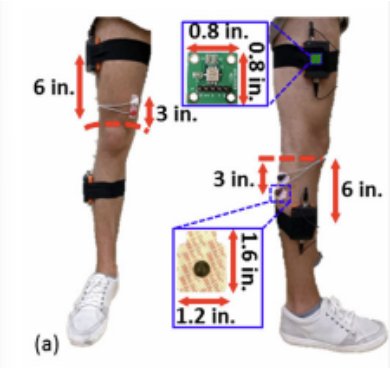


**Figure 2.9:** Hersek et al. electrode and knee sleeve placement

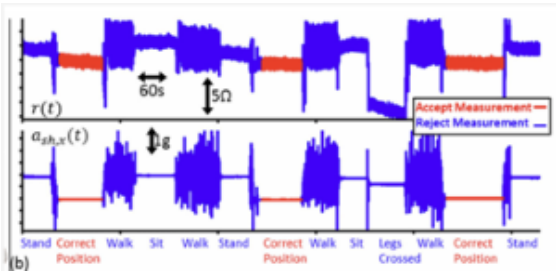


**Figure 2.10:** Dual axis accellerometer to detect when the knee is straight - Hersek et al.

### 2.5.2 University of Alabama's Solution (Critcher et al.)

Critcher and colleagues from the University of Alabama proposed a device that takes both longitudinal and transverse bioimpedance measurements, offering a more comprehensive assessment of knee health. Despite this advantage, their design lacks an IMU, limiting its functionality in dynamic, real-time joint position tracking [7]. Their solution is shown in 2.11

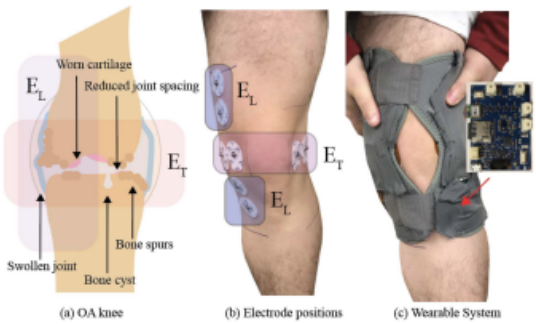


**Figure 2.11:** Critchel et al. developed knee sleeve

### 2.5.3 Richardson's Device

Developed by Richardson et al., this device also focuses on longitudinal EBI measurements and includes an IMU, but the latter was not used to detect a straight leg, but for general analysis and gait detection. Its primary limitation is the requirement for patients to remain seated during data collection, reducing its applicability in daily activity monitoring [14], as the device is not really a wearable and portable solution, as shown in 2.12

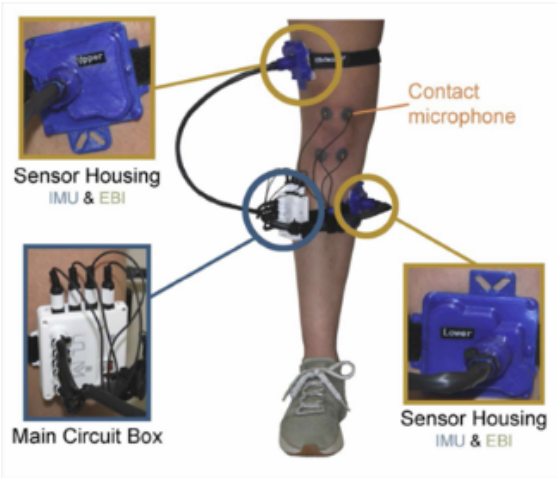


**Figure 2.12:** Richardson et al. device implementation

### 2.5.4 Goktug's Rigid Brace

Goktug's design employs a rigid and non adjustable brace, which can be uncomfortable and non adaptable to different knee sizes. Its invasive nature and lack of

comfort could deter regular use, especially in non- linical settings [15], as noticed in 2.13. This was still a very complete solution that deeply inspired my work.

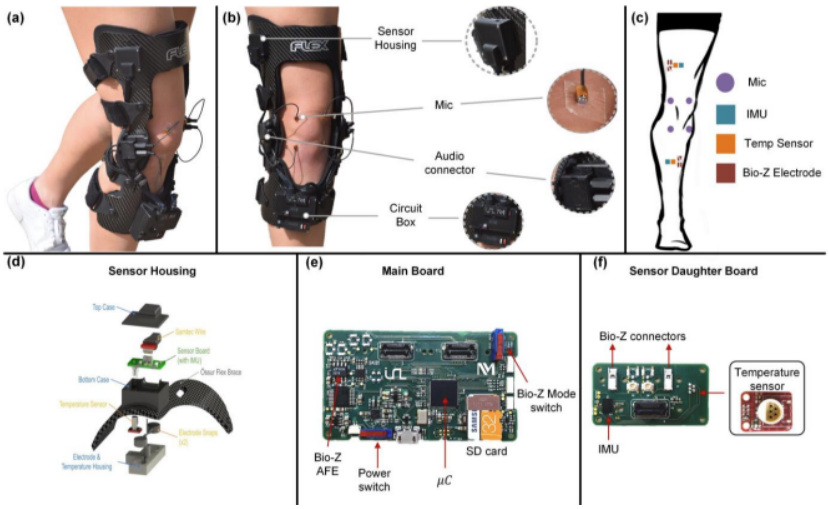


**Figure 2.13:** (a) Side and (b) front view of the brace. (c) Sensor placement. Exploded views of (d) circuit box and (e)sensor housing. The pictures of PCBs: (f) audio board, (g) main board, and (h) sensor daughter board.- Goktug's et al.

### 2.5.5 Ferreira's Textile-Based Solution

Ferreira's innovative approach utilizes textile electrodes made from biocompatible silver-based conductive Shieldex P130 + B fabric. This design incorporates an intermediate 3 mm foam layer for mechanical pressure, providing a less invasive and more comfortable alternative to traditional wet electrodes [16], for the study if the boy composition in the ankle. This suggest that it could be possible to substitute the wet classic Ag-Ag electrodes with dry textile electrodes, thus creating a much more comfortable and easy to use solution.

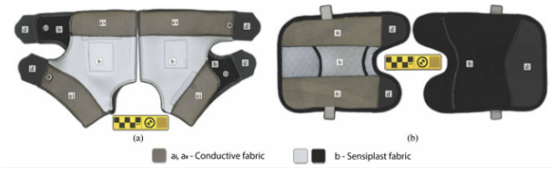


**Figure 2.14:** Textile ankle body composition device

### 2.5.6 Discussion

Each of these solutions presents unique contributions to the field of knee health assessment. While devices like those from Hersek and Critcher offer detailed bioimpedance measurements, the integration of IMUs by Georgia Tech facilitates better tracking of joint position during physical activities. On the other hand, Ferreira's use of textile electrodes proposes a user-friendly approach that could enhance patient compliance in long-term monitoring scenarios.

These varied approaches underscore the ongoing innovation in wearable knee health technologies, each catering to different aspects of patient care and monitoring. As the field advances, combining the strengths of these diverse technologies could lead to more holistic and effective solutions for knee health assessment.

## 2.6 Conclusion

The exploration of bioimpedance (BioZ) applications in the field of knee health, particularly in the context of osteoarthritis (OA), reveals both the potential and the limitations of current research and technology. Despite the significant advancements in wearable devices and measurement techniques discussed in this chapter, there remains a notable gap in the literature regarding the definitive proof of BioZ's efficacy in diagnosing and monitoring osteoarthritis. This gap is primarily due to the variability in study designs, the limited number of participants in most research, and the lack of long-term, comprehensive studies that integrate various biomarkers and symptomatic data.

### 2.6.1 Identified Gaps and Limitations

Current studies have provided valuable insights into the electrical properties of knee tissues and their correlation with health states. However, these studies often involve small sample sizes and do not uniformly consider factors like varying stages of disease progression, different activity levels of patients, or the long-term effects of treatment interventions. Moreover, while some wearable devices have introduced innovative approaches to measuring knee bioimpedance, many lack integration of essential features such as real-time data processing, multimodal sensing, or adaptive algorithms that can personalize the monitoring to each patient's specific condition.

### 2.6.2 Our Study's Contribution

This research final goal is to fill these gaps by developing a comprehensive device that incorporates the best solutions identified to date, such as transverse bioimpedance measurements, integration of IMUs for movement tracking. By doing

so, we intend to provide a more definitive answer to the potential of BioZ in managing osteoarthritis. In conclusion, while the current state of the art in wearable bioimpedance devices for knee health assessment has laid a solid foundation, significant work remains. Our project is poised to bridge these critical gaps, contributing to a more robust understanding and application of bioimpedance technology in clinical settings. By integrating and building upon the best practices observed in existing research, we aim to establish a new standard in OA management and patient care.

# Chapter 3

# Bioimpedance Analysis

## 3.1 Introduction

This chapter focuses on the analysis of bioimpedance as a tool for monitoring physiological changes and its potential application in the management of osteoarthritis. The discussion begins with an overview of the materials and equipment used in the experiments, including the development kit and electrodes.

Next, the chapter outlines the experiments conducted to explore various factors influencing bioimpedance measurements, such as electrode placement, and physiological changes. Each experiment is described in detail, including the methods used and the specific protocols followed, accompanied by a presentation of the results.

Finally, the chapter concludes with a discussion of the data collected, highlighting key trends and observations.

## 3.2 Materials

### 3.2.1 Bioimpedance Analysis Tools

The primary tool used for bioimpedance analysis in this study was the MAX30009EVKIT#, an evaluation kit designed to assess the performance and features of the MAX30009 Low-Power, High-Performance Bioimpedance (BioZ) Analog Front End (AFE). This tool is ideal for applications that require accurate bioimpedance measurements, such as fitness, wellness, and clinical diagnostics.

#### MAX30009EVKIT# Overview

The MAX30009EVKIT# provides a comprehensive platform for evaluating the MAX30009 BioZ AFE's capabilities. It consists of two primary boards:

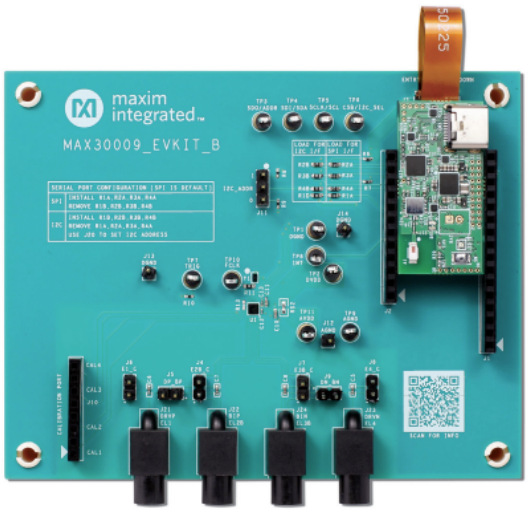


**Figure 3.1:** MAX30009EVKIT# Board

- The **MAX30009_EVKIT_B** sensor board, which contains the MAX30009 chip for bioimpedance measurements.
- The **MAXSENSORBLE_EVKIT_B** microcontroller (MCU) board, which manages data acquisition and communication with the PC via Bluetooth® Low Energy (BLE).

The kit is powered by a 105 mAh Li-Po battery, which can be recharged through a USB-C port. A variety of test points are provided on the board, allowing for easy access to measure signals at different stages of the bioimpedance analysis. The evaluation kit communicates with a user-friendly graphical user interface (GUI) on a Windows® system, enabling real-time monitoring, plotting, and logging of bioimpedance.

### Key Features and Capabilities

The MAX30009 is a complete analog front end designed specifically for bioimpedance applications. It offers a number of key features that make it well-suited for clinical and wearable devices:

- **High Input Impedance:** Ensures accurate measurements even in environments with high contact impedance.
- **Low Noise and High Common-Mode Rejection Ratio (CMRR):** The system includes filtering and protection mechanisms to enhance signal quality.

- **Programmable Gain and Filter Options:** The MAX30009 includes both high-pass and low-pass filters, as well as programmable gain, allowing for customizable configurations based on application needs.
- **Simultaneous I and Q Acquisition:** The system captures both the in-phase (I) and quadrature (Q) components of the bioimpedance signal, allowing for a full characterization of tissue impedance.
- **Ultra-Low Power Operation:** With power-saving features such as lead-off detection during standby mode, the device is suitable for battery-powered wearable applications.

### Data Acquisition and Configuration

The MAX30009EVKIT# is controlled through a dedicated GUI, which allows users to configure settings, start data acquisition, and view the results in real-time. Bioimpedance data can be acquired in both the in-phase (I) and quadrature (Q) channels, and the results are displayed graphically in the software interface.

The GUI provides options for configuring parameters such as:

- **Stimulus Drive Mode:** The system supports both current and voltage stimulation modes.
- **Amplifier Settings:** Users can adjust the amplifier range and bandwidth to optimize power consumption or signal quality, depending on the application.
- **Digital Filtering:** High-pass and low-pass filters are configurable based on the application's frequency range.
- **Data Logging:** The GUI offers logging options, allowing users to save bioimpedance data directly to a CSV file for later analysis.

### Experimental Setup with the MAX30009EVKIT#

In this study, the MAX30009EVKIT# was employed to measure the bioimpedance of the knee tissues in both healthy and osteoarthritic subjects. Electrode cables connected to the board facilitated the bioimpedance measurements, and real-time data was captured via the GUI software installed on a Windows® 10 system.

The setup also included the use of coupling capacitors (47nF) to block DC currents, ensuring the safety of the participants by preventing any direct current from entering the body. The kit's flexible configuration allowed the team to switch between different measurement modes and customize the settings to obtain high-accuracy bioimpedance data for further analysis.

### 3.2.2 MATLAB for Data Elaboration and Visualization

For the analysis and visualization of the bioimpedance data collected during the experiments, we employed MATLAB. MATLAB is a widely-used software tool for numerical computing, data analysis, and visualization, making it an ideal choice for handling the complex datasets generated by bioimpedance measurements.

MATLAB's capabilities allowed us to:

- **Import and process large datasets:** The bioimpedance data collected from the MAX30009EVKIT was stored in CSV format, which could be easily imported into MATLAB for further analysis.
- **Calculate bioimpedance parameters:** Using MATLAB's mathematical functions, we were able to compute key bioimpedance metrics such as impedance magnitude and phase from the in-phase (I) and quadrature (Q) components of the signals.
- **Generate plots and visualizations:** MATLAB's powerful plotting tools enabled us to create detailed graphs that illustrated the time-domain behavior of the bioimpedance signals, as well as the variations in impedance magnitude and phase across different conditions.
- **Perform statistical analysis:** MATLAB also provided tools for performing statistical analysis on the bioimpedance data, allowing us to quantitatively compare results between healthy individuals and osteoarthritis patients.

The flexibility and power of MATLAB allowed us to manage the large amounts of data collected, ensuring that we could efficiently process and visualize the results, which were essential for understanding the differences in bioimpedance between healthy and osteoarthritis-affected tissues. More detailed descriptions of the specific analyses and methods used are provided in the Methods section.

### 3.2.3 Lab Equipment

In addition to the bioimpedance sensor and electrodes, several other pieces of equipment were used to monitor and control the physiological parameters during the experiments. These devices allowed us to track heart rate and manage exercise conditions effectively. Below are the key devices used in our experiments.

#### Polar OH1 Heart Rate Monitor

The Polar OH1 is an optical heart rate sensor worn on the arm. It is known for its high accuracy and comfort, making it an ideal tool for real-time heart rate monitoring during the bioimpedance experiments. The data provided by the Polar

OH1 was used to track the subject's heart rate during both the upper and lower limb tests, helping us correlate heart rate changes with bioimpedance measurements.

**Figure 3.2:** Polar OH1 Heart Rate Monitor.

### SCIFIT Arm Cycle Ergometer

For the upper limb experiments, we used the SCIFIT Arm Cycle Ergometer. This machine allowed the subject to cycle using their arms, simulating upper body exertion while seated. The force level was set to 4.0 to ensure consistent resistance during the exercise. The arm cycle ergometer helped us explore how upper body movement influenced bioimpedance measurements on the lower limbs.

### BIODEX Treadmill

For the lower limb experiments, we used the BIODEX treadmill. This treadmill allowed us to vary the walking and running speeds in a controlled manner, with predefined speed settings for walking (2.7 m/h to 3.0 m/h) and running (4.0 m/h to 6.0 m/h). This device was crucial in observing how dynamic lower limb activity affected bioimpedance measurements.

### Govee Indoor Thermometer and Hygrometer

To ensure that environmental conditions such as temperature and humidity were stable and did not influence the bioimpedance measurements, we used the Govee Indoor Thermometer and Hygrometer. This device provided real-time monitoring of the room's temperature and humidity levels throughout the experiments.

The Govee thermometer-hygrometer was placed in the room where the tests were conducted, and data was recorded continuously. The accuracy of the device


**Figure 3.3:** SCIFIT Pro 1


**Figure 3.4:** BIODEX Trainer 3

helped us confirm that there were no drastic environmental changes during the bioimpedance measurements, which could have otherwise skewed the results. The data were then retrieve with the timestamo from the Govee official application.

These tools were essential in ensuring that the physiological changes observed in the bioimpedance measurements were well-controlled and could be correlated with specific physical activities and heart rate changes.


**Figure 3.5:** Govee Indoor Thermometer and Hygrometer.

## 3.3 Methods

### 3.3.1 Data Acquisition

The data acquisition process for bioimpedance analysis was carried out using the MAX30009 bioimpedance sensor. This section describes the setup and configuration of various parameters critical for accurate data collection.

#### Clock and timing parameters

The PLL was utilized to synchronize the sampling frequency with the stimulus frequency, ensuring accurate phase measurements.

The sampling rate for BioZ is given by:

$$SR_{\text{BIOZ}} = \frac{\text{PLL\_CLK}}{\text{NDIV} \times \text{BIOZ\_ADC\_OSR}}$$

where

$$\text{BIOZ\_ADC\_CLK} = \frac{\text{PLL\_CLK}}{\text{NDIV}} \quad \text{(must be between 16.0 kHz and 36.375 kHz)}$$

and

$$\text{PLL\_CLK} = M \times \text{REF\_CLK} \quad \text{(must be between 14 MHz and 28 MHz).}$$

The value of REF_CLK is 32.768 kHz.

The BioZ stimulus frequency is set by the following equation:

$$F_{\text{BIOZ}} = \frac{\text{PLL\_CLK}}{\text{KDIV} \times \text{BIOZ\_DAC\_OSR}}$$

where

$$\text{BIOZ\_SYNTH\_CLK} = \frac{\text{PLL\_CLK}}{\text{KDIV}} \quad \text{(must be between 4096 Hz and 28 MHz)}.$$

The ratio of $F_{\text{BIOZ}}$ to $SR_{\text{BIOZ}}$ must be 0.5 or an integer, so that each BioZ sample is integrated over a given number of stimulus cycles. This ratio, $C_{\text{BIOZ}}$, is calculated by the following equation:

$$C_{\text{BIOZ}} = \frac{F_{\text{BIOZ}}}{SR_{\text{BIOZ}}} = \frac{\text{NDIV} \times \text{BIOZ\_ADC\_OSR}}{\text{KDIV} \times \text{BIOZ\_DAC\_OSR}}.$$

In 3.6 the tab of the GUI relative to the PLL parameter is shown.

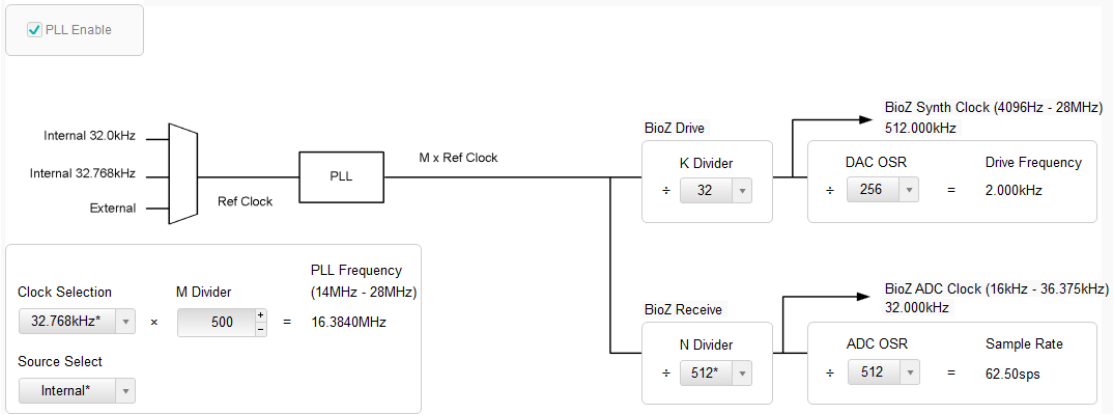


**Figure 3.6:** PLL tab of the MAX30009 GUI software

### Frequency Sweep Methodology

To determine the most effective stimulus frequency for our measurements, a frequency sweep was conducted. This approach involved systematically varying the stimulus frequency across a wide range to observe the response of the bioimpedance measurements. The sweep helped in identifying the frequency at which the bioimpedance data was most relevant and yielded the most interesting results.

## 3.3.2 Frequency Selection for Measurement

Based on the data acquisition needs, the following table lists the selected frequencies for the frequency sweep, from the lowest to the highest frequency, used to evaluate bioimpedance:

| M (MDIV + 1) | PLL CLK (Hz) | KDIV | BIOZ_DAC | F_BIOZ (Hz) | NDIV | BIOZ_ADC_OSR | INT. CYCLES | SR_BIOZ (sps) |
|---|---|---|---|---|---|---|---|---|
| 438 | 14352384 | 8 | 256 | 7008 | 512 | 256 | 64 | 109.5 |
| 750 | 24576000 | 16 | 256 | 6000 | 1024 | 256 | 64 | 93.75 |
| 625 | 20480000 | 16 | 256 | 5000 | 1024 | 256 | 64 | 78.13 |
| 500 | 16384000 | 16 | 256 | 4000 | 512 | 256 | 32 | 125 |
| 500 | 16384000 | 32 | 256 | 2000 | 512 | 256 | 32 | 62.5 |
| 500 | 16384000 | 64 | 256 | 1000 | 512 | 1024 | 32 | 31.25 |
| 500 | 16384000 | 128 | 256 | 500 | 512 | 1024 | 16 | 31.25 |
| 500 | 16384000 | 256 | 256 | 250 | 512 | 1024 | 8 | 31.25 |
| 500 | 16384000 | 512 | 256 | 125 | 512 | 1024 | 4 | 31.25 |
| 512 | 16777216 | 1024 | 256 | 64 | 512 | 1024 | 32 | 3.91 |
| 512 | 16777216 | 2048 | 256 | 32 | 512 | 1024 | 1 | 32 |
| 512 | 16777216 | 4096 | 256 | 16 | 512 | 1024 | 1 | 16 |

### BioZ Drive

The BioZ drive configuration involves several settings that are crucial for the accurate measurement of bioimpedance. The configuration settings are as follows:

- **Current DAC Drive Mode:** This setting determines the drive mode of the current DAC. The selected mode is "Current" which implies that a constant current is used for the impedance measurement.
- **Voltage Mode Amplitude (RMS):** The amplitude of the voltage mode, set at 35.4 mV RMS. This parameter defines the root mean square (RMS) value of the voltage applied during the measurement.
- **Amplifier Bandwidth:** The bandwidth of the amplifier is set to "Medium-High". This affects the frequency response of the amplifier, with a medium-high setting providing a balance between noise performance and response speed.
- **Amplifier Range:** Also set to "Medium-High", indicating the range of the amplifier which affects the dynamic range and sensitivity of the measurements.
- **Drive Frequency:** Calculated as 2.000 kHz, derived from the PLL Frequency divided by the K Divider and adjusted by the DAC OSR.
- **Use External Resistor and External Capacitor:** Checkboxes indicate that an external capcitor was used but not the external resistor
- **Current Drive Range Resistor:** Set to 5.525 kΩ, this resistor sets the range of current that can be driven through the circuit at 6.4 uArms, the current we chose out of the literature review and our own experiment as explained in the next section.

- **DC Restore:** A checked option that indicates the use of a DC restore circuit to stabilize the DC level in the signal path.

| STEP | BIOZ_IDRV_RGE | RANGE RESISTOR | BIOZ_VDRV_MAG | RMS CURRENT | FREQUENCY RANGE (Hz) | RECOMMENDED BIOZ_AMP_RGE |
|---|---|---|---|---|---|---|
| 1 | 1 (0x0) | 552.5kΩ | low (0x0) | 16nA | All frequencies | Low |
| 2 | 1 (0x0) | 552.5kΩ | low mid (0x1) | 32nA | All frequencies | Low |
| 3 | 1 (0x0) | 552.5kΩ | high mid (0x2) | 80nA | All frequencies | Low |
| 4 | 1 (0x0) | 552.5kΩ | high (0x3) | 160nA | All frequencies | Medium-Low |
| 5 | 2 (0x1) | 110.5kΩ | low (0x0) | 320nA | All frequencies | Medium-Low |
| 6 | 2 (0x1) | 110.5kΩ | low mid (0x1) | 640nA | All frequencies | Medium-Low |
| 7 | 2 (0x1) | 110.5kΩ | high mid (0x2) | 1.6µA | All frequencies | Medium-Low |
| 8 | 2 (0x1) | 110.5kΩ | high (0x3) | 3.2µA | All frequencies | Medium-Low |
| 9 | 3 (0x2) | 5.525kΩ | low (0x0) | 6.4µA | All frequencies | Medium-Low |
| 10 | 3 (0x2) | 5.525kΩ | low mid (0x1) | 12.8µA | All frequencies | Medium-High |
| 11 | 3 (0x2) | 5.525kΩ | high mid (0x2) | 32µA | All frequencies | Medium-High |
| 12 | 3 (0x2) | 5.525kΩ | high (0x3) | 64µA | All frequencies | Medium-High |
| 13 | 4 (0x3) | 276.25Ω | low (0x0) | 128µA | ≥ 512 | High |
| 14 | 4 (0x3) | 276.25Ω | low mid (0x1) | 256µA | ≥ 2048 | High |
| 15 | 4 (0x3) | 276.25Ω | high mid (0x2) | 640µA | ≥ 8192 | High |
| 16 | 4 (0x3) | 276.25Ω | high (0x3) | 1.28mA | ≥ 16384 | High |

**Figure 3.7:** Stimulus current options

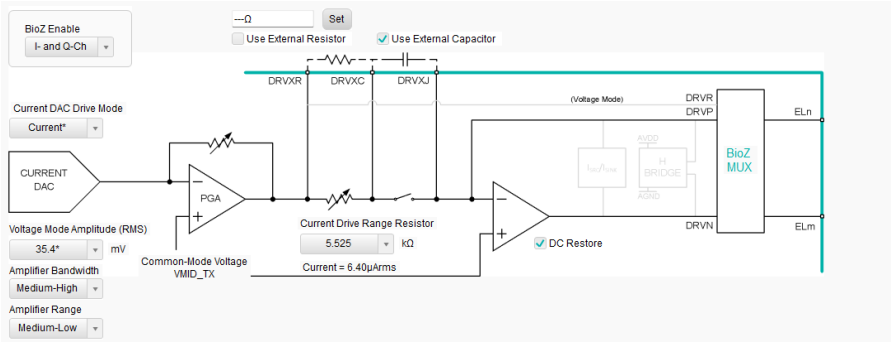


**Figure 3.8:** BioZ Drive Tab confguration

### BioZ Receive

The BioZ Receive Channel in the MAX30009 device features a sophisticated array of components designed for precise bioimpedance measurement. The channel consists of the following key components:

- **Input Multiplexer (MUX):** Equipped with Electrostatic Discharge (ESD)

protection, Electromagnetic Interference (EMI) filtering, programmable electrode assignment switches, lead biasing, DC lead-off detection, and ultra-low power lead-on detection.

- **Analog High-Pass Filter (HPF):** This programmable filter is bypassable and is crucial for removing DC components from the input signal, ensuring that only AC components are amplified.
- **Instrumentation Amplifier (INA):** Provides low-noise amplification of the differential signal, high input impedance, and excellent common-mode rejection ratio (CMRR), crucial for minimizing interference and enhancing measurement accuracy.
- **Demodulators:** Two demodulators are employed to down-convert the measurement frequency to DC, with one demodulator set at 0°for the I channel and the other at 90°for the Q channel.
- **Programmable Gain Amplifiers (PGAs):** These amplifiers allow for the adjustment of signal amplification, facilitating flexible gain settings across the measurement process.
- **Anti-Aliasing Filters (AAFs):** Positioned after the PGAs, these two-pole active low-pass filters operate with a -3dB cutoff at 600 Hz, significantly attenuating any frequencies above this threshold.
- **Analog-to-Digital Converters (ADCs):** Two 20-bit sigma-delta ADCs convert the analog signal into a digital format, allowing for further digital processing and analysis. The resolution of these ADCs is enhanced by the selectable oversampling ratios.

**Configuration and Functionality:**

- The total channel gain is configurable to 1V/V, 2V/V, 5V/V, or 10V/V through the `BIOZ_GAIN` setting. This gain influences both the INA and the PGA, adapting the system for different measurement needs.
- The phase and frequency of the demodulators are matched with the frequency of the BioZ stimulus (F_BIOZ) to effectively isolate the desired signal components.
- The digital filters in the channel, including a SINC3 decimation filter and programmable HPF and LPF, are critical for defining the signal bandwidth and improving the measurement's signal-to-noise ratio.

The BioZ Receive Channel is integral to applications such as Body Impedance Analysis (BIA), Galvanic Skin Response (GSR) measurement, and other bioimpedance-based diagnostic and monitoring tasks. Its design ensures high fidelity in signal acquisition and processing, essential for accurate and reliable bioimpedance measurements.

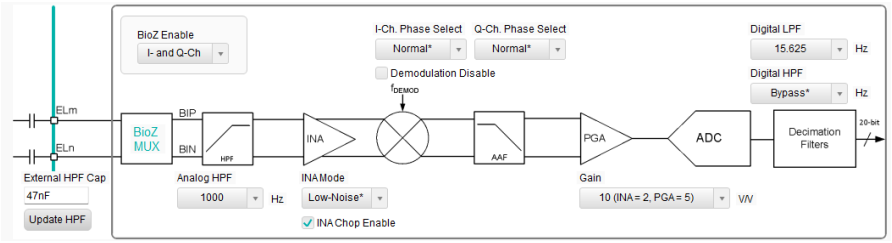


**Figure 3.9:** BioZ Receive Tab

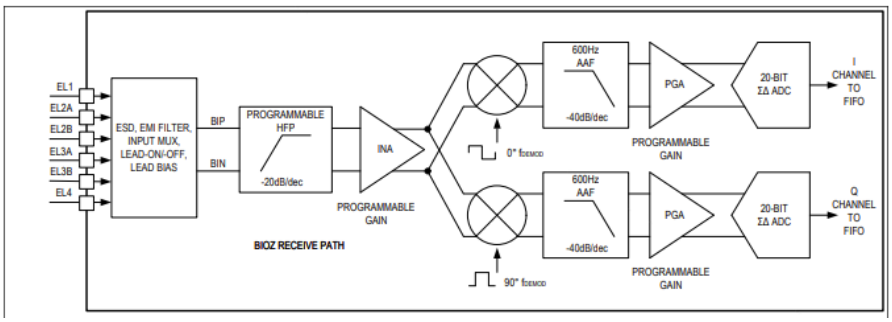


**Figure 3.10:** BioZ Receive channel

### BioZ Multiplexer

The system was set to operate in both bipolar and tetrapolar configurations to suit different types of measurements. The flexibility in mode selection allowed for comprehensive analysis by comparing results from different electrode setups.

### BioZ Calibration

Calibration was performed using internal trimmed resistors to ensure high absolute impedance accuracy. This step was critical for validating the system's accuracy before performing measurements on biological tissues.

The calibration of the MAX30009 BioZ channel is crucial for achieving high accuracy in bioimpedance measurements, specifically targeting an impedance magnitude error of 0.1% and phase error of 0.1°. The process can be conducted using

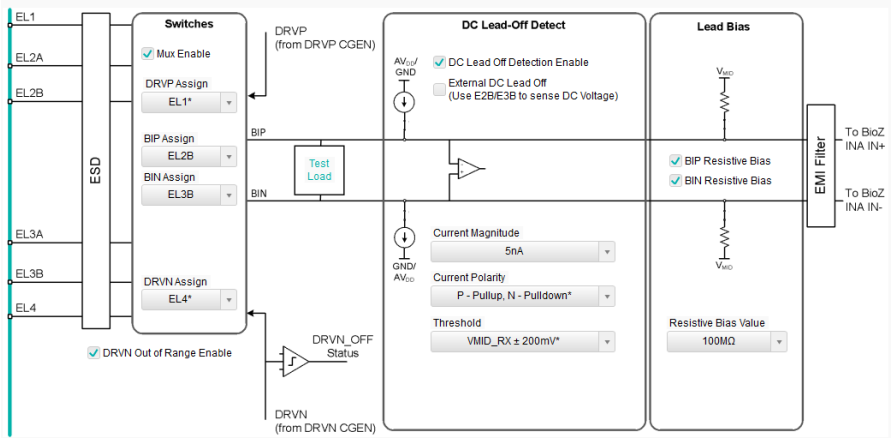


**Figure 3.11:** BioZ Mux Tab

either factory settings with a precision resistor connected to the device electrodes or onboard by attaching a precision resistor to the CALx pins. Key steps involved in the calibration process are as follows:

1. **Initial Setup:**
   - Select the synthesis frequency appropriate for the desired measurement.
   - Connect the precision resistor
   - Assert the necessary MUX and calibration enable bits in the registers to activate the correct paths for calibration.
2. **Offset Measurements:**
   - Set the stimulus current to the minimum (16 nARMS) to reduce influence on the measurement.
   - Apply a short circuit across the load to stabilize the current flow.
   - Enable the I and Q channels and record the offset values in impedance after the signal has settled.
3. **Impedance Measurements:**
   - Increase the stimulus current to the desired level for actual measurements.
   - For in-phase measurements, ensure the demodulation clocks for both channels are synchronized.
   - Record the impedance values with the calibration resistor in circuit, first in-phase and then in quadrature-phase.

4. **Calculation of Calibration Coefficients:**
    - Subtract the previously recorded offsets from the measured impedance values.
    - Calculate the calibration magnitude and phase delay coefficients using the adjusted values.
5. **Application of Calibration Coefficients:**
    - Perform measurements on the actual load and apply the calibration coefficients to adjust for any magnitude and phase discrepancies.
    - Compute the real and imaginary components of the load impedance.
    - Calculate the corrected load impedance magnitude and phase angle using the real and imaginary components.

This procedure is carried out by the program and was implemented in the firmware. Through the GUI in 3.12 is showed the relative tab, where the parameterand the internal resistance are setted. It's also possible to choose at which frequency to perform the calibration.

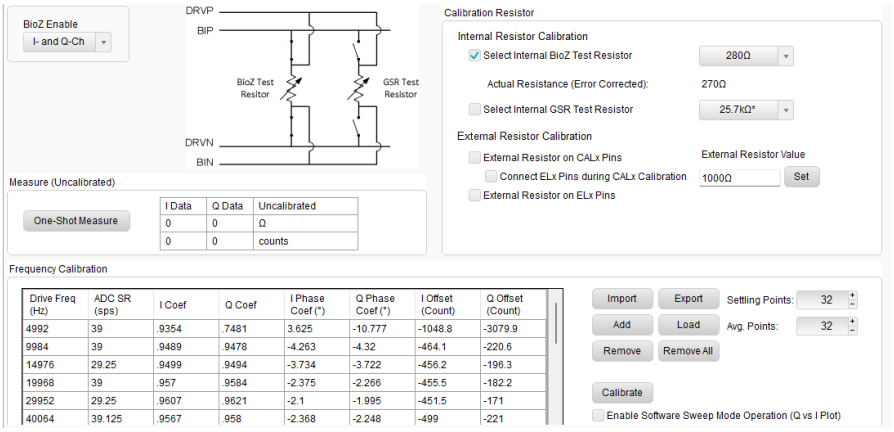


**Figure 3.12:** BioZ Calibration Tab

### 3.3.3 Safety and Regulations

Patient safety is the paramount concern when designing devices that apply voltage or current to the human body. This is especially crucial in medical and wearable devices where the integrity and functionality can significantly impact health outcomes.

The International Electrotechnical Commission (IEC) sets forth standards to ensure the safety and performance of medical electrical equipment. One of the

key standards, IEC 60601-1, outlines the general requirements for basic safety and essential performance. This standard specifies limits on patient auxiliary currents, emphasizing that the maximum allowable AC patient auxiliary current under normal condition is 100$\mu$A at low frequencies such as 50Hz or 60Hz, with allowances for increased currents at higher frequencies.

### Safety Mechanisms in the MAX30009

To aid in adherence to safety guidelines, the MAX30009 incorporates several safety mechanisms:

- **Current Drive Limitation:** The device limits the drive current according to the stimulus frequency. This is a crucial feature that prevents excessive currents from being delivered at frequencies that may be harmful to the patient.
- **Automatic Parameter Adjustment:** If parameters set by the host controller exceed the allowed safety thresholds, the MAX30009 automatically adjusts them to stay within safe limits. This includes adjustments to the frequency divider and current magnitude register fields.
- **Lockout Features:** For high-frequency, high-current stimulus settings, the device requires specific sequences in setting the frequency and current parameters to ensure that unsafe conditions are not inadvertently programmed.

### Additional Considerations for Wearable and Medical Devices

In the broader context of wearable and medical devices, designers must also consider:

- **Electromagnetic Compatibility (EMC):** Devices must be designed to comply with EMC standards to avoid interference with other medical equipment.
- **Usability:** Devices should be designed for ease of use, considering the ergonomic and interface needs of patients and healthcare providers.
- **Data Security:** Ensuring the confidentiality and integrity of patient data is critical, especially for devices that store or transmit health information.
- **Long-Term Reliability:** Medical devices should be reliable over their intended lifespan, requiring rigorous testing and quality control processes.

The integration of these safety features and adherence to international standards are not just regulatory requirements but are essential for the trust and safety of the patients who rely on these medical devices. Designers and manufacturers must be

diligent in their application of these standards throughout the product development lifecycle.

### 3.3.4 Electrode Placement

Electrode placement is crucial for accurate bioimpedance measurements. As supported by existing literature, we chose a transversal electrode placement strategy for our experiments. This approach is designed to optimize the detection of impedance variations due to anatomical differences and physiological changes across the measurement site.

The choice of transversal placement aligns with findings from previous studies, which suggest that this orientation can enhance sensitivity to changes in tissue properties and is beneficial for applications such as monitoring fluid accumulation or tissue health.

**Figure 3.13:** Electrode Placement Front View

**Figure 3.14:** Electrode Placement Side View

**Figure 3.15:** Illustration of the transversal electrode placement on the subject.

#### Data Processing and Visualization Using MATLAB

After collecting the bioimpedance data this MATLAB code automates several essential steps, including importing data from CSV files, applying conversions to transform the data into usable units, and visualizing key characteristics such as resistance, reactance, magnitude, and phase.

The workflow of this code is divided into the following stages:

1. **Data Import**: The bioimpedance data, collected during frequency sweep measurements, is imported from CSV files. Each file contains the real (I) and imaginary (Q) components of the impedance across a range of frequencies.

   The code allows the user to select one or more CSV files containing the bioimpedance data. Each file is then processed individually.

```
[File, Path] = uigetfile('../../Data/*.csv', 'Select
Bioimpedance file...', 'MultiSelect', 'on');
 FreqSweepData(i) = {importfileSweepFreq([Path, File{i}])};

```

   - **File Selection**: The `uigetfile` function opens a dialog for selecting CSV files containing the bioimpedance data.
   - **MultiSelect**: The function allows the user to select multiple files at once for batch processing.
   - **Data Import**: The function `importfileSweepFreq` (defined elsewhere) reads the CSV file and extracts the frequency sweep data for processing.

2. **Data Conversion**: The I and Q components are converted into impedance values (resistance and reactance) using a predefined conversion factor based on the sensor parameters, such as stimulus current and gain, as better explained in the next section The BioZ channel samples are digitized into a 20-bit left-justified 2's complement format. This formatting ensures that each sample accurately represents the voltage measured at the output of the Analog-to-Digital Converter (ADC). The path of the signal includes processing through an Instrumentation Amplifier (INA), a demodulator, a Programmable Gain Amplifier (PGA), and an Anti-Aliasing Filter (AAF).

   - The **INA and PGA** apply a combined configurable gain of 1V/V, 2V/V, 5V/V, or 10V/V, adjustable via `BIOZ_GAIN[1:0](0x24)`.
   - The **demodulator** processes the incoming waveform (either sine-wave or square-wave) by multiplying it with a square-wave of frequency $F_{BIOZ}$.
   - The **AAF** is a two-pole low-pass filter with a corner frequency of 600 Hz, which helps reduce higher frequency noise and artifacts.
   - The **decimation filter** in the ADC narrows the bandwidth to approximately $0.26 \times SR_{BIOZ}$, enhancing the signal's clarity and focus within the desired frequency range.

For absolute impedance measurements, crucial in applications such as Body Impedance Analysis (BIA/BIS), the following formula is applied to convert the DC component of the demodulated voltage into impedance:

$$Z_{BIOZ}(\Omega) = \frac{ADC\_COUNT \times VREF}{2^{19} \times BIOZ\_GAIN \times \frac{2}{\pi} \times I_{MAG}}$$

where:

- $ADC\_COUNT$ is the digital count output from the ADC in signed magnitude format.
- $VREF$ is typically 1V (refer to the Electrical Characteristics section of the datasheet).
- $BIOZ\_GAIN$ is the gain setting, with options including 1V/V, 2V/V, 5V/V, and 10V/V.
- $I_{MAG}$ is the stimulus current in APK, set by `BIOZ_VDRV_MAG[5:4](0x22)` and `BIOZ_IDRV_RGE[3:2](0x22)`.

The input-referred voltage amplitude for different stimulus types can be calculated using the equations:

$$V_{BIOZ}^{VPK}(\text{sine-wave}) = \frac{ADC\_COUNT \times VREF}{2^{19} \times BIOZ\_GAIN \times \frac{2}{\pi}}$$

And this is the resulting code:

```
1    ConversionFactor = VREF/(IMAG*(2^19)*BIOZ_GAIN*2/pi) ;
2    Resistance(:,i) = FreqSweepData{i}.ICalibratedcounts.*
     ConversionFactor;
3    Reactance(:,i) = FreqSweepData{i}.QCalibratedcounts.*
     ConversionFactor;
4    Mag(:,i) = sqrt((FreqSweepData{i}.ICalibratedcounts.*
     ConversionFactor).^2 + (FreqSweepData{i}.QCalibratedcounts.*
     ConversionFactor).^2);
5    Ph(:,i) = atan(FreqSweepData{i}.QCalibratedcounts./
     FreqSweepData{i}.ICalibratedcounts).*180./pi;
6
```

- **Magnitude**: The impedance magnitude is calculated using the Pythagorean theorem applied to the I and Q components.

- **Phase**: The phase angle in degrees is calculated from the ratio of Q to I using the arctangent function.

3. **Mathematical Operations**: Key calculations, such as the impedance magnitude and phase, are performed to transform the raw measurements into a format suitable for analysis.

```
1    Mag(:,i) = sqrt((FreqSweepData{i}.ICalibratedcounts.*
     ConversionFactor).^2 + (FreqSweepData{i}.QCalibratedcounts.*
     ConversionFactor).^2);
2    Ph(:,i) = atan(FreqSweepData{i}.QCalibratedcounts./
     FreqSweepData{i}.ICalibratedcounts).*180./pi;
3
```

- **Magnitude**: The impedance magnitude is calculated using the Pythagorean theorem applied to the I and Q components.
- **Phase**: The phase angle in degrees is calculated from the ratio of Q to I using the arctangent function.

4. **Visualization**: The processed data is visualized through various plots that allow us to assess how impedance and phase change with frequency. This step is crucial for characterizing the bioimpedance data and understanding the physiological implications of the measurements, and also to compare different measurements.

The following subsections provide a detailed explanation of each part of the code and its purpose in the context of bioimpedance data analysis.

## 3.4 Experiments Done

The series of experiments conducted were designed to explore the functionalities and performance characteristics of the MAX30009 sensor. These experiments were aimed at understanding how different parameters affect BioZ measurements, evaluating the repeatability of the sensor, and observing physiological changes. The experiments were divided into three main sections: parameter tuning, repeatability tests, and analysis of physiological changes.

### 3.4.1 Parameter Tuning

In the first set of experiments, we focused on tuning various parameters of the MAX30009 sensor to optimize its performance for bioimpedance measurements.

This included adjusting settings such as the drive current, frequency settings, and the gain configurations. Through iterative testing and adjustments, we established a set of parameters that balanced measurement precision with power consumption.

### Current Intensity

Selecting the appropriate current intensity was critical for achieving accurate bioimpedance measurements. We performed an intense literature reseach on the topic and also conducted our self some test using an RC model to check different currents behaviour on the frequency sweep. The setup is shown in the following photos.

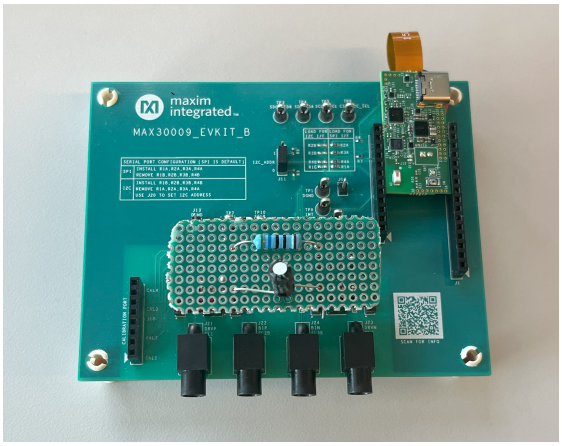


**Figure 3.16:** RC model setup

### Waveform Type

We also experimented with both sine and square waveform types to understand their impact on the sensor's performance. While square waves are typically used for their simplicity in bioimpedance measurements, we found that sine waves, despite slightly higher current consumption, provided more stable and repeatable measurements. This decision was supported by observations of reduced noise and artifacts in the sine wave mode.

## 3.4.2 Wet electrode comparisons

In our bioimpedance measurements, we conducted a series of experiments to compare the performance of different wet electrodes. Specifically, we evaluated 3M electrodes against Kendall electrodes, shown in 3.17. The main criteria for this comparison were signal quality and practical implementation for our use case.

To minimize artifacts in the bioimpedance measurements due to varying blood flow, I, the subject, remained seated for 10 minutes before the measurements. This ensured a period of normalization, reducing the likelihood of artifacts caused by posture changes or sudden muscle movements. After this rest period, bioimpedance measurements were taken while I was standing with the leg in a straight position. This posture was chosen to ensure consistency between measurements and to avoid variations in impedance due to changes in leg orientation or muscle contractions.

We used the 3M electrodes in two different conditions: old electrodes that had been in use for several experiments, and new electrodes taken directly from the packaging. Additionally, Kendall electrodes were also tested to assess any performance differences due to their smaller form factor. Each measurement was taken on both knees, with timestamps recorded for each session. The table below summarizes the setup for each measurement:

| **Timestamp** | **Type** | **Knee** |
|---|---|---|
| 11:57 am | 3M old | L |
| 11:57 am | 3M old | R |
| 12:04 pm | 3M | L |
| 12:04 pm | 3M | R |
| 12:13 pm | 3M new | L |
| 12:13 pm | 3M new | R |
| 12:19 pm | Kendall | L |
| 12:19 pm | Kendall | R |

**Table 3.1:** Summary of measurements taken with 3M and Kendall electrodes

As shown in the table, we first used the 3M electrodes, both old and new, for measurements on the left (L) and right (R) knees. Following these tests, we switched to Kendall electrodes, applying them on both knees to evaluate their performance under the same conditions.

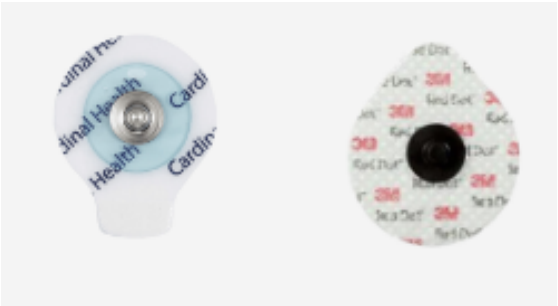

**Figure 3.17:** On the right: Kendall electrode - on the left: 3M electrode

### 3.4.3 Repeatability Tests

The second phase of testing involved conducting repeatability tests to ensure the sensor's consistency over multiple trials. This was crucial to verify the reliability of the MAX30009 in clinical and research settings. We performed these tests under controlled conditions, measuring both myself and a colleague to account for individual variability. All measurements were taken in a controlled temperature environment, after a 10-minute rest period, and the subject remained seated between measurements. Measurements were taken while standing with legs straight.

#### Electrode Positioning Repeatability

In the first experiment, we tested the repeatability of the bioimpedance measurements by evaluating the effect of slight variations in electrode positioning. I was the subject for this experiment, with electrodes placed on both knees. On the left knee, we replaced the 3M electrode between measurements to observe the impact of slight variations in electrode placement. Although we aimed to place the electrode in the same spot each time, slight variations were inevitable. On the right knee, the 3M electrode was not replaced, and the experiment was designed to observe how the bioimpedance measurements changed over time as the gel dried. We took four measurements every 10 minutes on both knees.

To further validate this experiment, we repeated the procedure on another subject (female) with Kendall electrodes. For this subject, the electrodes were fixed on the left knee and replaced on the right knee between measurements, similar to the previous trial. The time interval remained the same, with four measurements taken every 10 minutes over a 30-minute period.

In these tests, the electrodes were consistently placed on the same areas of both knees to minimize variation, and the environment was controlled to maintain a stable temperature. Measurements were performed after a 10-minute rest, while the subject stood with legs straight during the data acquisition process.

### 3.4.4 Physiological Changes

The final set of experiments was designed to observe how physiological changes affect BioZ measurements. This involved monitoring changes under various conditions before and after exercise. These tests helped in understanding how physiological factors could influence bioimpedance measurements and the sensor's responsiveness to such changes.

### Upper Limb Experiments

The aim of the upper limb experiments was to determine if movement in the arms could significantly influence blood flow and modify the bioimpedance (BioZ) measurements. Specifically, we wanted to see if BioZ measurements were sensitive enough to detect changes due to upper limb movements. The experiment involved cycling for the arms while the subject was seated, using a cycle ergometer with the force level set to 4.0.

Every 5 minutes, the subject stood up, and BioZ measurements were taken from both legs. During the experiment, heart rate (HR) was recorded using the POLAR device, and temperature and humidity were monitored in the room to ensure no drastic changes occurred that could influence the measurements. The experiment was conducted twice: once with me as the subject and once with a female subject to account for any potential sex-related differences. After the exercise we also recorded the cool down phase, to see if the values were going back to the before-exercise values and how fast this was happening.

The following tables summarize the data from both trials:

| **Timestamp** | **Heart Rate (bpm)** | **Temperature (°C)** | **Humidity (%)** |
|---|---|---|---|
| 12:22 pm | 69 | 23.8 | 47 |
| 12:28 pm | 85 | 23.5 | 48 |
| 12:33 pm | 90 | 23.6 | 48 |
| 12:38 pm | 94 | 23.6 | 48 |
| 12:44 pm | 92 | 23.8 | 47 |
| 12:49 pm | 95 | 23.7 | 47 |
| 12:54 pm | 105 | 23.3 | 49 |
| 1:04 pm | 68 | 23.3 | 48 |

**Table 3.2:** First trial: Male subject

| **Timestamp** | **Heart Rate (bpm)** | **Temperature (°C)** | **Humidity (%)** |
|---|---|---|---|
| 12:30 pm | 90 | 26.3 | 42 |
| 12:40 pm | 108 | 25.0 | 45 |
| 12:50 pm | 118 | 24.0 | 47 |
| 1:00 pm | 125 | 23.4 | 49 |
| 1:10 pm | 82 | 24.5 | 47 |
| 1:20 pm | 92 | 24.7 | 47 |
| 1:30 pm | 92 | 25.1 | 47 |
| 1:40 pm | 90 | 25.0 | 47 |

**Table 3.3:** Second trial: Female subject

### Lower Limb Experiments

The lower limb experiments were aimed at investigating whether a direct exercise on the legs, specifically affecting the knees with increased blood flow and muscle stress, would influence the bioimpedance (BioZ) measurements. These tests were designed to determine how exercise-related physiological changes could impact the BioZ values.

We performed two runs of the experiment on myself. The first run had issues due to the electrodes detaching from the skin because of sweat. The second run followed an updated protocol to address this issue. Additionally, a third set of experiments was performed on another male subject, recorded over two consecutive days with intensive leg training on the evening between the two sessions.

#### Protocol for the First Experiment

1. Static bioimpedance
2. 30 squats
3. Static bioimpedance
4. Walk/Run protocol:
   (a) 5 minutes walking at 2.7 m/h
   (b) Static bioimpedance
   (c) 5 minutes walking at 3.0 m/h
   (d) Static bioimpedance
   (e) 5 minutes running at 4.5 m/h
   (f) Static bioimpedance
   (g) 5 minutes running at 5.5 m/h
   (h) Static bioimpedance
   (i) 5 minutes running at 6.0 m/h
   (j) Static bioimpedance
5. Cool down static measurement:
   (a) Bioimpedance every 10 minutes for 40 minutes

During the experiment, we monitored heart rate, temperature, and humidity, as shown in the following table.

| Timestamp | Heart Rate (bpm) | Temperature (°C) | Humidity (%) | Knee |
|---|---|---|---|---|
| 3:47 pm | 74 | 22.3 | 52 | L/R |
| 3:50 pm | 120 | 22.1 | 53 | L/R |
| 3:57 pm | 92 | 21.7 | 54 | L/R |
| 4:04 pm | 93 | 21.6 | 55 | L/R |
| 4:11 pm | 128 | 21.5 | 56 | L/R |
| 4:18 pm | 137 | 21.5 | 56 | L/R |
| 4:27 pm | 148 | 21.6 | 57 | L/R |
| 4:37 pm | 75 | 21.4 | 56 | L/R |
| 4:47 pm | 68 | 23.3 | 51 | L/R |
| 4:57 pm | 74 | 26.8 | 45 | L/R |
| 5:07 pm | 70 | 27.3 | 48 | L/R |
| 5:24 pm | 59 | 27.3 | 49 | L/R |

**Table 3.4:** First run: Heart rate, temperature, and humidity measurements.

**Protocol for the Second Experiment**

The second experiment addressed the issue of electrode detachment by performing skin preparation steps to minimize sweat-related interference with the skin-electrode impedance. The revised protocol was as follows:

1. Skin preparation
2. Static bioimpedance
3. 30 squats
4. Walk/Run protocol:
   (a) 15 minutes walking at 2.7 m/h
   (b) 10 minutes running at 4.0 m/h
5. Skin preparation
6. Cool down static measurement:
   (a) Bioimpedance every 10 minutes for 40 minutes

The key difference in this protocol is the exclusion of measurements during the activity itself, focusing on post-activity measurements after re-preparing the skin to reduce the influence of sweat.

| Timestamp | Heart Rate (bpm) | Temperature (°C) | Humidity (%) |
|---|---|---|---|
| 4:14 pm | 58 | 22.0 | 54 |
| 4:48 pm | 100 | 22.4 | 54 |
| 5:05 pm | 67 | 22.3 | 53 |
| 5:20 pm | 64 | 22.3 | 54 |
| 5:40 pm | 62 | 22.2 | 54 |

**Table 3.5:** Second run: Post-activity heart rate, temperature, and humidity measurements.

**Protocol for the Third Experiment**

This experiment was conducted on another male subject, recorded over two consecutive days. The subject performed intensive leg training between the two sessions, with the goal of capturing baseline measurements on the first day and observing any changes during the follow-up session the next day.

The protocol was the same for both days:

1. Static bioimpedance
2. Walk/Run protocol:
   (a) 10 minutes walking at 2.7 m/h
   (b) Static bioimpedance
   (c) 5 minutes running at 4.0 m/h
   (d) Static bioimpedance
   (e) 5 minutes running at 5.5 m/h
   (f) Static bioimpedance
   (g) 5 minutes running at 5.5 m/h
   (h) Static bioimpedance
3. Cool down static measurement

The following tables summarize the results from both days:

| Timestamp | Heart Rate (bpm) | Temperature (°C) | Humidity (%) |
|---|---|---|---|
| 11:29 am | 60 | 21.8 | 56 |
| 11:40 am | 69 | 21.7 | 56 |
| 11:48 am | 100 | 21.6 | 56 |
| 11:56 am | 116 | 21.6 | 56 |
| 12:03 pm | 137 | 21.6 | 57 |
| 12:15 pm | 80 | 21.6 | 56 |
| 1:29 pm | 60 | 21.5 | 56 |

**Table 3.6:** Third experiment, Day 1: Heart rate, temperature, and humidity measurements.

| Timestamp | Heart Rate (bpm) | Temperature (°C) | Humidity (%) |
|---|---|---|---|
| 11:32 am | 55 | 21.8 | 57 |
| 11:39 am | 65 | 21.7 | 57 |
| 11:45 am | 95 | 21.6 | 57 |
| 11:53 am | 108 | 21.5 | 58 |
| 12:01 pm | 133 | 21.5 | 57 |
| 1:46 pm | 60 | 21.6 | 57 |

**Table 3.7:** Third experiment, Day 2: Heart rate, temperature, and humidity measurements.

These tests allowed us to explore how bioimpedance is affected by different levels of physical activity and muscle recovery, while controlling for environmental factors like temperature and humidity.

## 3.5 The 'Investigation of Biomechanics During Movement in Healthy Athletes' Study

The data collection for this study was conducted in collaboration with Dr. Adam Tenforde as part of a broader investigation into the biomechanics of healthy athletes during various forms of physical activity. The main goal of this study was to create a normative database of biomechanical data, including bioimpedance measurements, which could be used to compare injured athletes with healthy ones, and to detect potential predictors of injury.

### 3.5.1 Study Presentation and Goals

The study, titled *Investigation of Biomechanics During Movement in Healthy Athletes*, aimed to evaluate the biomechanics involved in walking, running, and jumping among healthy, uninjured athletes. The specific goals of the study were to:

- Establish a normative database of biomechanical parameters for healthy athletes during movement.
- Compare the biomechanical differences between habitual distance runners and multi-directional sport athletes.
- Examine how speed and footwear affect gait biomechanics.
- Assess physiological parameters like knee range of motion, strength, and bone health.

Bioimpedance spectroscopy (BIS) played a critical role in assessing physiological changes at the knee joint, particularly in understanding joint conductivity and inflammation. This is especially relevant for detecting early indicators of joint issues, such as those related to osteoarthritis (OA), which are common in some former athlete populations.

### 3.5.2 Bioimpedance Measurement Focus

The study included bioimpedance measurements to evaluate the electrical characteristics of the knee joint. These measurements were taken before and after biomechanical assessments to track changes during movement. Bioimpedance was measured at multiple frequencies ranging from 1 kHz to 1 MHz, using tetrapolar electrodes placed on either side of the knee joint. The electrodes were positioned transversely on the medial and lateral surfaces of the knee, following the protocol for transverse bioimpedance measurement as highlighted in the literature. This placement was chosen to optimize sensitivity to tissue changes across the knee joint, particularly in the context of inflammation and tissue conductivity.

A low-amplitude sinusoidal current, compliant with IEC 60601-1 safety standards, was applied to measure impedance. The results of these measurements could potentially be used as predictive markers for knee pain and inflammation, especially for athletes prone to knee-related conditions such as osteoarthritis.

### 3.5.3 Research Questions

In this study, our main goal is to explore how bioimpedance measurements can help distinguish between healthy subjects and patients with Osteoarthritis (OA). Specifically, we aim to address the following research questions:

**Figure 3.18:** Bioimpedance measurements setup during the data collection

### Baseline Differences Hypothesis

We hypothesize that OA patients will show a higher limb-to-limb difference in bioimpedance measurements compared to healthy individuals. This difference is expected to provide a baseline indicator of the impact of OA on fluid distribution and tissue properties in the knees.

As showed in [5] study, knee injuries typically cause a reduction in bioimpedance, approximately 5% on average, when compared to healthy knees, where the difference is nearly 0%. This reduction in bioimpedance in the affected knee highlights the importance of comparing both knees of the same individual, as this comparison is more meaningful than comparing knees between different individuals.

- Knee injuries resulted in a 5% reduction in bioimpedance, compared to nearly 0% in healthy knees.
- Comparing both knees of the same individual provides more accurate insights than comparing knees across different subjects.

### Effect of Running on Healthy Subjects vs OA Hypothesis

We expect running on a treadmill to alter bioimpedance measurements in OA patients more significantly than in healthy subjects, resulting in larger changes in limb-to-limb differences in OA patients. The reasoning behind this is that physical activity, such as running, influences the distribution and volume of interstitial fluid. For OA patients, particularly those with edema, post-exercise changes in bioimpedance are expected to be more pronounced. In contrast, healthy individuals without edema are expected to show only minor changes, attributed to normal physiological responses such as muscle perfusion and minor fluid shifts, as proved in [3] and [4] studies.

$$H_a = \frac{\Delta R(5k)_{extension-flexion}}{\Delta R(100k)_{extension-flexion}} \tag{3.1}$$

**Effect of Shockwave Therapy on OA Patients Hypothesis**

As demonstrated in [5] study, we hypothesize that after 4 months of shockwave therapy, OA patients will exhibit bioimpedance measurements that are more similar to those of healthy subjects. Specifically, the difference in resistance ($\Delta R$) between the injured and healthy knee is expected to decrease after rehabilitation.

- $\Delta R_{injured} = 11.8\Omega > \Delta R_{healthy} = 4.9\Omega$
- After rehabilitation, $\Delta R_{injured}$ decreases from 11.8 Ω to 1 Ω, and $\Delta X_{injured}$ decreases from 4.9 Ω to 2.3 Ω.

Injured subjects initially exhibit lower resistance in the affected knee compared to the healthy knee, but shockwave therapy brings the resistance values closer to those observed in healthy subjects.

### 3.5.4 Data Integration and Future Goals

The bioimpedance data collected in this study is expected to provide valuable insights into joint health, especially in relation to tissue conductivity changes and inflammation. The collected data will contribute to building a comprehensive normative database that can be compared with future studies involving injured athletes, aiding in both injury prevention and treatment strategies.

This study represents an important step in understanding how bioimpedance can be utilized in sports science to monitor joint health and prevent injuries in athletes.

## 3.6 Results and discussion

The results of the laboratory experiments provided valuable insights into the behavior of the BioZ sensor and the factors influencing its measurements. By systematically varying parameters such as electrodes, current amplitude, and frequency we established a baseline for BioZ measurements and informed the subsequent development of the knee sleeve.

This section presents a detailed analysis of the experimental results, highlighting the impact of different configurations on measurement accuracy and consistency. The discussion focuses on how these findings shaped our understanding of the sensor's performance and guided the optimization of the final design.

### 3.6.1 Current Magnitude

The experiments on the RC model gave the expected results, particularly when analyzing the resistance over reactance graph, which displayed the typical semicircle shape, as shown in 3.19 This confirmed the correctness of our measurements. We repeated the measurements using different drive currents, and the results remained consistent and comparable across trials, as shown in 3.20.

To finalize the decision on which current to use, we conducted an extensive literature review. Inspired by the findings in *Localized Bioimpedance Measurements with the MAX3000x Integrated Circuit: Characterization and Demonstration* by Critcher and Freeborn [17], we opted for a drive current close to 6.4 $\mu$A, slightly below their used 8 $\mu$A, as it was the nearest available setting on our device.

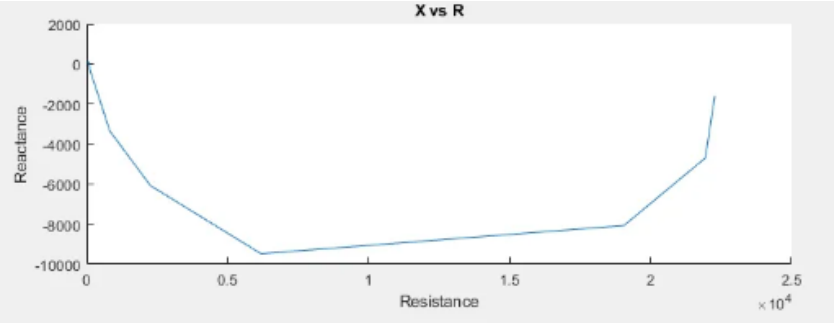


**Figure 3.19:** RC model measurements at 256 uA

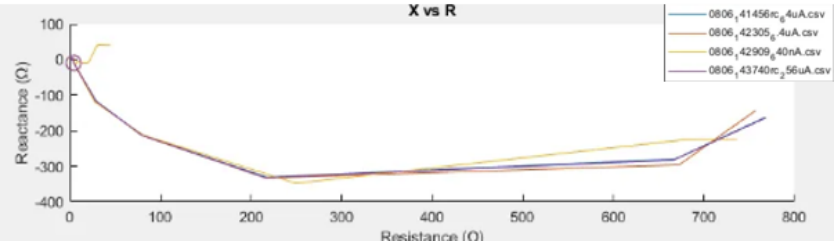


**Figure 3.20:** RC model with different current intensities

### 3.6.2 Wet electrode comparisons

The results of the experiments showed no significant difference in terms of signal quality between the two types of electrodes. Both 3M and Kendall electrodes provided comparable results with minimal variation. The variation observed was primarily in the form of an offset difference, which is expected due to the different skin-electrode impedance. This impedance can vary depending on the materials and design of the electrodes, leading to slight differences in the initial baseline measurements. However, this offset does not affect the overall quality or reliability of the signal, as both types of electrodes consistently captured the bioimpedance data with high accuracy. These findings suggest that both electrodes are suitable for bioimpedance measurements, with the minor differences in skin-electrode impedance falling within acceptable ranges for such experiments.
However, when considering other factors, particularly the form factor of the electrodes, Kendall electrodes offered a distinct advantage. Due to their smaller size, Kendall electrodes allow for closer placement on the subject's skin. This proximity between the electrodes enhances the measurement accuracy by reducing the negative sensitivity that can occur when the power and sensing electrodes are too far apart.

Thus, despite the equivalence in signal performance, we opted for Kendall electrodes in our experimental setup. Their compact form factor improves the overall quality of the measurements by mitigating potential distortions caused by excessive spacing between the electrodes.

In 3.21 and 3.22 we can see in yellow the Kendall electrode measurement, in blue the 3M old electrode and in red the new 3M electrode measurement. We can notice a slight offset between the Kendall and 3M, while there is no significant difference between the 3M and old 3M electrode measures.

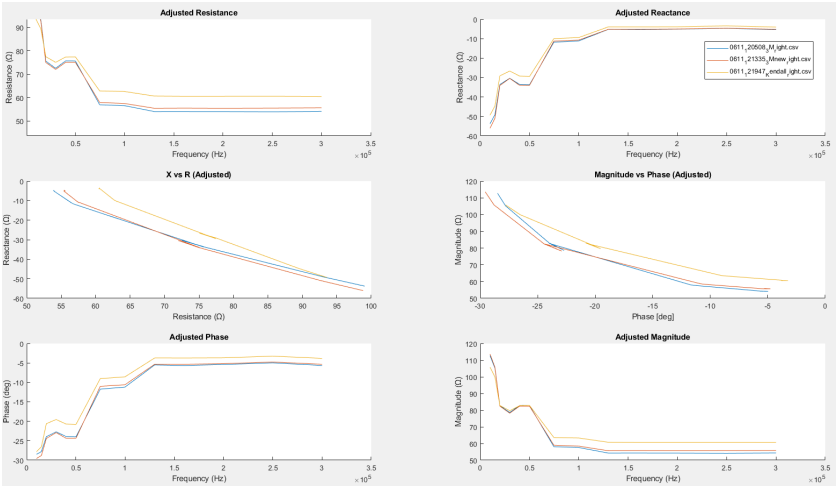


**Figure 3.21:** Wet electrode comparison - right leg

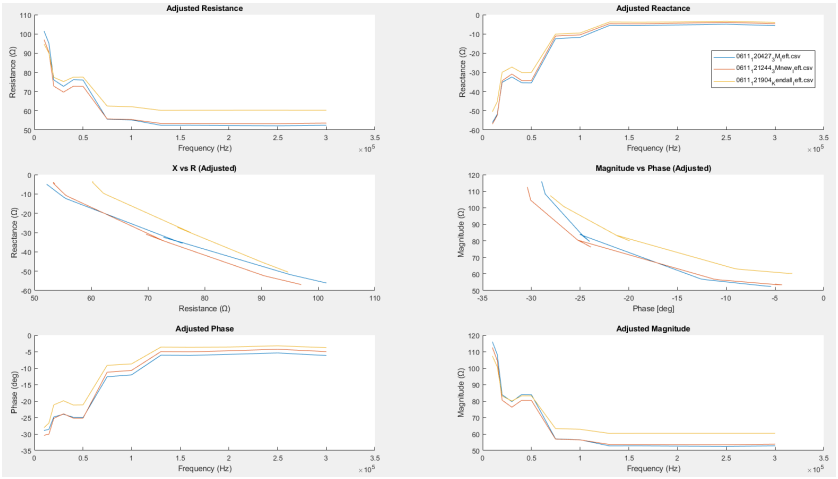


**Figure 3.22:** Wet electrode comparison - right leg

### 3.6.3 Repeatability test

The results of the repeatability experiments provide critical insights into the stability and consistency of BioZ measurements under varying conditions.

**Electrode Drying:**

Figure 3.23 shows the results of the electrode drying experiment, with resistance and reactance plotted across multiple frequencies. At 50 kHz, the drying process introduced a variability of approximately 0.4 Ω in reactance and 1.5 Ω in resistance. Despite these variations, the overall impact of electrode drying on BioZ measurements was minor and remained well within acceptable limits. This suggests that the drying process does not significantly impair the reliability of BioZ data over time, provided the electrodes maintain adequate contact with the skin.

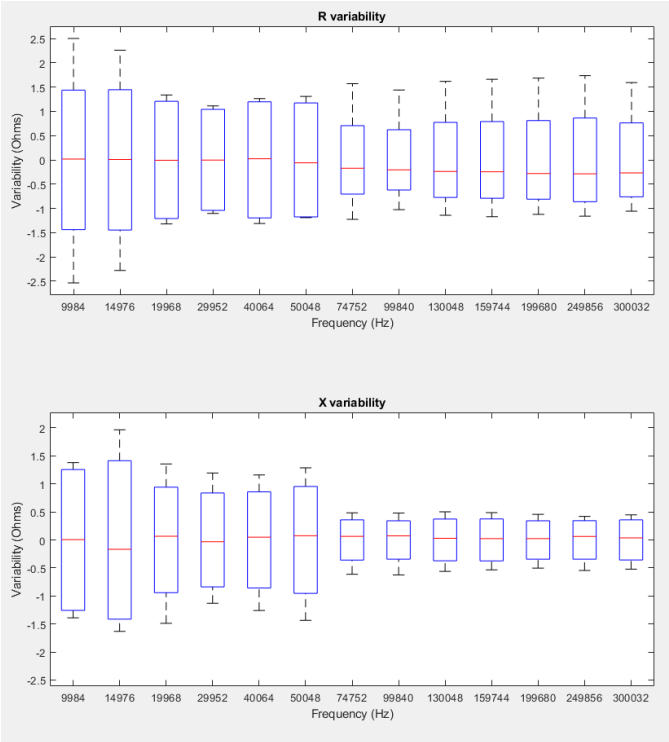


**Figure 3.23:** Resistance and reactance variability due to electrode drying. Each box represents the median (central mark), the 25th and 75th percentiles (box edges), and the whiskers extend to the most extreme non-outlier points. Outliers are shown with '+' symbols.

### Electrode Repositioning:

The results of the electrode repositioning experiment, presented in Figure 3.24, show a more pronounced impact on BioZ measurements compared to electrode drying. At 50 kHz, variability reached approximately 3 Ω for both resistance and reactance. These results highlight the importance of precise and consistent electrode placement to minimize measurement discrepancies. The observed variability underscores the need for careful electrode handling during application, particularly in wearable devices where electrodes may be repositioned frequently.

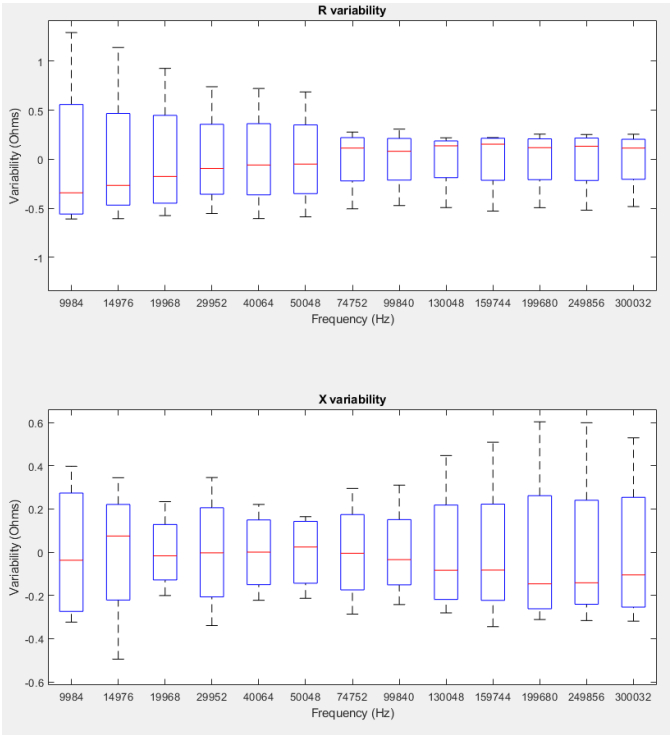


**Figure 3.24:** Resistance and reactance variability due to electrode repositioning. The box plot follows the same format as described for Figure 3.23.

### Discussion:

The repeatability experiments revealed that:

- Electrode drying introduces limited variability in BioZ measurements, making it a minor concern for most applications.
- Electrode repositioning introduces more significant variability, with measurement discrepancies of up to 3 Ω, emphasizing the need for consistent electrode placement.

- Both experiments confirmed the robustness of BioZ measurements when performed under controlled conditions. Similar trends were observed for the two subjects, demonstrating that these findings are broadly applicable.

These results confirm that, while external factors like electrode drying and repositioning can affect BioZ measurements, their impact can be minimized through proper electrode placement and handling. These findings informed the design of the knee sleeve to ensure stable and reliable measurements during use.

### 3.6.4 Physiological changes

The results of the physiological changes observed during the experiments are presented in separate graphs for the upper and lower limbs, with data shown for both male and female subjects. Each graph is structured into multiple sections to provide a detailed view of the BioZ measurements and their variations over time.

**Graph Structure:** Each graph consists of the following sections, organized from top to bottom:

1. **Resistance:** The top section shows the resistance measurements for the left limb (on the left) and the right limb (on the right).
2. **Reactance:** Below the resistance, this section presents the reactance measurements for the left and right limbs.
3. **Relative Difference to Baseline:** This section displays the percentage variation of the BioZ magnitude with respect to the initial baseline measurement.
4. **Difference Between Limbs:** The bottom section shows the difference in BioZ magnitude between the two limbs (right minus left).

In each part of the graph, different curves represent the measurements at various frequencies used during the experiment. Additionally, the red-shaded area represents the heart rate (HR), used for monitoring the subject's activity. Specifically, an increase in HR indicates that the subject is exercising, while a decrease in HR corresponds to resting periods. This provides additional context for interpreting the changes in bioimpedance measurements relative to the physical effort. The HR scale is provided on the right y-axis.

The following sections provide a detailed discussion of the results for the upper and lower limbs.

### Upper Limb Results

**Male Subject** The results for the male subject's upper limb are shown in Figure 3.25. The graph reveals a noticeable decrease in both resistance and reactance, even during exercises focused solely on the upper limb, while the knee remained relaxed. This suggests that upper limb activity can still influence bioimpedance measurements in the upper limb region, likely due to physiological changes such as increased blood flow or systemic effects.

Additionally, the subject was sweating during the exercise, which may have contributed to the observed variations by altering the skin-electrode interface and affecting the bioimpedance measurements. This highlights the importance of considering external factors like perspiration when interpreting BioZ data.

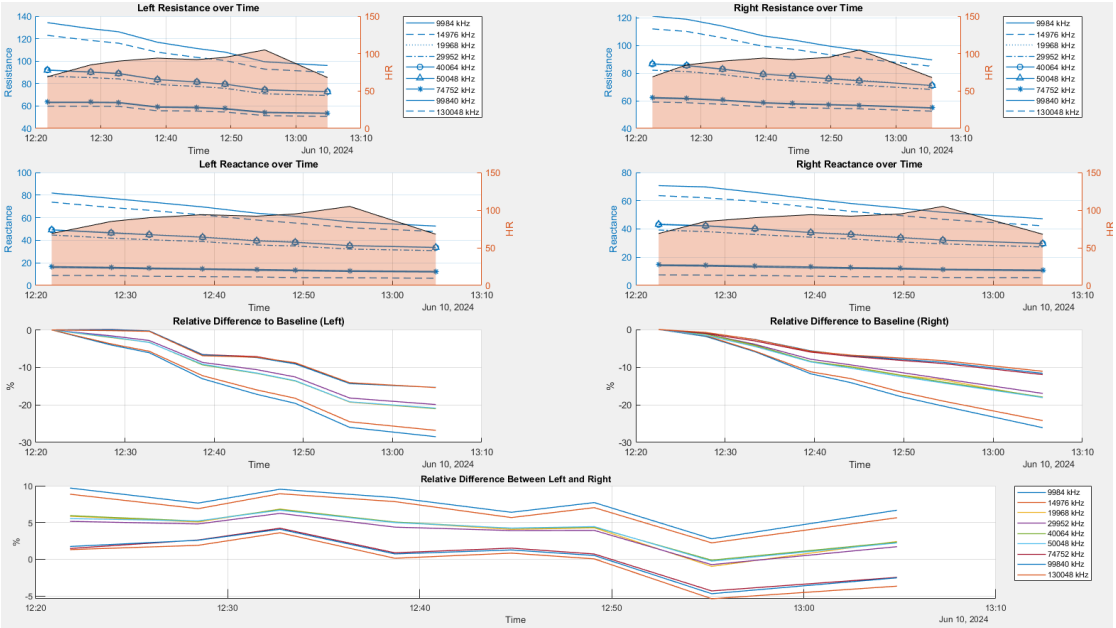


**Figure 3.25:** Male subject during upper limb exercise

**Female Subject**

The results for the female subject's upper limb are shown in Figure 3.26. In this case, the variations in bioimpedance were more subtle compared to the male subject. Specifically, resistance showed a variation of only around 3%, while reactance varied by approximately 5%.

Unlike the male subject, the female subject did not report sweating during the exercise, which likely contributed to the smaller variations observed in the measurements. Additionally, despite having a similar heart rate (HR) during the session, the physical effort was self-reported to be lower. This discrepancy can be attributed to differences in the participants' levels of athleticism, emphasizing the importance of considering individual fitness levels when interpreting BioZ results.

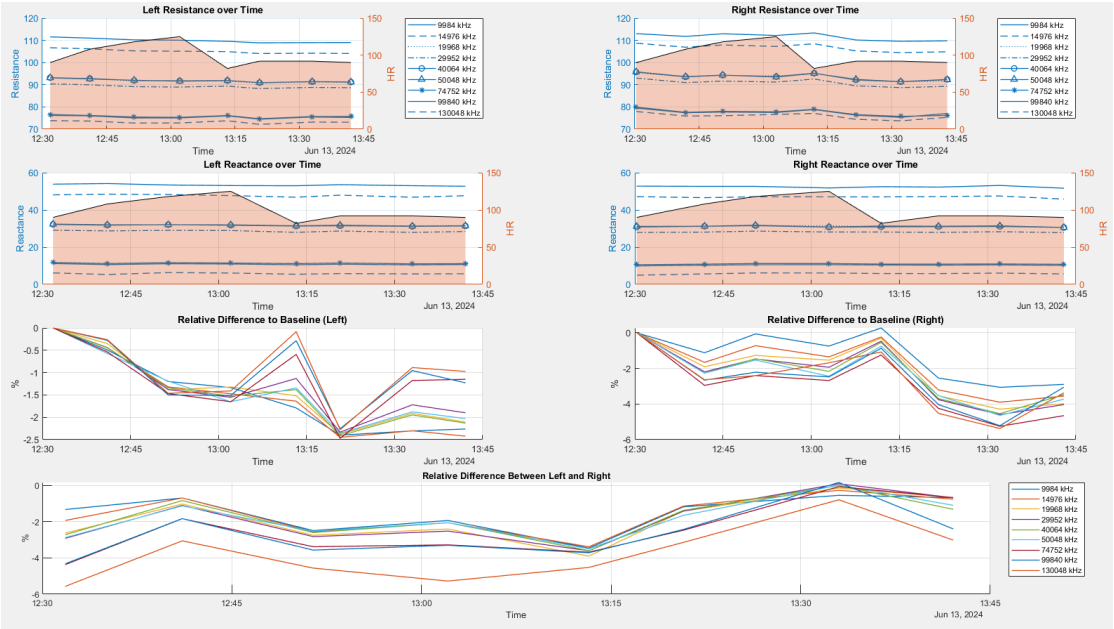


**Figure 3.26:** Female subject during upper limb exercise

### Lower Limb Results

### Male Subject #001

For subject #001, two protocols were performed due to an issue encountered during the first trial.

**Protocol 1** In the first protocol, as we can notice in 3.27 we had a problem between 16:15 and 16:30 due to the detachment of the gel electrodes caused by excessive sweating. This highlighted the importance of stable electrode placement for accurate bioimpedance measurements.

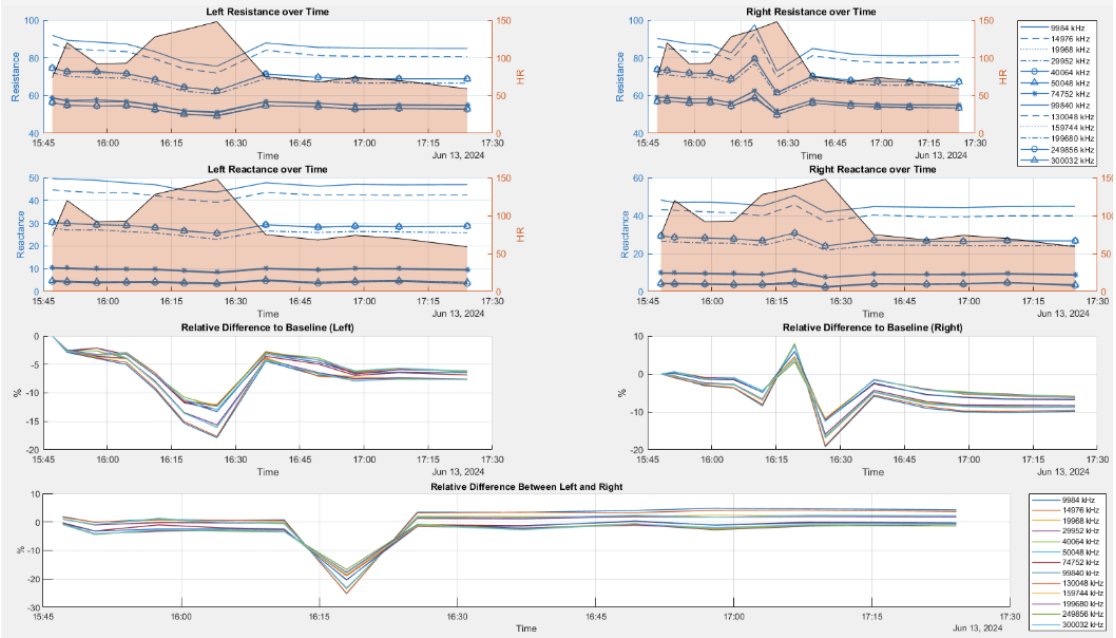


**Figure 3.27:** Male subject #001 during lower limb exercise - protocol 1

**Protocol 2** To address the issue, Protocol 2 was conducted with the modifications described in the method section. The results showed in 3.28 a significant deviation from baseline, with differences of up to 15%, similar to the trends observed in the upper limb of the male subject and much larger than those of the upper limb of the female subject.

Resistance and reactance consistently decreased during exercise and gradually increased back during the rest phases. However, the bioimpedance values exhibited a delayed recovery, taking a long time to return to baseline after the exercise. This trend underscores the physiological effects of sustained physical activity on bioimpedance measurements.

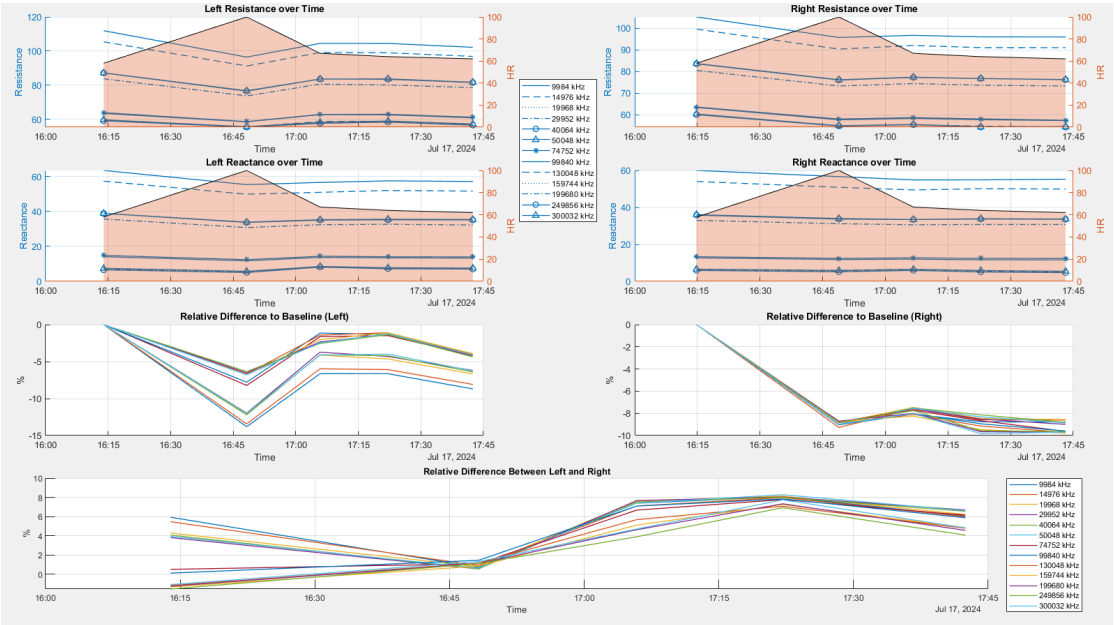


**Figure 3.28:** Male subject #001 during lower limb exercise - protocol 2

### Male Subject #002

For subject #002, baseline and follow-up measurements were taken as described in the method section. The results in 3.29 and 3.30 showed minimal differences between baseline and follow-up, suggesting that the intensive exercise performed the night before did not significantly influence the bioimpedance measurements taken the following day.

Despite this, the overall trends in resistance and reactance for subject #002 aligned with those observed for subject #001. Specifically, resistance and reactance decreased during physical activity and increased during resting phases, providing consistency in the observed patterns across subjects.

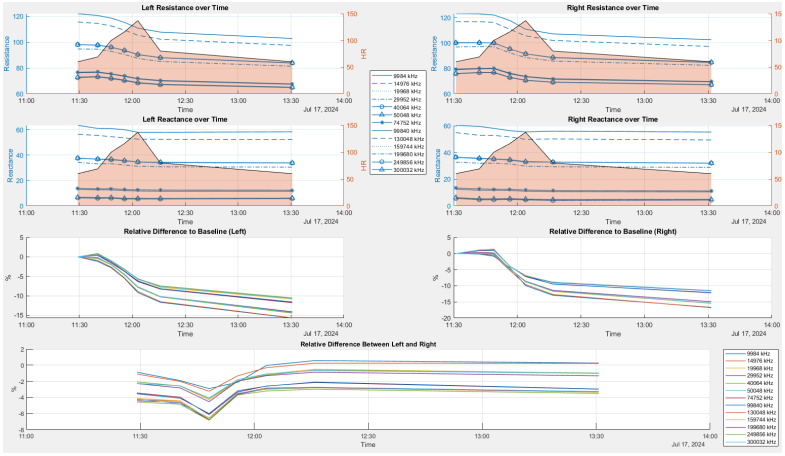


**Figure 3.29:** Male subject #002 during lower limb exercise at baseline

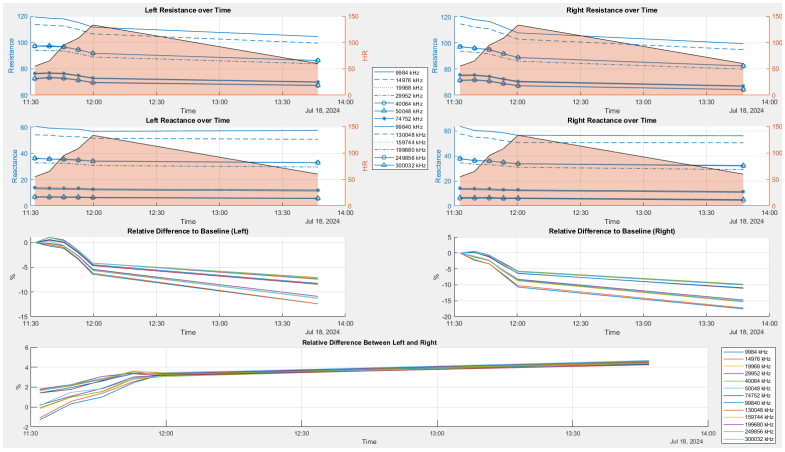


**Figure 3.30:** Male subject #002 during lower limb exercise at follow up

### 3.6.5 Dr. Adam study data collection

As part of the ongoing research, data collection has begun with the first five subjects, all of whom are healthy individuals. These subjects will contribute to establishing normative data for the study, which will later be expanded to include participants with osteoarthritis (OA) to allow for comparisons. At this stage, no comments or conclusions can be drawn as the current dataset consists solely of healthy subjects.

The results are presented in Figures 3.31 and 3.32. Each graph compares the bioimpedance measurements taken before and after exercise for the left and right legs.

**Graph Structure:** The solid lines represent the bioimpedance measurements taken before exercise, while the dashed lines show the measurements after exercise. The left leg is shown in green, and the right leg is shown in red. This format provides a clear visual representation of any changes in resistance and reactance between the two time points for each subject.

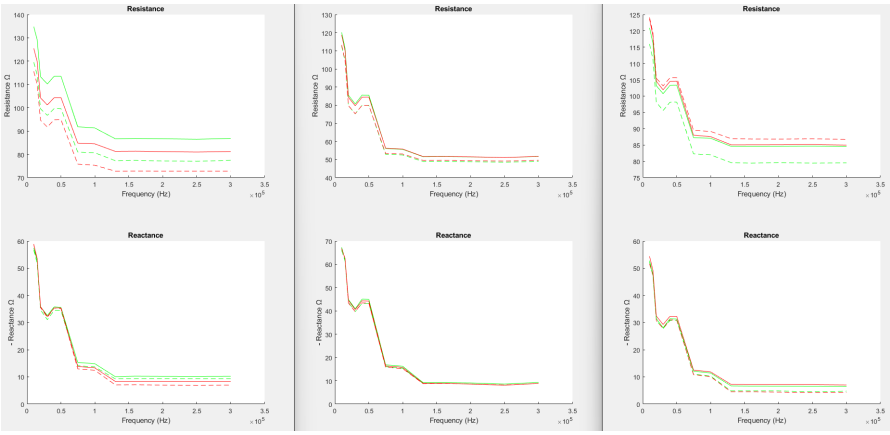


**Figure 3.31:** BioZ measurements for subject HAS0001, HAS0002 and HAS0003 before and after exercise

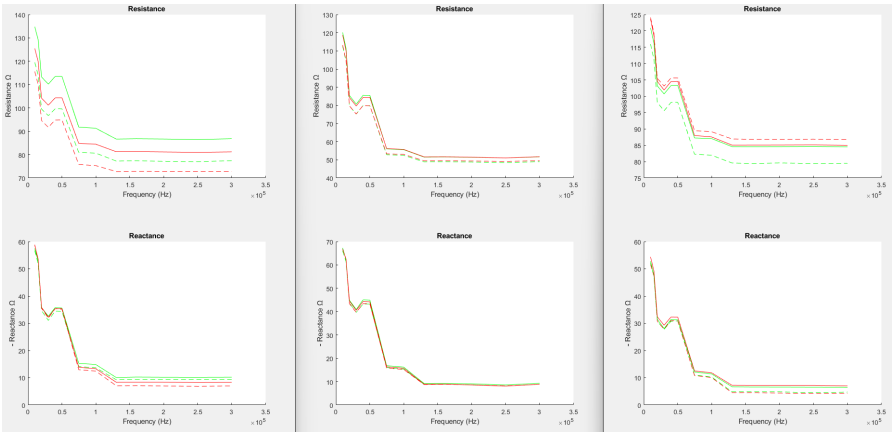


**Figure 3.32:** BioZ measurements for subjects HAS0004 and HAS0005 before and after exercise

# Chapter 4

# Development of the Knee Sleeve

## 4.1 Introduction to Knee Sleeve Development

The development of a wearable knee sleeve capable of measuring bioimpedance in real-time offers potential benefits in various applications, including healthcare, sports, and research. This introduction will discuss the limitations of the current lab-based setup, the benefits of a portable embedded solution, and the potential applications of such a device.

### 4.1.1 Limitations of the Current Lab-Based Setup

Currently, the bioimpedance measurement devices used in the lab setup are constrained by several factors that limit their use outside controlled environments.

1. **Mobility Constraints:** The current development kit requires connection to a PC and is not wearable, limiting its use to specific times and controlled environments where data can be collected.
2. **User Accessibility:** Operating the device requires specialized training, making it impractical for daily use by patients or athletes without technical support.
3. **Real-World Data Collection:** The inability to measure bioimpedance during everyday activities may result in data that does not capture typical physiological variations experienced by patients and athletes.

These constraints underscore the need for a portable, wearable solution that can overcome the limitations of lab-based setups.

### 4.1.2 Benefits of a Portable, Embedded Solution

An embedded, portable solution integrated into a knee sleeve would offer several benefits over the current setup, addressing the limitations mentioned above.

1. **Continuous Monitoring:** A wearable device embedded in the knee sleeve would allow for continuous or periodic monitoring of bioimpedance in real-world conditions, enabling the collection of more comprehensive and ecologically valid data.
2. **Early Detection and Prevention:** By continuously monitoring bioimpedance, deviations from baseline can be detected early, enabling timely interventions to prevent injuries or manage chronic conditions such as osteoarthritis.
3. **Convenience and Compliance:** A user-friendly, portable device increases the likelihood of regular use, improving patient compliance and providing more consistent data over time.

This solution could bridge the gap between controlled lab measurements and real-world data collection, enhancing the quality and scope of bioimpedance research.

### 4.1.3 Potential Applications of the Knee Sleeve

The development of a wearable bioimpedance knee sleeve has potential applications in various fields, including healthcare, sports, and research.

1. **Everyday Life Remote Monitoring:** Healthcare providers can remotely monitor patients' knee health, offering timely interventions and adjustments to treatment plans based on real-time data. Patients recovering from knee surgery can also use the device to track their progress and adjust exercises as needed.
2. **Sports and Athletics:** Athletes can use the knee sleeve to detect early signs of strain or injury, allowing for preventative measures to be taken before the injuries become severe.
3. **Research and Development:** The knee sleeve can be a valuable tool for studies and data collection in various real-world scenarios, offering new insights into physiological responses during activities.

These applications highlight the versatility of the knee sleeve as a tool for both clinical and research settings, supporting the development of personalized treatment plans and enhancing the understanding of knee health in different populations.

### 4.1.4 How the Device Works

The knee sleeve device consists of several key components, including a PCB located on the top right, a battery positioned on the top left, bioimpedance electrodes placed transversally on the plane of the knee, and two IMUs: one positioned on the thigh and the other on the shank. As shown in Figure 4.1, the concept highlights the placement of these components and illustrates the overall structure of the device.

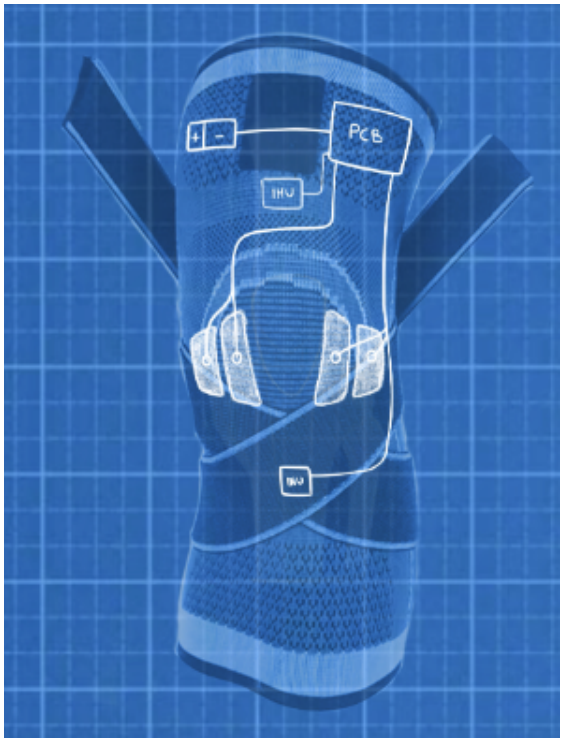


**Figure 4.1:** Concept drawing - components placement on the knee sleeve

The device operates in two distinct modes:

1. **Daily Recording Mode:** In this mode, we expect less severe changes in bioimpedance, so a measurement is taken approximately every 10 minutes. This mode is designed for continuous long-term monitoring.

2. **Activity Mode:** This mode captures more frequent measurements, taking a reading every 30 seconds. However, this mode operates for a shorter period due to its higher sampling frequency, making it ideal for capturing data during physical activity.

The bioimpedance measurements are captured when the leg is in a straight position. This is determined using data from the two IMUs, which, thanks to a

sensor fusion algorithm, can detect when both IMUs are aligned on the same plane, indicating that the leg is straight.

Communication with external devices such as a PC or smartphone is facilitated via Bluetooth. This connection allows the device to receive necessary parameters and offload data for further analysis. In the next section, we will explore the details of the PCB development process.

An important consideration in the design of the knee sleeve was ensuring that the device could be easily washed. To address this, all of the electronic components are housed in removable pockets. This allows the user to take out the electronics before washing the sleeve, ensuring that the device remains functional while maintaining hygiene and user comfort. The placement of these pockets was carefully integrated into the overall design to maintain ease of use without compromising the performance or durability of the sleeve.

### 4.1.5 Electrode Types

In the concept, we have visualized three different types of electrodes that are used or considered for future iterations of the device:

- **Snap Electrodes:** These are wet electrodes, the same as those used in our experiments and data collection. Wet electrodes are known for their superior measurement accuracy and reliability, making them ideal for comparison with the lab-based development kit. Their high fidelity in measuring bioimpedance makes them the current standard for validating the device's performance.
- **Velcro Electrodes:** Also known as stem electrodes, these electrodes are more reusable due to their washable nature. They offer a practical advantage for long-term use, as they can be easily cleaned and reapplied. While not as accurate as wet electrodes, their reusability makes them a good option for non-experimental or prolonged daily use.
- **Textile Electrodes:** These electrodes are designed for comfort and are embedded into the fabric of the knee sleeve. While they offer better comfort for the user, their measurement quality is currently less reliable than that of the wet electrodes. However, they present an exciting avenue for future development as material science and electrode technology improve, potentially providing a solution that balances comfort and accuracy.

Each of these electrodes has its own strengths and limitations, and future iterations of the knee sleeve may incorporate different types of electrodes depending on the specific use case and the required balance between comfort, accuracy, and reusability.

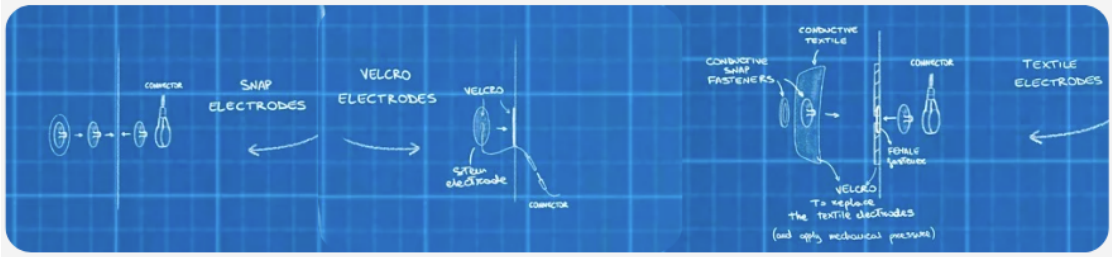


**Figure 4.2:** Concept drawings - different electrodes alternatives

## 4.2 Materials

### 4.2.1 Software Tools

The development of the knee sleeve required the use of specialized software tools for both the hardware and firmware components. The two primary software platforms used were Altium Designer for PCB development and Code Composer Studio for firmware development.

#### Altium Designer

Altium Designer was the main software used for the development of the PCB. This tool provided a comprehensive environment for creating both the schematic and the PCB layout. In the schematic phase, Altium allowed for the precise selection and connection of components, ensuring that all electrical and functional requirements were met. The PCB layout functionality of Altium enabled detailed control over component placement, trace routing, and layer design, which was crucial for the compact design of the knee sleeve. With Altium's extensive library of components and real-time design verification, the software ensured that the PCB met all technical specifications while maintaining a small form factor.

#### Code Composer Studio

For firmware development, Code Composer Studio (CCS) was the primary tool used. CCS is an integrated development environment (IDE) specifically designed for Texas Instruments (TI) microcontrollers. In this project, CCS was used to write, compile, and debug the firmware running on the TI microcontroller embedded in the knee sleeve. The IDE provided all necessary tools to manage the microcontroller's peripheral settings, implement sensor data acquisition from the IMUs and bioimpedance electrodes, and handle the Bluetooth communication with external devices. Additionally, CCS facilitated the testing and debugging of the firmware,

ensuring that the code performed reliably under various conditions and across the different operational modes of the device.

### 4.2.2 Testing and Validation Equipment

To ensure the proper functionality and accuracy of the knee sleeve device, several testing and validation tools were used throughout the development process.

#### JLink EDU Segger

For debugging and testing, the *JLink EDU Segger* was utilized, specifically configured to use cJTAG. A custom cable was assembled to connect the debugger to the board, ensuring minimal space occupation. This was a crucial aspect in maintaining the compact design of the knee sleeve while still allowing for efficient testing and debugging of the system's firmware.

#### Development Kit for Validation

A development kit was used as a reference platform to validate the bioimpedance measurements taken with our custom knee sleeve device. This kit served as a benchmark, ensuring that the bioimpedance data collected by the knee sleeve was accurate and consistent with established measurement standards. By comparing the results from our device to those obtained from the development kit, we were able to fine-tune the knee sleeve's performance and ensure reliable data acquisition in real-world scenarios.

## 4.3 PCB Development

The development of the printed circuit board (PCB) for the knee sleeve was a critical phase in the project, requiring careful consideration of both the design and component selection. The goal was to create a compact, efficient system capable of managing the bioimpedance measurements, IMU data, and Bluetooth communication while maintaining low power consumption and usability in real-world scenarios.
In Figure 4.3, the PCB block diagram for the knee sleeve is presented, illustrating how the device will function. Below is a step-by-step explanation of the workflow:

1. The user presses the Bluetooth (BT) button to enable the Bluetooth connection. This allows the device to receive settings and parameters from the PC, which are set by the user through a graphical user interface (GUI).

2. The microcontroller (uC) receives these settings and configures the registers of both the bioimpedance (BioZ) sensor and the IMU sensors accordingly.
3. The IMU begins acquiring data continuously.
4. The microcontroller saves the IMU data in the flash memory and checks the leg's position to determine whether it is straight, using data from the IMUs.
5. Once the leg is straight, the microcontroller initiates the bioimpedance data acquisition process.
6. After acquiring bioimpedance data, the uC saves it into the flash memory.
7. At the end of the activity, the user presses the BT button again to establish a connection with the PC and offload the data saved in memory for further analysis.

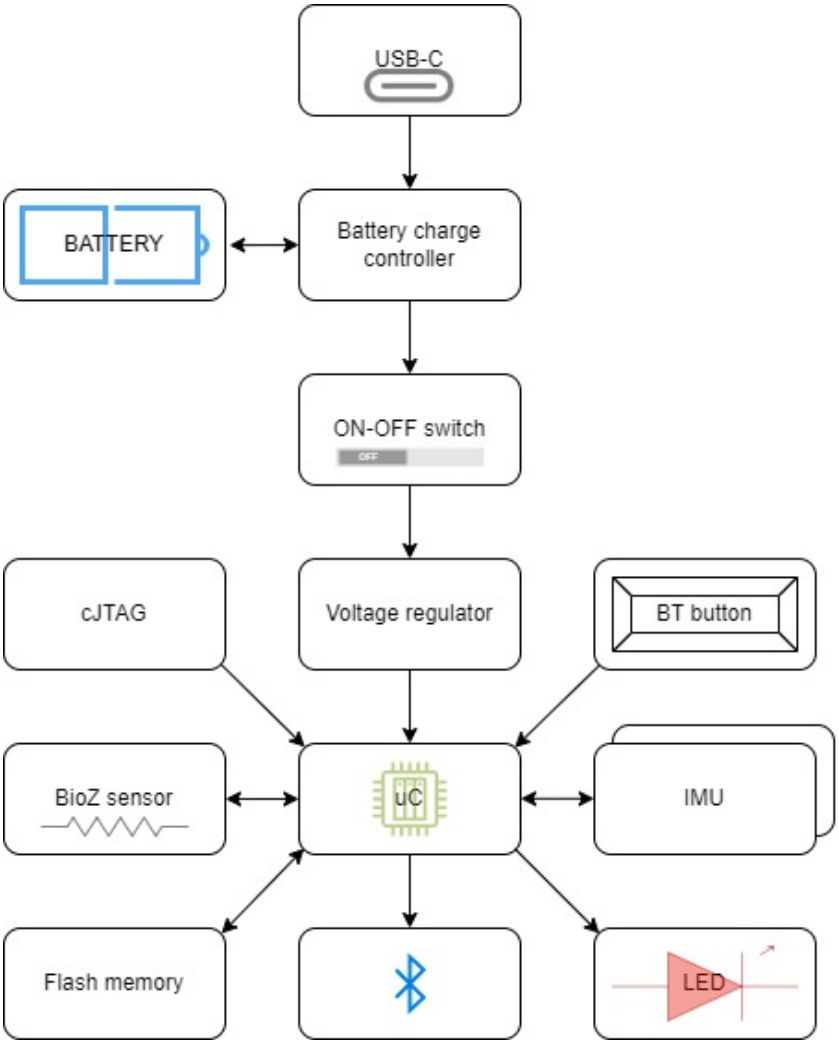


**Figure 4.3:** PCB block diagram

### 4.3.1 Component Selection

The following components were selected to meet the functional requirements of the device:

- **USB-C Connector:** Positioned on the top of the device, it is used for recharging the Li-Polymer battery.
- **Battery Charger:** Responsible for charging the Li-Polymer battery and managing the correct discharge patterns to ensure the battery's longevity and safety.
- **Li-Polymer Battery (350 mAh):** Powers the entire system, providing sufficient capacity for both daily recordings and more frequent activity monitoring sessions.
- **On/Off Switch:** Allows the system to be turned on after the battery management system (BMS), ensuring that the battery can be charged even when the system is turned off.
- **Voltage Regulator:** Provides a stable output of 3.3V, which is necessary for the operation of the microcontroller and other components.
- **cJTAG Interface:** Compact JTAG interface supported by the microcontroller, allowing for debugging and programming with fewer pins, minimizing space requirements.
- **Microcontroller:** Manages all operations, including data collection from the bioimpedance sensor (via SPI) and the IMUs (via I2C). It also stores data in the flash memory and communicates with external devices through the Bluetooth module.
- **Bioimpedance Sensor (MAX30009ENA+):** Same as the sensor used in the development board, responsible for measuring bioimpedance from the electrodes placed on the knee.
- **IMU Sensors:** Detect the orientation of the leg, particularly when it is straight, to guide the timing of bioimpedance data acquisition.
- **RGB LED:** Provides user feedback, indicating Bluetooth connection status and other states of the microcontroller.
- **Flash Memory:** Stores the data collected from the IMUs and bioimpedance sensor for later transmission and analysis.

- **Bluetooth Module:** Facilitates communication with external devices, allowing parameters to be received and data to be offloaded.
- **Button:** Activates Bluetooth to enable wireless communication when needed.

In the following subsections, we will expand on the criteria used for selecting each component and the role that each plays in the overall functionality of the knee sleeve device.

### Microcontroller CC2652

The CC2652R microcontroller, part of the SimpleLink™ MCU platform by Texas Instruments, is a versatile and powerful choice for applications requiring efficient data handling and low power consumption. It integrates a 48 MHz Arm® Cortex®-M4F processor, providing ample processing power for complex operations, such as managing data from multiple inertial measurement units (IMUs) and performing necessary computations.

The CC2652R has dual SPI interfaces, which facilitate seamless communication with bioimpedance sensors and flash memory, keeping them separate. This is crucial for applications that demand high-speed data transfer and reliable storage. Additionally, the microcontroller supports I2C communication, enabling efficient interaction with IMUs, making it suitable for sensor-rich environments.

The CC2652R excels in power efficiency, making it ideal for wearable technology. Its ultra-low-power sensor controller operates independently from the main CPU, sampling and processing sensor data with minimal energy consumption. The on-chip buck DC/DC converter is extremely handy because it can power the bioimpedance sensor and the IMU without requiring external components.

For debugging and programming, the CC2652R includes a 2-pin cJTAG interface, simplifying development and decreasing the number of necessary pins and routes. On the JTAG interface, we added a RESET signal for the microcontroller to avoid the need for a dedicated button on the PCB, thus saving valuable space. The integrated RF module supports multiple wireless protocols, including Bluetooth® 5.2 Low Energy and IEEE 802.15.4, making it suitable for a wide range of wireless applications without the need for additional components, but simply with a 2.4 GHz chip antenna and the relative conditioning circuit.

Other main characteristics of this microcontroller include a comprehensive set of peripherals, such as general-purpose timers, a 12-bit ADC, UARTs, comparators, and cryptographic accelerators, which add to its versatility and applicability in various domains. With 352 kB of in-system programmable flash and 80 kB of ultra-low leakage SRAM, the CC2652R offers sufficient memory resources for most embedded applications.

In summary, the CC2652R microcontroller is an optimal choice for applications requiring robust processing capabilities, efficient data handling, and low power consumption, particularly in wearable technologies.

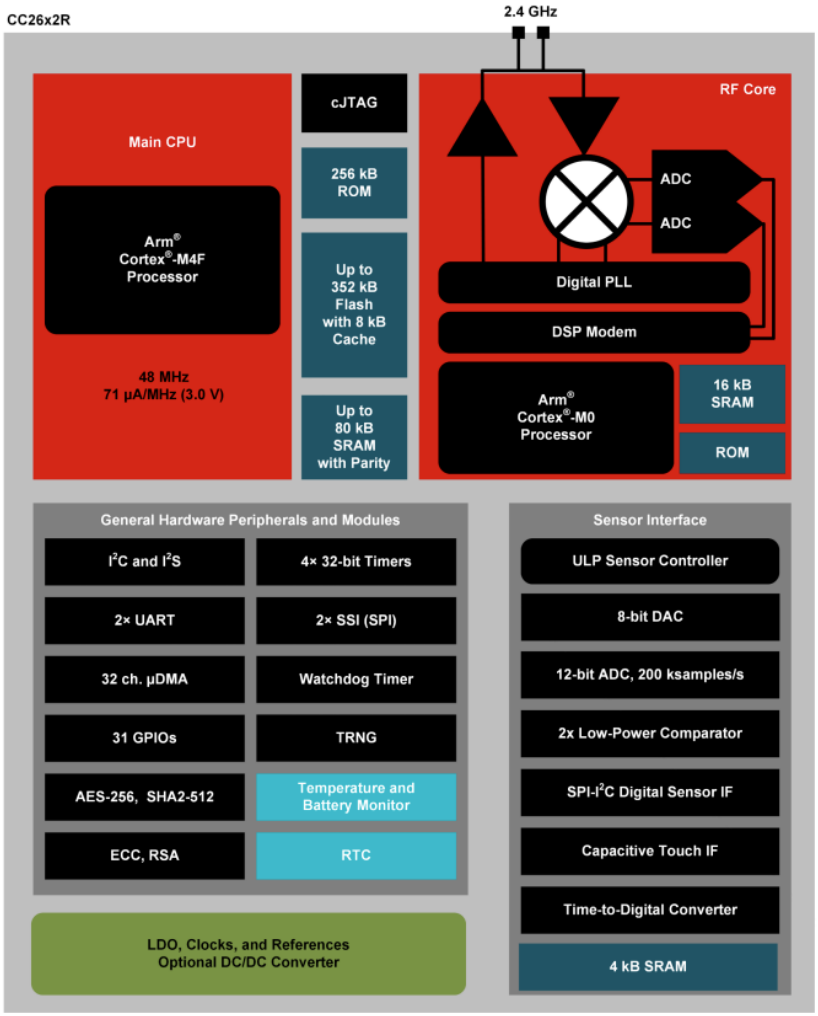


**Figure 4.4:** CC2652 block diagram

### Oscillating Crystals

The selection of oscillating crystals for the knee sleeve PCB was based on the required frequency and input impedance specified in the CC2652R microcontroller's datasheet, as shown in 4.5 and 4.6. Additionally, we took into consideration the equivalent series resistance (ESR) to ensure that it met the parameters outlined for stable oscillation.

We selected two crystals, both manufactured by Abracon:

| | PARAMETER | MIN | TYP | MAX | UNIT |
|---|---|---|---|---|---|
| | Crystal frequency | | 48 | | MHz |
| ESR | Equivalent series resistance<br>6 pF < $C_L$ ≤ 9 pF | | 20 | 60 | Ω |
| ESR | Equivalent series resistance<br>5 pF < $C_L$ ≤ 6 pF | | | 80 | Ω |
| $L_M$ | Motional inductance, relates to the load capacitance that is used for the crystal ($C_L$ in Farads)[5] | | < 3 × $10^{-25}$ / $C_L$ $^2$ | | H |
| $C_L$ | Crystal load capacitance[4] | 5 | 7[3] | 9 | pF |
| | Start-up time[2] | | 200 | | µs |

**Figure 4.5:** 48 MHz oscillator requirements

| | | MIN | TYP | MAX | UNIT |
|---|---|---|---|---|---|
| | Crystal frequency | | 32.768 | | kHz |
| ESR | Equivalent series resistance | | 30 | 100 | kΩ |
| $C_L$ | Crystal load capacitance | 6 | 7[1] | 12 | pF |

**Figure 4.6:** 32 kHz oscillator requirements

- **ABS07-32.768KHZ-7-T:** A 32.768 kHz crystal with a 7 pF load capacitance. This crystal is used for the low-frequency oscillator. To fine-tune its frequency, we used external 12 pF capacitors in parallel, calculated based on the formula from the microcontroller datasheet, as shown in Figure **??**.
- **ABM8W-48.0000MHZ-7-D1X-T3:** A 48 MHz crystal, also with a 7 pF load capacitance, which serves as the high-frequency oscillator. This crystal can be fine-tuned using the internal variable load capacitors available within the microcontroller, eliminating the need for external tuning components.

$$C_L = \frac{C_1 \times C_2}{C_1 + C_2} + C_{\text{parasitic}} \approx \frac{\text{load capacitor value}}{2} + C_{\text{parasitic}} \tag{4.1}$$

The low-frequency 32.768 kHz crystal plays a crucial role in maintaining accurate timing for the system, especially during low-power modes, while the 48 MHz crystal is essential for the microcontroller's main clock, enabling fast and efficient data processing and communication. By selecting crystals with the correct load capacitance and tuning them appropriately, we ensured that the oscillators provide stable and precise timing signals required for the system's operation.

### Flash Memory

For the storage requirements of the knee sleeve, we selected the **Winbond W25Q01JV-DTR**, which provides the ability to communicate via SPI, enabling fast and reliable data transfers between the components.

### Bioimpedance Sensor

The bioimpedance sensor used in this project is the **MAX30009ENA+**, the same as the development kit used in our data collection, which is capable of performing tetrapolar measurements, dynamic measurements, and frequency sweeps. These features allow the sensor to provide highly accurate bioimpedance readings, which are crucial for the knee sleeve's intended applications.

The MAX30009ENA+ is designed to handle a range of bioimpedance measurement scenarios, including those where dynamic data collection is required, such as during physical activity, as well as frequency sweeps that provide detailed impedance profiles. This sensor offers a high degree of flexibility in terms of measurement frequency and accuracy, making it an ideal choice for wearable applications.

With its low power consumption and high precision, the MAX30009ENA+ is particularly well-suited to the knee sleeve, where continuous monitoring is needed without significantly draining the battery. The sensor's SPI interface allows for efficient communication with the microcontroller, ensuring that data is transferred quickly and accurately for further processing and storage.

### IMU Sensors

For the knee sleeve device, the **ICM-20948** IMU sensors were chosen due to their advanced features, low power consumption, and compatibility with the I2C communication protocol. The ICM-20948 is a 9-axis MotionTracking device, combining a 3-axis gyroscope, 3-axis accelerometer, and 3-axis magnetometer in a single, compact 3 mm x 3 mm x 1 mm package.

The key reasons for choosing this sensor include:

- **Sensor Fusion:** The ICM-20948 includes an embedded Digital Motion Processor (DMP) that performs sensor fusion, offloading computational tasks from the microcontroller. This allows for efficient real-time motion tracking and orientation calculations, which are critical for determining when the leg is straight during bioimpedance measurements.
- **Power Efficiency:** With a power consumption as low as 2.5 mW, the sensor is optimized for low-power applications, making it ideal for wearable devices like the knee sleeve, where battery life is a key consideration.
- **I2C Communication:** The sensor supports communication via I2C, which simplifies integration with the microcontroller and allows for efficient data transfer between components at up to 400 kHz.

These features, combined with the device's small form factor and robust performance, make the ICM-20948 a perfect choice for the knee sleeve application, where accurate motion tracking and power efficiency are essential.

### LEDs

Two LEDs were incorporated into the knee sleeve design for communication and status indication:

- **RGB LED:** The RGB LED produced by KingBright is used to communicate various states of the device, particularly the Bluetooth connection status, as well as indicating when data is being recorded. We chose the AAA3528LSEEZGKQBKS that operates on a 3.3V supply, which aligns with the system's overall power requirements and eliminates the need for a 5V regulator. With a current consumption of only 2 mA, it provides an energy-efficient solution for user feedback.

**Figure 4.7:** RGB led

- **Red LED:** A red LED is dedicated to indicating battery charging status. It lights up when the battery is being charged and turns off when charging is complete. Like the RGB LED, the red LED (APT1608LSECK/J3-PRV) was chosen for its low current consumption, which is also 2 mA, ensuring that it does not significantly impact the system's power usage during operation.

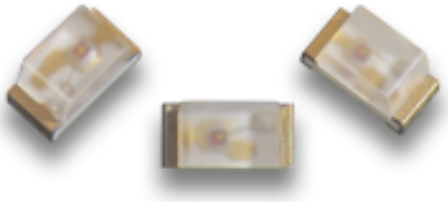

**Figure 4.8:** RED led

These LEDs provide crucial feedback to the user while maintaining minimal power consumption, contributing to the overall efficiency of the knee sleeve system.

### Connectors

Several connectors were used in the knee sleeve PCB design to ensure secure and stable connections between various components, all while minimizing space occupation:

- **5-pin Molex MICRO-LOCK PLUS 1.25:** These connectors were selected for the IMU, battery, and JTAG interfaces. Each connector features a clip for additional mechanical stability, ensuring a secure connection even with movement and potential wear. Despite their small size, these connectors offer reliable performance and mechanical durability, making them ideal for a compact, wearable device like the knee sleeve.

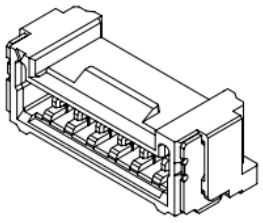

**Figure 4.9:** Molex MICRO-LOCK PLUS 1.25 connector

- **USB-C Connector:** A USB-C connector was used for charging the device's battery. This connector was chosen for its widespread compatibility, compact size, and ability to handle higher charging currents. The USB-C port allows for easy charging and contributes to the overall compact design of the knee sleeve.

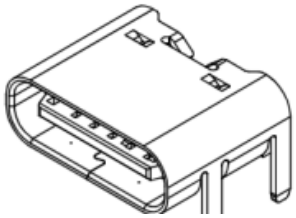

**Figure 4.10:** USB-C connector

These connectors ensure reliable connections throughout the device while maintaining the compact form factor required for a wearable system.

### Logic Level Shifters

The microcontroller (CC2652) operates at a 3.3V logic level, while some of the sensors, such as the IMUs and the MAX30009 bioimpedance sensor, operate at a lower voltage level of 1.8V. Without proper voltage translation, communication between these devices would not be possible. A direct connection between components with different logic levels could result in damage to the lower-voltage components or unreliable communication.

To address this, logic level shifters are used to convert the 3.3V signals from the microcontroller to 1.8V, and vice versa, ensuring safe and reliable communication. The I2C bus, which connects the microcontroller to the IMUs, and the SPI bus, which connects the microcontroller to the MAX30009 sensor, both require level shifting to match the voltage levels of the different components.

The inclusion of level shifters not only protects the components but also ensures that communication between the microcontroller and the sensors is stable and consistent, allowing for accurate data collection and processing.

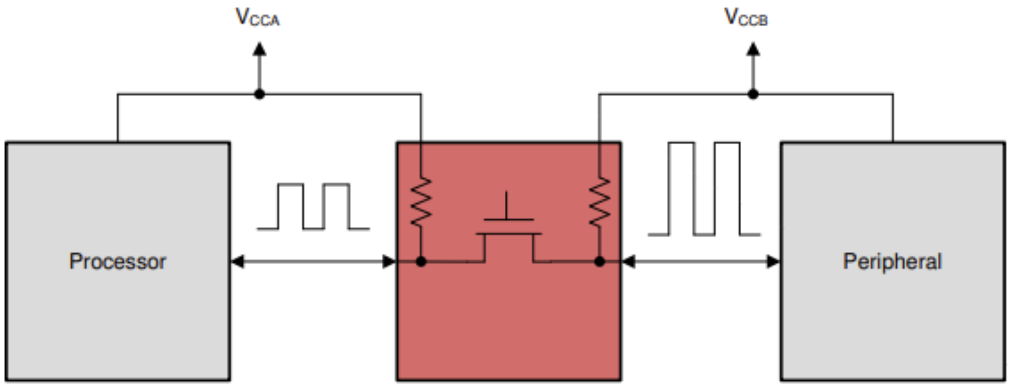


**Figure 4.11:** Block diagram of logic level shifter between the microcontroller and sensors.

The diagram in Figure 4.11 illustrates the role of the level shifters in the system, translating signals between the 3.3V microcontroller and the 1.8V sensors.

For the knee sleeve device, we utilized two types of level shifters to enable communication between the 3.3V microcontroller and 1.8V sensors.

**TXS0102 for I2C:** The **TXS0102** is a 2-bit bidirectional voltage-level translator chosen for the I2C communication with the IMUs. It supports voltage translation between 1.65V to 3.6V on the A port and 2.3V to 5.5V on the B port, making it ideal for the 1.8V IMU sensors and 3.3V microcontroller. The TXS0102 requires no direction control signal, making it simple to implement for I2C, and

supports data rates up to 2 Mbps, sufficient for standard I2C operations.

**TXB0104 for SPI:** The **TXB0104** is a 4-bit bidirectional voltage-level translator used for the SPI communication with the bioimpedance sensor (MAX30009). It supports voltage levels between 1.2V to 3.6V on the A port and 1.65V to 5.5V on the B port. With a data rate of up to 100 Mbps, it is well-suited for high-speed SPI communication. Additionally, the TXB0104 features automatic direction sensing, which is ideal for bidirectional communication on the SPI bus.

### Battery Charger

The battery charger chosen for the knee sleeve device is the **MCP73831**, a miniature single-cell, fully integrated Li-Ion/Li-Polymer charge management controller. This charger was selected because it efficiently converts the 5V USB input into a regulated 4.2V output, which is ideal for charging the Li-Polymer battery used in the device.

Key reasons for choosing the MCP73831 include:

- **Input Voltage:** The charger accepts a 5V input, making it compatible with standard USB power sources.
- **Regulated Output Voltage:** The MCP73831 provides a fixed 4.2V output, ensuring safe and reliable charging for the Li-Polymer battery.
- **Programmable Charge Current:** The charge current can be programmed using an external resistor, allowing for flexibility in controlling the charging process, with a range from 15 mA to 500 mA.
- **Small Form Factor:** The compact size of the MCP73831 allows for minimal space occupation on the PCB, an important consideration for the wearable knee sleeve.

Additionally, the MCP73831 includes reverse discharge protection and thermal regulation, further ensuring the safety and longevity of the battery during the charging process.

### Voltage Regulator

The voltage regulator chosen for the knee sleeve device is the **TPS7A02**, a nanowatt IQ low-dropout (LDO) voltage regulator that ensures a stable 3.3V output for the microcontroller. The device was selected due to its ultra-low quiescent current (25 nA) and its ability to handle up to 200 mA of output current, making it ideal for low-power applications like wearables.

Key reasons for choosing the TPS7A02 include:

- **Input and Output Range:** The regulator supports an input voltage range of 1.5V to 6.0V, while providing a stable output voltage of 3.3V, which is necessary for powering the microcontroller and other components.
- **Low Quiescent Current:** The ultra-low quiescent current (25 nA typical) significantly extends the battery life of the system, ensuring efficient operation even when the device is idle.
- **Small Form Factor:** The TPS7A02 is available in compact package options such as the X2SON (1.0 mm × 1.0 mm) and SOT-23-5, which are ideal for space-constrained designs.
- **Low Dropout Voltage:** With a maximum dropout voltage of 270 mV at 200 mA, the regulator ensures stable operation even when the input voltage is close to the output voltage.

The TPS7A02 provides excellent transient response and power efficiency, making it a reliable choice for powering the 3.3V rail of the knee sleeve system while optimizing battery usage.

### Power Estimation

To ensure that the knee sleeve operates efficiently over extended periods, we performed power consumption calculations for each of the system's components and estimated the necessary battery capacity based on average current draw during typical operation.

**Microcontroller (CC2652R):** The microcontroller operates with a peak current of 9.1 mA during Bluetooth transmission. However, since Bluetooth transmission occurs only for about 20 seconds per hour to transfer data (as estimated by 10 ms per KB of data for a total of 1 MB), its average current consumption is approximately 2.87 mA during operation. The breakdown is as follows:

$$I_{\text{microcontroller}} = 1.45\,\text{mA} + (31\,\mu\text{A} \times 24\,\text{MHz}) = 2.194\,\text{mA}$$

With the addition of peripheral currents that account for 670 uA, the total average current is 2.87 mA.

**MAX30009 Bioimpedance Sensor:** The bioimpedance sensor operates at an average current of 0.616 mA, assuming it takes one minute for a frequency sweep or dynamic measurement and operates for half of the device's active time.

$$@50\,\text{kHz} - 1.222\,\text{mA} \quad | \quad \text{idle} = \text{few}\,\mu\text{A}$$

So on average:

$$I_{\text{avg}} = \frac{(5 \times 0.01) + (5 \times 1.222)}{10} = 0.616\,\text{mA}$$

**LEDs:** The RGB LED, used to indicate Bluetooth and measurement states, operates with an average current of 1 mA, based on being active for half of the device's operational time, and consuming 2 mA during operation and with a negligible leakage current when not in use.

**IMU (ICM20948):** The IMU runs continuously during data collection and has a current consumption of 7.8 mA.

**Flash Memory:** Flash memory has a low standby current of 80 µA and consumes up to 30 mA during read/write operations. However, since data is only written briefly during the collection of IMU data (at 200 Hz), the time spent writing to memory is minimal. Based on the following calculations the time spent writing per hour is around 10 seconds, resulting in a negligible impact on average current.

**Write Speed Calculation**

- **Page Size:** 256 bytes
- **Number of Pages to Write 3 MB:**

$$\frac{3\,\text{MB}}{256\,\text{bytes}} = \frac{3 \times 1024 \times 1024\,\text{bytes}}{256\,\text{bytes}} = 12288\,\text{pages}$$

- **Total Write Time:**

$$12288\,\text{pages} \times 0.5\,\text{ms/page} = 6144\,\text{ms} = 6.144\,\text{seconds}$$

**Read Speed Calculation**

- **SPI Clock Frequency:** 4 MHz
- **Data Transfer Rate:**

$$\text{Data Transfer Rate} = \text{Clock Frequency} \times \text{Data Width} = 4\,\text{Mbps}$$

- **Data Transfer Rate in Bytes:**

$$4\,\text{Mbps} = 4 \times 10^6\,\text{bits per sec} = \frac{4 \times 10^6}{8}\,\text{B per sec} = 500{,}000\,\text{B per sec}$$

- **Total Read Time:**

$$\frac{3\,\text{MB}}{500{,}000\,\text{B per sec}} = \frac{3 \times 1024 \times 1024\,\text{bytes}}{500{,}000\,\text{B per sec}} \approx 6.29\,\text{seconds}$$

At a data acquisition rate of 100 Hz from the IMU (with bioimpedance data being negligible in comparison), each reading consists of 6 bytes (3 axes each for the accelerometer and gyroscope). Over the course of one second, this results in:

$$100\,\text{readings/second} \times 6\,\text{bytes/reading} = 0.6\,\text{kB/second}$$

Over the span of one hour (3600 seconds), the total data generated would be:

$$0.6\,\text{kB/second} \times 3600\,\text{seconds} = 4.32\,\text{MB}$$

Based on the write and read speed calculations (as shown in the previous section), writing or reading this data to/from memory would take at most 10 seconds per hour, ensuring efficient data management. Thus the average current consumption is:

$$\frac{(30 \times 10 + 0.08 \times 3590)}{3600} = 0.1631$$

**Battery Size Calculation:** The battery capacity required to support the system was calculated using the formula:

$$\text{Battery capacity} = \frac{\text{total time}}{\text{average current}}$$

From 4.12, the total current consumption is estimated at 12.478 mA on average, and with a 350 mAh battery, the operational time is over 20 hours, so more than enough for ou

All components in the power section, including the switch, were selected to ensure they can handle the maximum current of each component, with the average current used to estimate the necessary battery capacity.

| | Component | MAX current (mA) | | | Average current (mA/h) | |
|---|---|---|---|---|---|---|
| 1 | Microcontroller | 9.1 | | | 2.87 | |
| 1 | BioZ sensor | 2.7 | | | 0.616 | |
| 1 | Voltage regulator | 0.0000025 | | | 0 | |
| 1 | Battery charger | 0.05 | | | 0 | |
| 1 | RGB led | 6 | | | 1 | |
| 1 | SPI level shifter | 0.0144 | | | 0.0144 | |
| 1 | I2C level shifter | 0.01 | | | 0.01 | |
| 2 | IMU 9 DoF | 7.8 | | | 7.8 | |
| 1 | Flash memory | 35 | | | 0.163 | |
| | | | | | | |
| | TOTAL | 60.6744025 | mA | | 12.4734 | mA/h |

**Figure 4.12:** Power estimation summary table

### Memory Estimation

To estimate the required memory capacity for the system, the data rate of each component was analyzed. The BioZ sensor will get a frequency sweep every other second generating data at a rate of **6 byte per second**. This is an overestimation of the actual data because probably the patient will not have the leg extended every other second. For the IMU we considered a 100 Hz sampling rate, sufficient to detect when the patient is standing with the leg straight, and to collect data for gait analysis. To calculate the average amount of data the following considerations are made:

1. **IMU Data:** The ICM-20948 generates 16-bit (2 bytes) data for each axis of the gyroscope, accelerometer, and magnetometer:
   - Gyroscope: 3 axes $\times$ 2 bytes = 6 bytes
   - Accelerometer: 3 axes $\times$ 2 bytes = 6 bytes
   - Magnetometer: 3 axes $\times$ 2 bytes = 6 bytes

   **Total:** $6 + 6 + 6 = 18$ bytes per sample.
2. **Total Data Rate:** Multiply the data per sample by the sampling rate:

   $$\text{Data Rate} = 18\,\text{bytes/sample} \times 100\,\text{samples/second} = 1800\,\text{bytes/second}.$$

   Converting to kilobytes:

   $$1800\,\text{bytes/second} = 1.8\,\text{kB/second}.$$

So the average data generated by the ICM-20948 is **1.8 kB/s** and the total combined data rate of the system is therefore **1.8 kB/s**, considering the bioimpedance data rate negligible.

To calculate how long a system with a data rate of **1.8 kB/s** can run on a **1 Gb** memory (Gigabit), the following steps are performed:

1. **Convert Memory Size:** A memory size of 1 Gigabit is converted to bytes:

   $$1\,\text{Gb} = \frac{1{,}000{,}000{,}000}{8} = 125{,}000{,}000\,\text{B}.$$

2. **Calculate Duration:** The total duration in seconds is calculated by dividing the memory size by the data rate:

   $$\text{Time (in seconds)} = \frac{\text{Memory Size}}{\text{Data Rate}} = \frac{125{,}000{,}000}{1{,}800} \approx 69{,}444\,\text{seconds}.$$

3. **Convert to Hours:** To convert the duration into hours:

$$\text{Time (in hours)} = \frac{\text{Time (in seconds)}}{3600} = \frac{69{,}444}{3600} \approx 19.3\,\text{hours}.$$

**Conclusion:** A system with a data rate of **1.8 kB/s** can store data for approximately **19.3 hours** on a **1 Gb** memory. This estimation demonstrates that the system is well-suited for long-term monitoring applications without exceeding memory limits.

### 4.3.2 Schematic Design

In this section we will go through the description of the schematic design for the PCB.

#### Microcontroller

The CC2652R1 microcontroller is central to the PCB design, managing data acquisition, communication, and power management. The pin assignments and peripheral connections are as follows:

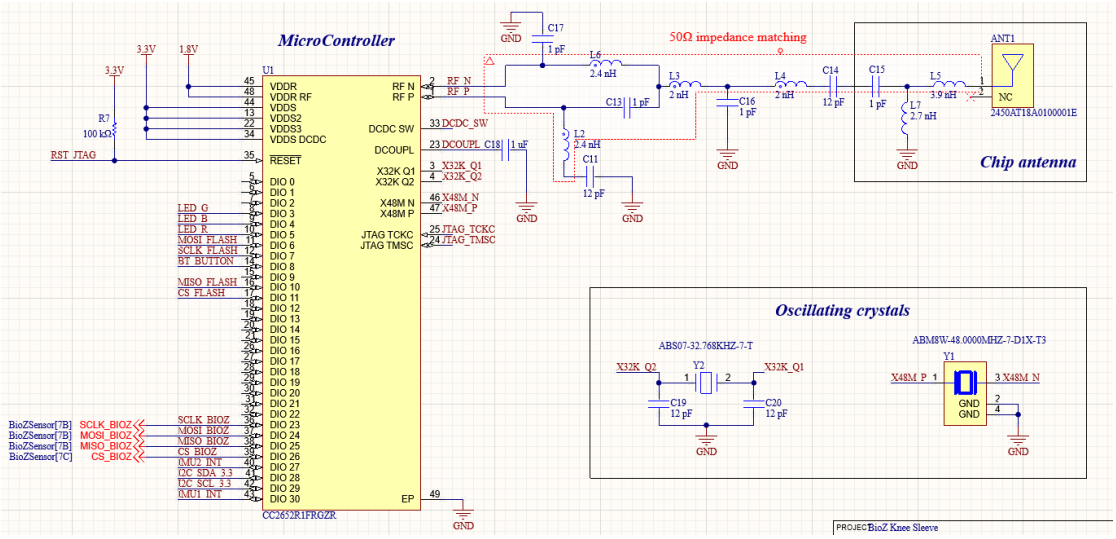


**Figure 4.13:** Microcontoller schematic focus

- **Oscillator Crystals:** The X32K and X48M oscillators are connected to the microcontroller with proper decoupling capacitors to ensure stable operation. The 32 kHz crystal uses external capacitors for load regulation, while the 48 MHz crystal is internally regulated by the microcontroller.

- **RF and Antenna:** The RF signals (RF_N, RF_P) are routed to the antenna through an impedance matching circuit, according to the microcontroller's RF design guidelines. The chip antenna also has his own impedance matching circuit, according to its datasheet.
- **SPI Connections:** Two separate SPI buses are used to interface with the flash memory and the bioimpedance sensor (MAX30009). MISO, MOSI, SCLK, and CS lines for both devices are separated to avoid timing conflicts.
- **RESET signal:** The reset signal is pulled up with a 100 kOhm resistance and can be pulled down by the JTAG.
- **Power Management:** The CC2652R1 is powered by a 3.3V source, and the internal DC-DC converter generates a 1.8V output (DCDC_SW) for powering the VDDR net, supplying the peripherals.

### Decoupling networks

The decoupling capacitors, ferrite bead, and inductors were chosen according to the recommendations in the microcontroller and component datasheets, ensuring proper filtering, noise suppression, and stable power delivery throughout the system.

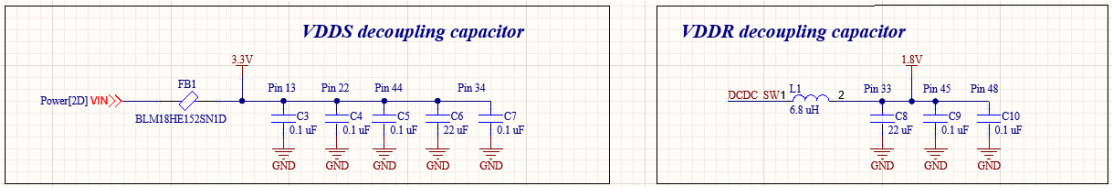


**Figure 4.14:** Decoupling networks

**LED Connections**

The RGB LED is controlled by three GPIO pins (LED_R, LED_G, LED_B) to signal different states like Bluetooth connection or recording activity.

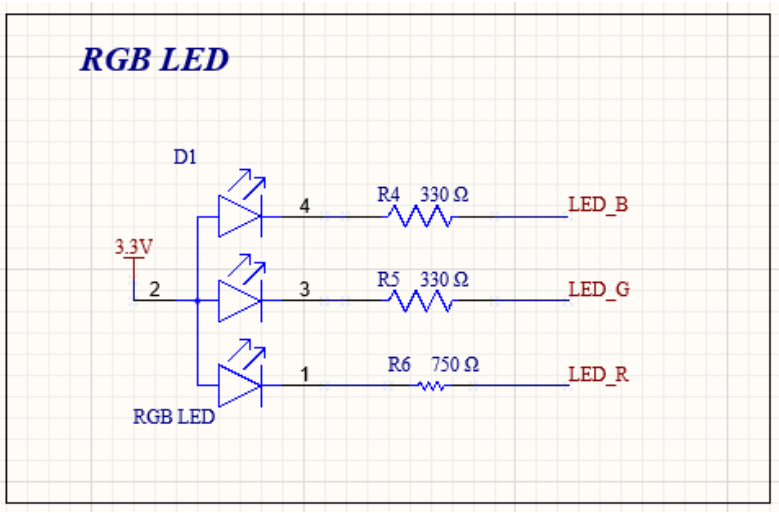


**Figure 4.15:** RGB LED

Using Ohm's Law:

$$R = \frac{V_{cc} - V_f}{I_f}$$

Having $V_{cc} = 3.3\,\text{V}$:

1. **Red LED Resistor Calculation:**

$$R_{\text{red}} = \frac{3.3\,\text{V} - 1.8\,\text{V}}{0.002\,\text{A}} = \frac{1.5\,\text{V}}{0.002\,\text{A}} = 750\,\Omega$$

2. **Green LED Resistor Calculation:**

$$R_{\text{green}} = \frac{3.3\,\text{V} - 2.65\,\text{V}}{0.002\,\text{A}} = \frac{0.65\,\text{V}}{0.002\,\text{A}} = 325\,\Omega$$

3. **Blue LED Resistor Calculation:**

$$R_{\text{blue}} = \frac{3.3\,\text{V} - 2.65\,\text{V}}{0.002\,\text{A}} = \frac{0.65\,\text{V}}{0.002\,\text{A}} = 325\,\Omega$$

**Choosing Standard Resistor Values:** Standard resistor values close to the calculated ones are:

- **Red LED:** 750 Ω (or the closest standard value, 680 Ω or 820 Ω, if 750 Ω is not available)
- **Green LED:** 330 Ω (nearest standard value)
- **Blue LED:** 330 Ω (nearest standard value)

**BT button**

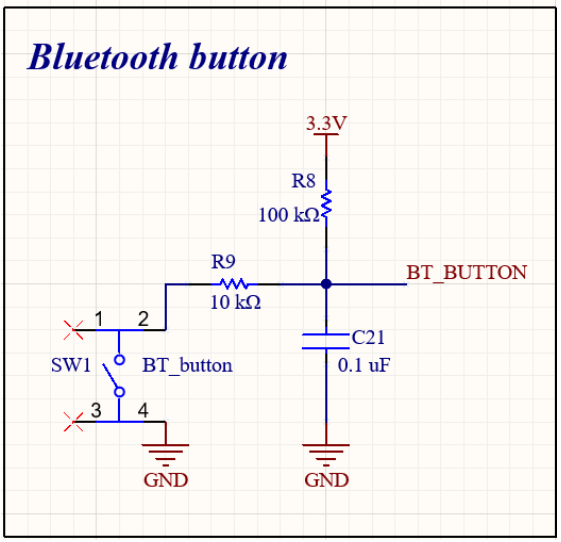


**Figure 4.16:** Debouncing button network

The Bluetooth button uses a debouncing circuit with a 10 kΩ resistor in series with a 0.1 µF capacitor, providing a time constant ($\tau$) of 1 ms to ensure stable signal input.

### FLASH memory

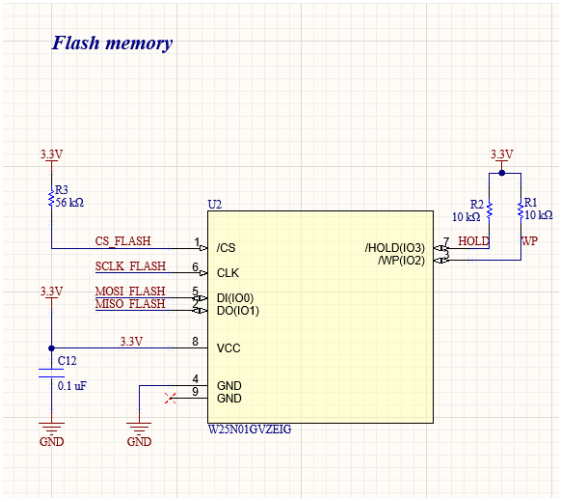


**Figure 4.17:** Flash memory circuit

The flash memory has a pull-up resistor on the Chip Select (CS) line to avoid glitches during power-up and eliminate the need to use the output enable (OE) on the level shifter. A 56 kΩ resistor is chosen for the pull-up to ensure that the level shifter can still pull the line down properly, as recommended for values greater than 50 kΩ.

Both the HOLD and WRITE PROTECT pins are pulled up since they are not used, as the SPI bus is dedicated and not shared with other peripherals. Additionally, a 0.1 µF decoupling capacitor is placed according to the datasheet specifications. The SPI connections to the microcontroller follow standard communication lines (MISO, MOSI, SCLK, CS) for data transfer.

### JTAG Interface

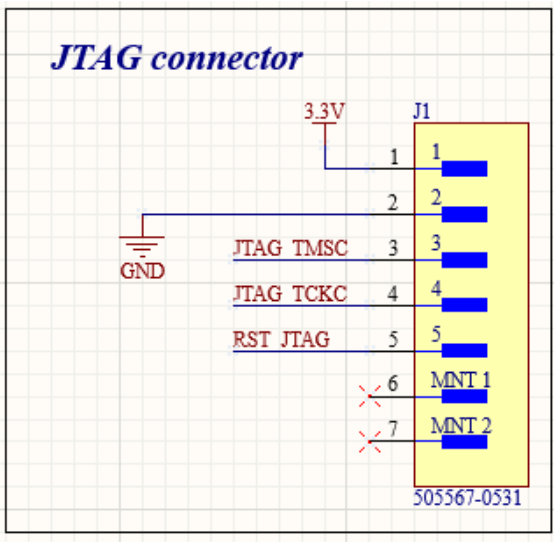


**Figure 4.18:** JTAG connector

A 2-pin cJTAG is connected for debugging, with the RESET pin pulled high via resistor R3 and can be pulled down for reset via the JTAG.

### I2C Connections

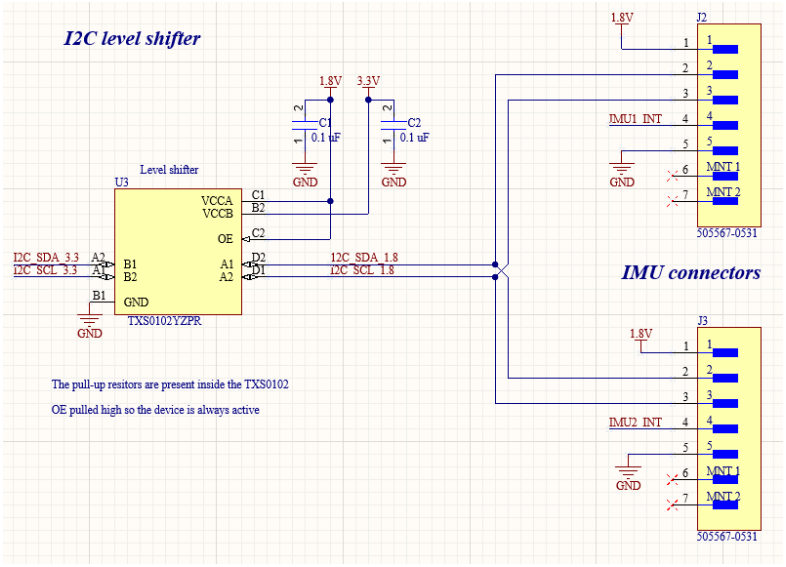


**Figure 4.19:** I2C network

The I2C bus is used to communicate with the IMU sensors. The I2C lines (SCL, SDA) are connected via a level shifter to accommodate the 1.8V IMUs. Decoupling capacitor are placed to stabilize the VCCA and VCCB power lines. The pull-up resistor are not placed because they are already present inside the level shifter as shown in 4.20. The OE pin is pulled up to reduce the footprint needed for a control signal, because in our application the level shifter will be always active.

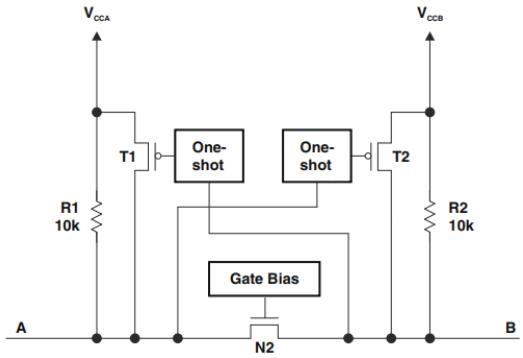


**Figure 4.20:** Level shifter internal structure

### BioZSensor

The bioimpedance sensor is connected to the electrodes as follows:

- **Electrode Connections:** EL1 and EL4 are used to input the sine-wave current into the knee, while EL2B and EL3B detect the resulting voltage. To minimize noise interference, EL2A and EL3A are connected to guard traces to shield the B traces from noise and improve signal integrity.
- **Capacitors:** A 47 nF capacitor is connected between DRVSJ and DRVXC to AC-couple the VDRV and IDRV amplifiers, as required for sine-wave current-drive applications.
- **Electrode Connections:** To minimize measurement error, the electrode cables will be soldered directly onto the PCB pads rather than using connectors, which can introduce unwanted variations in the signal.
- **Calibration Pins:** The CAL pins are not used since the internal resistances provided by the bioimpedance sensor are sufficient for our application.

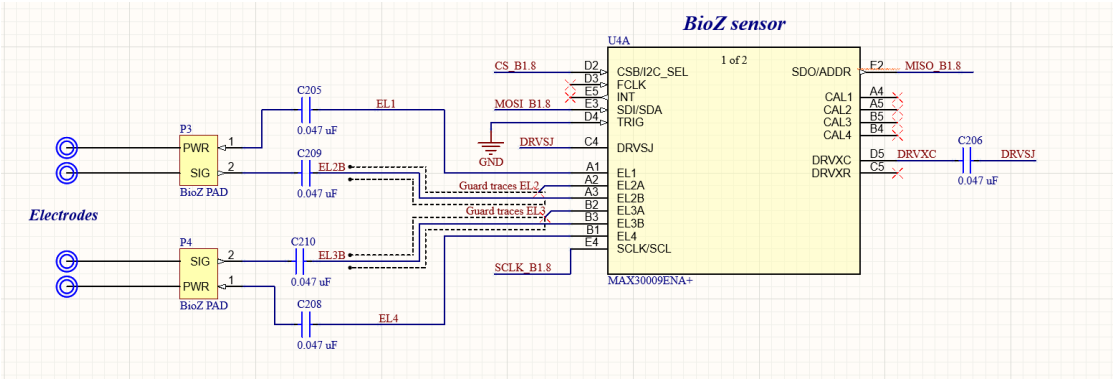


**Figure 4.21:** MAX30009ENA+ circuit

### SPI level shifter

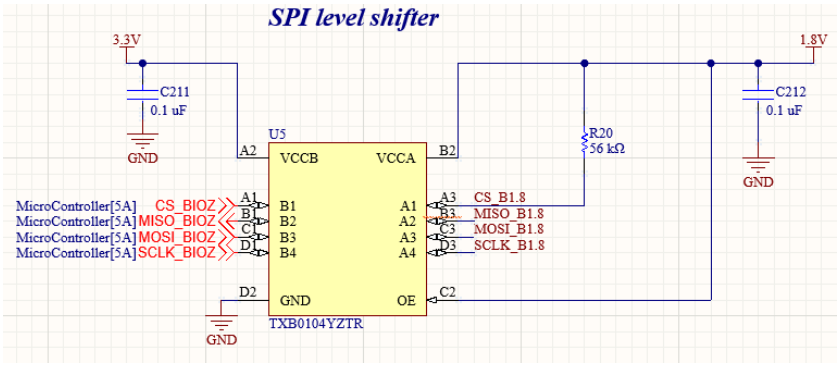


**Figure 4.22:** SPI level shifter

The SPI level shifter is configured with VCCA set to 1.8V for the bioimpedance sensor and VCCB set to 3.3V for the microcontroller. No termination resistors are required on the SPI lines, as the operating frequency is only 6 MHz, and the traces are kept short to minimize signal integrity issues. There are no resistor on termination because the SPI will work at only 6 MHz max and traces are short enough to not have undesired reflections. The CS lines of both the Flash memory and the MAX30009 are kept high by a pull-up resistor to avoid glitches during startup that could lead to random values to be written into registers.

**Power section of BioZSensor**

The power lines are decoupled as advised in the datasheet.

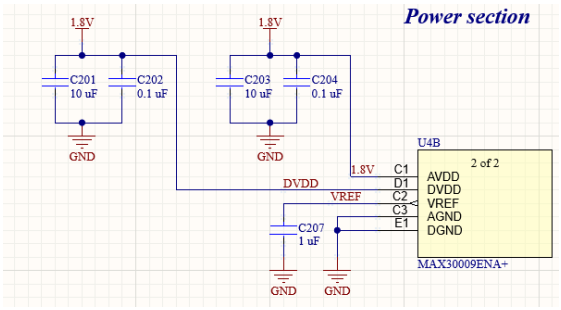


**Figure 4.23:** Power section

## Power

Discussion on the power design and power components.

### USB-C connector

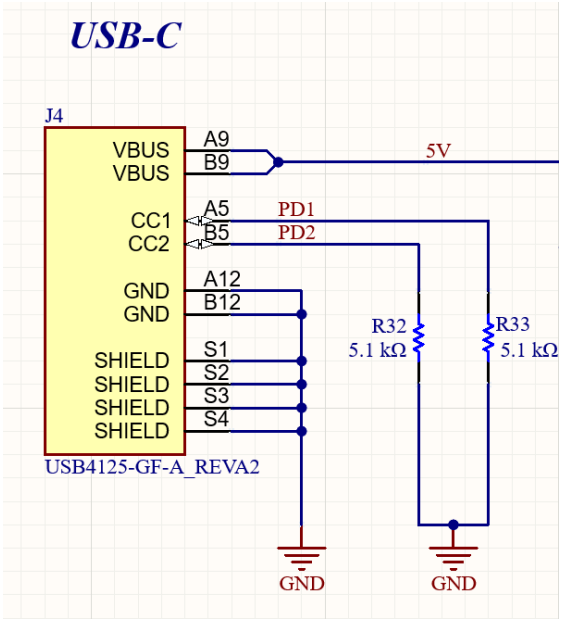


**Figure 4.24:** USB connector

The USB-C connector uses only 6 pins dedicated to power delivery. The CC1 and CC2 pins are pulled down with 5.1 kΩ resistors, in accordance with the USB-C protocol, allowing the power source to recognize the device as a current sink.

### Battery charger

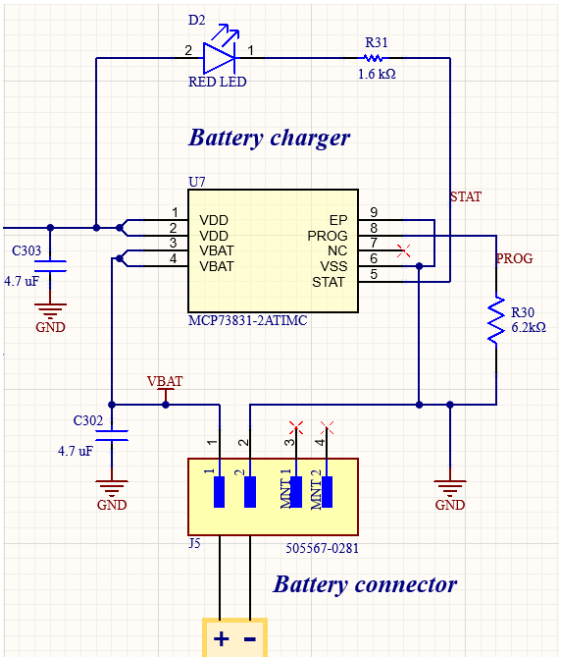


**Figure 4.25:** Battery charger

The battery charger receives 5V on the VDD pin and outputs 4.2V on the VBAT pin to charge the battery at a rate of 0.5C, which corresponds to 175 mA for the 350 mAh battery. The charging current is determined by a 6.2 kΩ resistor, using the formula:

$$I_{\text{charge}} = \frac{V_{\text{PROG}}}{R_{\text{PROG}}} \times 1000$$

where $V_{\text{PROG}}$ is typically 1V. Rearranging to solve for $R_{\text{PROG}}$:

$$R_{\text{PROG}} = \frac{1V}{I_{\text{charge}}} \times 1000$$

For a charge current of 175 mA:

$$R_{\text{PROG}} = \frac{1V}{0.175A} \times 1000 = 5714\,\Omega$$

Since the closest standard resistor value is 6.2 kΩ, the charging current becomes:

$$I_{\text{charge}} = \frac{1V}{6200\,\Omega} \times 1000 \approx 161.29\,\text{mA}$$

This current is safely below the 175 mA threshold.

Additionally, the red LED, which indicates charging, is pulled down by the PROG pin during charging and uses a 1.6 kΩ resistor. The value is calculated as follows:

$$R = \frac{V_{\text{dd}} - V_f}{I_f} = \frac{5V - 1.8V}{0.002A} = \frac{3.2V}{0.002A} = 1600\,\Omega$$

Thus, a 1.6 kΩ resistor is used for the battery LED.

**Voltage regulator**

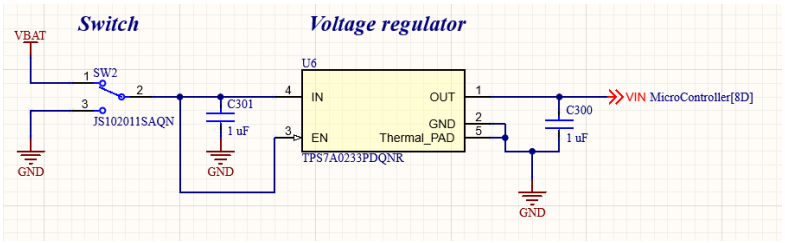


**Figure 4.26:** Switch and voltage regulator

The JS102011SAQN is a mechanical on/off switch rated to handle up to 300 mA at 6 VDC. This switch controls the power supply from the battery (VBAT) to the voltage regulator.

The TPS7A0233PDQNR voltage regulator is used to step down the VBAT to a fixed output of 3.3V, supplying power to the microcontroller and other components. A 1 µF decoupling capacitor is placed at the input of the regulator to ensure stable operation and filter any noise.

---

**IMU**

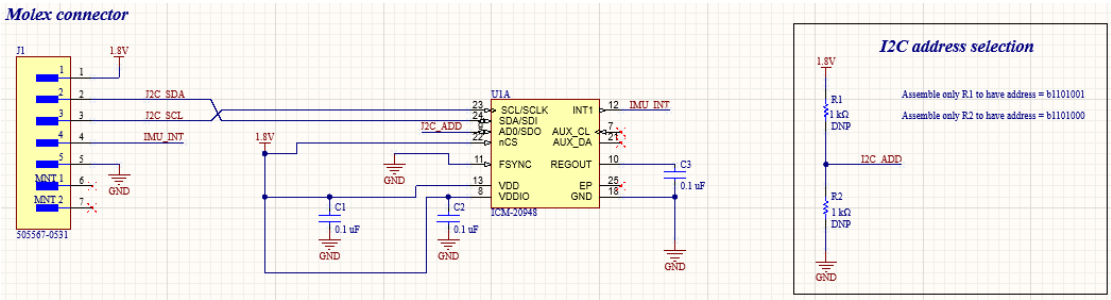


**Figure 4.27:** IMU schematic

The IMU (Inertial Measurement Unit) in our design is connected through a Molex connector that supplies power (1.8V) and ground. The connector also carries the two $I^2C$ signals at 1.8V and receives the interrupt from the INT1 pin of the IMU.

To ensure stable power supply and minimize noise, a 0.1 µF decoupling capacitor was placed close to the IMU, as recommended in the datasheet.

We are not using the AUX interface since the ICM20948 IMU is not operating as a master in $I^2C$ communication.

The $I^2C$ address of the IMU can be configured as either 'b1101001' if AD0 is pulled high or 'b1101000' if AD0 is pulled low. To allow flexibility in selecting the address, two resistors were included for hand soldering, making it possible to choose the address dynamically. We opted for 1206 package components for these resistors to facilitate manual soldering.

This design ensures compatibility with our power requirements, signal levels, and communication protocol while providing flexibility in $I^2C$ addressing.

### 4.3.3 PCB Layout

The printed circuit board (PCB) is a fundamental component of the BioZKneeSleeve, serving as the platform that interconnects all the electronic components of the device. Given the wearable nature of the project, the PCB design required careful attention to both size constraints and performance.

For the design and manufacturing of the BioZKneeSleeve PCB, we selected JLCPCB as our manufacturer. JLCPCB is well-known for offering high-quality and cost-effective PCB fabrication services, making it an ideal choice for our project.

Before starting any design work, we thoroughly reviewed JLCPCB's design guidelines and proceeded to set all the necessary design rules within our CAD software. These rules included specifications for trace width, spacing, via sizes, minimum drill diameters, and other critical design parameters.

Throughout the design process, we ensured that all design choices adhered to these rules, ensuring compatibility with JLCPCB's fabrication capabilities. Upon finalizing the PCB layout, a comprehensive design rule check (DRC) was performed, confirming that all the design rules were respected.

By adhering to the manufacturer's guidelines from the outset, we ensured a smooth and efficient transition from design to fabrication, minimizing potential issues during production.

#### BioZKneeSleeve PCB Layout

The design of the PCB was driven by the goal of minimizing its size, as the device is intended to be wearable. Therefore, the final dimensions of the main PCB were kept as compact as possible, measuring 28.975 mm x 42.075 mm. This small form

factor ensures that the device can be comfortably worn while maintaining all the necessary functionality.

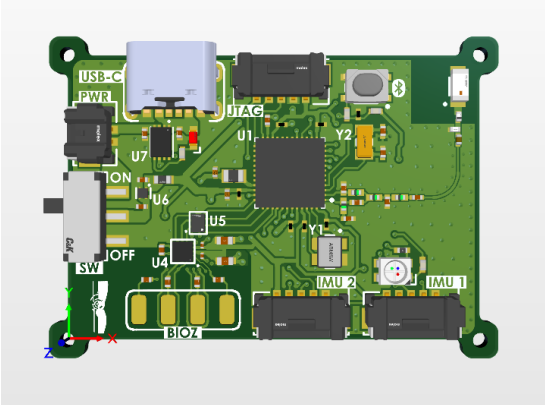


**Figure 4.28:** BioZKneeSleevePCB top view

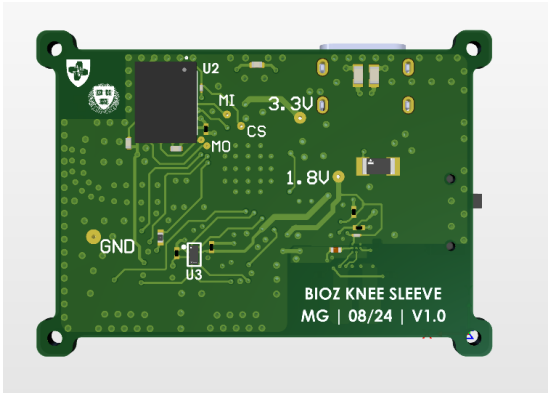


**Figure 4.29:** BioZKneeSleevePCB bottom view

For the layer configuration, we chose a 4-layer stackup with a signal-gnd-gnd-signal configuration. In this layout, the power traces share the same layer as the signal traces, which allowed us to optimize space while maintaining power integrity. The use of double ground layers provided signal stability, especially for the critical signals on the bottom layer, such as the SPI lines.

This stackup and layer configuration helped us achieve both the necessary electrical performance and the size constraints required for a wearable device.

For further details on the layout of each layer, the Gerber files are provided in the appendix, where the full design of each layer can be examined.

### General Design Choices

The PCB layout for the BioZKneeSleeve was carefully designed to ensure proper signal integrity and controlled impedance, especially for the RF section. The stackup we selected was critical in achieving this, as we needed a 50-ohm controlled impedance for the RF traces, which was a key requirement of the microcontroller specifications.

For the thickness of the layers, we followed the guidelines from the microcontroller datasheet, specifically for the RF section, as shown in the image below (Fig. 4.30). These recommendations helped us to maintain optimal RF performance and minimize signal loss across the traces.

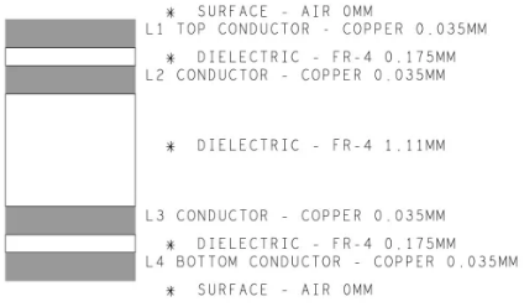


**Figure 4.30:** Microcontroller RF section guidelines.

Based on the availability of the manufacturer, we selected the following PCB stackup (Fig. 4.31). This stackup was chosen to ensure a controlled impedance of 50 ohms, which was necessary for the RF lines. The stackup consisted of a copper layer thickness of 0.035mm for the top and bottom layers, with dielectric materials and copper thickness for the inner layers, as specified in the image.

| Name | Material | Type | Weight | Thickness | Dk | Df |
|---|---|---|---|---|---|---|
| Top Overlay | | Overlay | | | | |
| Top Solder | SM-001 | Solder Mask | | 0.03048mm | 3.8 | 0.03 |
| Top Surface Fini... | PbSn | Surface Finish | | 0.02mm | | |
| L1 (signal) | CF-004 | Signal | 1oz | 0.035mm | | |
| Dielectric 2 | PP-006 | Prepreg | | 0.084mm | 3.91 | 0.02 |
| Dielectric 1 | PP-017 | Prepreg | | 0.0764mm | 3.91 | 0.02 |
| L2 (GND) | CF-004 | Signal | 1/2oz | 0.0152mm | | |
| Dielectric 3 | Core-039 | Core | | 1.065mm | 4.6 | 0.02 |
| L3 (GND) | CF-004 | Signal | 1/2oz | 0.0152mm | | |
| Dielectric 5 | PP-017 | Prepreg | | 0.0764mm | 3.91 | 0.02 |
| Dielectric 4 | PP-006 | Prepreg | | 0.084mm | 3.91 | 0.02 |
| L4 (signal) | CF-004 | Signal | 1oz | 0.035mm | | |
| Bottom Surface... | PbSn | Surface Finish | | 0.02mm | | |
| Bottom Solder | SM-001 | Solder Mask | | 0.03048mm | 3.8 | 0.03 |
| Bottom Overlay | | Overlay | | | | |

**Figure 4.31:** PCB stackup chosen based on manufacturer availability.

This stackup allowed us to achieve the necessary electrical performance while balancing the mechanical requirements of the board.

A key factor was the variation in trace widths across different sections of the board. The power lines, for example, have a width of 0.7 mm to handle the necessary current, while the more critical and space-constrained sections, such as the BioZ sensor, use much narrower lines, down to 0.1 mm. This ensures proper signal integrity and power distribution across the PCB.

### Component Placement

The component placement strategy focused on addressing the most critical components first to ensure optimal functionality and signal integrity. Here are the key placement decisions:

**Microcontroller Placement** The microcontroller (uC) was placed at the center of the PCB for several important reasons. This central location allows for symmetric routing of signals and ensures that critical traces such as RF and SPI lines can be routed effectively to minimize trace length and signal degradation. Placing the uC centrally also allows for easier access to other components, like decoupling capacitors, oscillators, and peripherals.

**Decoupling Capacitors and DDR Network** The decoupling capacitors for the uC were positioned as close as possible to their respective pins to minimize noise and maintain stable voltage levels. Proper decoupling is critical for reducing power supply noise and maintaining signal integrity.

Additionally, the DDR network includes the inductor L1, which was placed as close as possible to the related uC pin (Fig. 4.32).

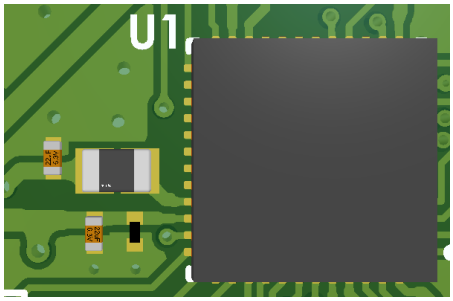


**Figure 4.32:** DDR network with inductor L1 close to the uC.

**Oscillator Placement** Both the high-frequency 48 MHz oscillator and the 32 kHz oscillator were placed very close to the uC to ensure accurate timing and reduce the risk of signal distortion due to long traces (Fig. 4.33).

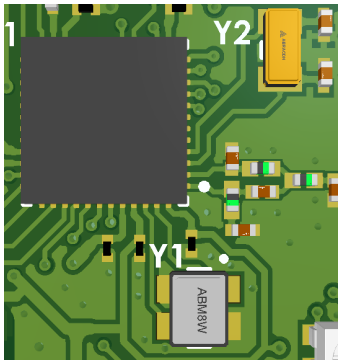


**Figure 4.33:** Oscillator placement: 48 MHz HF and 32 kHz very close to the uC.

**RF Circuit Section** The RF circuit required careful placement and routing to maintain signal integrity at 2.4 GHz. First, we placed the BALUN filter (Fig. 4.34), which is used to convert the balanced RF signal from the microcontroller into an unbalanced one suitable for the antenna. This was followed by the RF conditioning circuit of the uC.

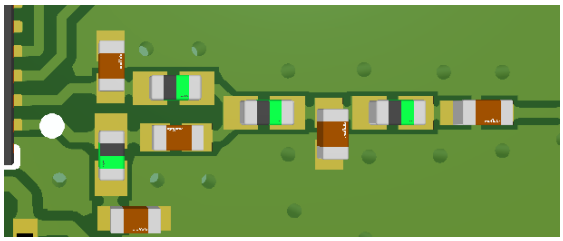

**Figure 4.34:** Placement of the BALUN filter in the RF section.

The RF traces were designed with a 50-ohm controlled impedance, calculated using coplanar waveguide geometry, with the width and spacing of the traces were evaluated thanks to Altium built-in impedance line calculator that gave us the parameter shown in **??**.

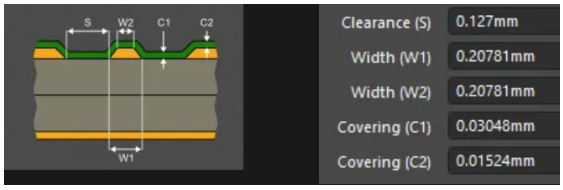


**Figure 4.35:** 50 Ohm coplanar line parameters

The curve was made smooth to avoid impedance mismatches, as shown in 4.36.

The vias were placed at a distance calculated to be less than 1/20 of the wavelength at 2.4 GHz, which corresponds to less than 3 mm, to minimize signal reflection.

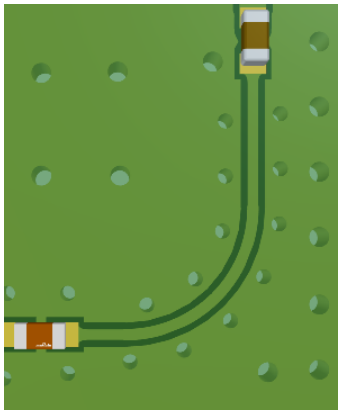

**Figure 4.36:** Coplanar line smooth curve

Finally, we included a T-shaped matching circuit for the antenna to adapt the 50-ohm impedance of the line, ensuring there were no reflections in the RF path. The antenna circuit was placed as per the datasheet recommendations (Fig. 4.37 and 4.38).

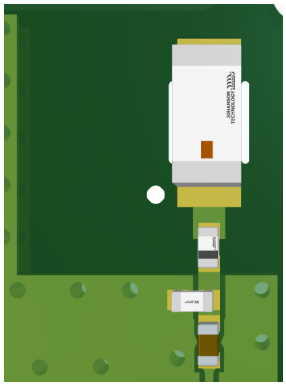

**Figure 4.37:** Antenna matching circuit

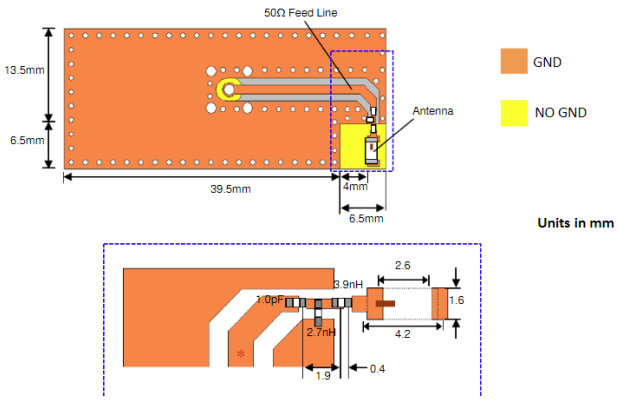


**Figure 4.38:** Datasheet recommendation matching circuit

**SPI Lines for the BioZ Sensor and Flash Memory** The SPI lines for the BioZ sensor were carefully routed with a level shifter placed in the middle to ensure correct voltage levels. The SPI lines were spaced at a distance greater than three times the trace width to avoid crosstalk between them (Fig. 4.39).

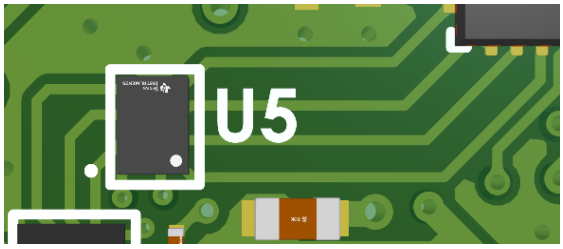


**Figure 4.39:** SPI lines for the BioZ sensor with level shifter in the middle.

The SPI lines for the flash memory were routed on the bottom side of the PCB. This decision was made to keep the lines short, preventing signal reflection and distortion in the high-frequency signals. Since the flash memory was one of the few components that could be placed on the bottom layer, it helped maintain the compact size of the board. Similar to the BioZ sensor, the SPI lines were kept short and distant from each other to avoid interference (Fig. 4.40).

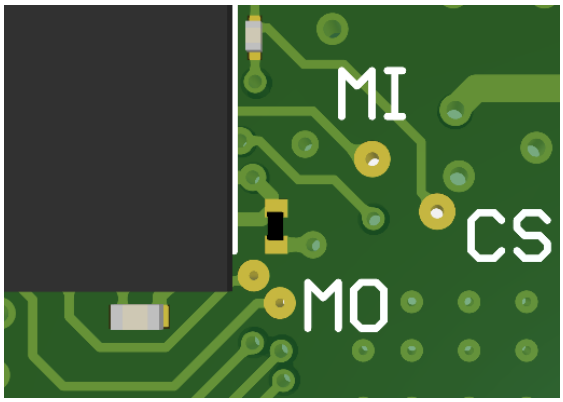


**Figure 4.40:** SPI lines for the flash memory, placed on the bottom layer.

### Power Section

The power section of the PCB was strategically placed in the top-left corner of the board. This decision was made to ensure that the power-related signals did not interfere with the other sensitive signals on the board, such as those related to the RF section or BioZ sensor.

**Power Connections** The primary power connections are located in this corner, consisting of the USB-C connector, the battery connector, and the on-off switch. The USB-C connector was designed with only six pins, as it is solely used for power delivery. The remaining unused pins were omitted to save space. Additionally,

two pull-down resistors were placed on the bottom layer (4.42, as specified by the USB-C standard (Fig. 4.41).

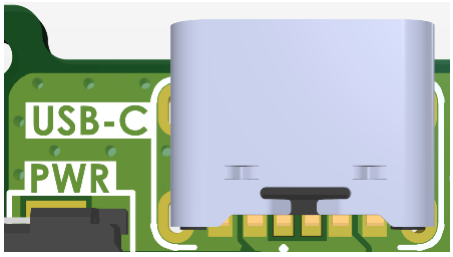


**Figure 4.41:** USB-C connector with six pins for power.

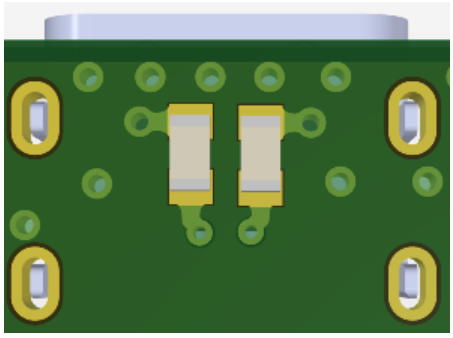

**Figure 4.42:** Bottom layer pull-down resistor

The battery connector is a Micro-Lock connector, chosen specifically to ensure it remains securely connected, even under movement or vibrations, reducing the risk of disconnection (Fig. 4.43).

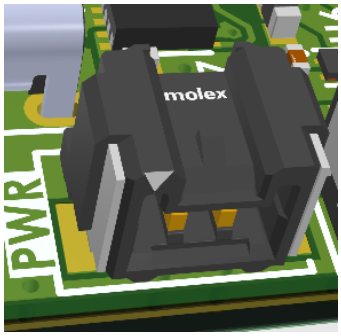


**Figure 4.43:** Micro-Lock battery connector to prevent accidental disconnection.

The on-off switch was positioned nearby to provide easy access for manual

control of the power supply to the board.

**Polygon Pour for Power Section** To ensure robust power delivery, a polygon pour was used for the power section. This technique allowed us to provide a low-resistance, wide path for the power lines, minimizing voltage drops and ensuring stable power across the entire PCB. The polygon pour covered the entire power section and helped to isolate the power signals from other sensitive areas.

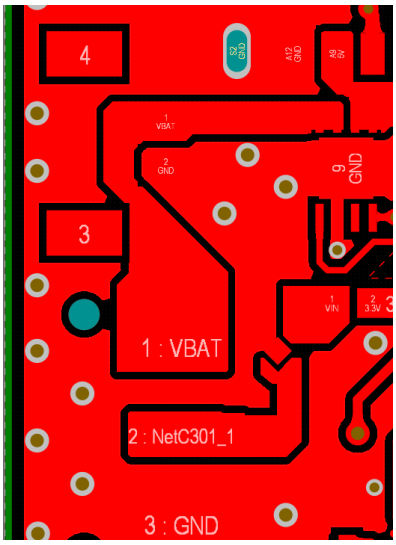


**Figure 4.44:** Poligon pour for power delivery

**Battery Charger and Voltage Regulation** Between the USB-C connector and the battery connector, we placed the battery charger circuit, which is responsible for managing the battery's charge and ensuring the device operates safely. This circuit was surrounded by the necessary decoupling components to minimize noise and ensure stable operation. A red LED was added to provide a visual indication of the battery charging status, that turns on while the battery is charging(Fig. 4.45). The current flowing into the battery during the charge is tuned by a resistance, as explained in the schematic section. We chose a bigger resistance for this, to able to substitute it in case a bigger or smaller battery would be needed. For its dimensions I decided to place it in the bottom layer as shown in 4.46.

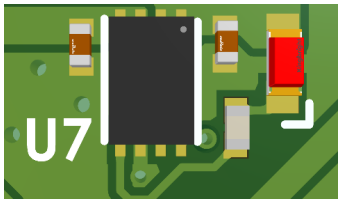


**Figure 4.45:** Battery charger circuit with decoupling capacitors and LED.

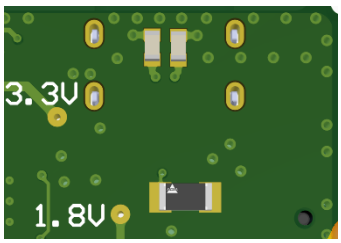


**Figure 4.46:** Current tuning resistance on the bottom layer

Following the battery charger, the power flows through the on-off switch to the voltage regulator. The voltage regulator steps down the input voltage from the battery to 3.3V, which is used to power the microcontroller and other circuits on the board (Fig. 4.47). The power signal flows through a Ferrite Bead to increase the stability of the power delivery.

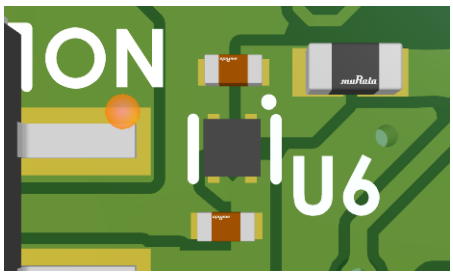


**Figure 4.47:** Voltage regulator providing 3.3V to the PCB.

By isolating the power section in the top-left corner and implementing a polygon pour for robust power distribution, we minimized potential interference with sensitive signal lines and ensured stable power delivery to all components.

**BioZ Sensor** The layout for the BioZ sensor closely follows the design of the development kit to ensure optimal performance. Specifically, there is no ground plane under the pads to avoid noises to degrade the measures. Additionally we

implemented separate ground planes for the digital and analog sections on both layers 2 and 3. These two ground planes are connected at a single point through the bottom layer, ensuring proper grounding and minimizing noise interference. The same separation was applied to the 1.8V power lines on the top layer, with distinct paths for digital and analog power, as shown in the image below (Fig. 4.48).

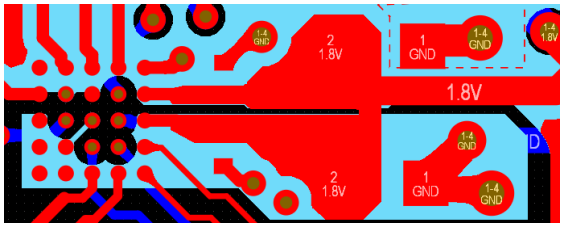


**Figure 4.48:** Power and ground separation between digital and analog sections.

The sensor uses a ball grid array (BGA) package with 0.25 mm pad diameter and 0.4 mm spacing between the pads. This design required very small vias, but these dimensions were still within the manufacturing limits specified by JLCPCB. To manage this, we used via-in-pad technology, where the vias are filled during the manufacturing process to maintain signal integrity and prevent solder wicking (Fig. 4.49).

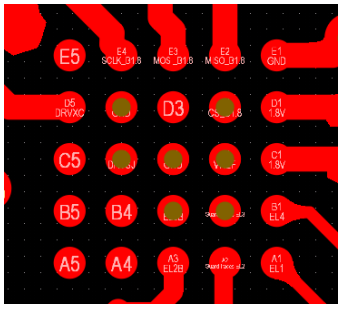


**Figure 4.49:** Via-in-pad for the BGA package.

The sensor pads are located on the bottom layer of the PCB and were designed to be symmetrical with respect to the MAX30009ENA+ to ensure equal trace lengths for both the power and sensing lines. The power pads are placed on the outer edges of the layout, while the sensing voltage pads are located on the inside. Guard traces were placed around the sensing lines on layer 1 to minimize interference, with corresponding guard pads on the layer below (Fig. 4.50).

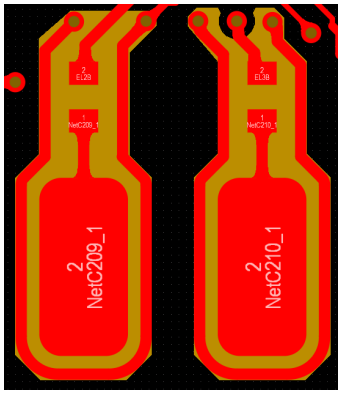


**Figure 4.50:** Guard traces on layer 1 in red and guard pads on the layer below in yellow

The decoupling capacitors were also placed symmetrically around the sensor pads to ensure stable power delivery and to minimize any noise that could affect the sensor's performance.

**I²C Lines and IMU Connector** The I²C lines were routed on the bottom layer, along with the I²C level shifter (Fig. 4.51), because they are less sensitive than SPI lines. Since the I²C bus operates at a lower frequency, the traces can be longer without negatively affecting signal integrity. The I²C lines terminate at the IMU connector, which is a Micro-Lock Molex connector designed to ensure that the connection remains secure, even under movement or vibration. The connector also carries the 1.8V and ground lines to supply power to the IMU, as well as the interrupt signal coming from the IMU (Fig. 4.52).

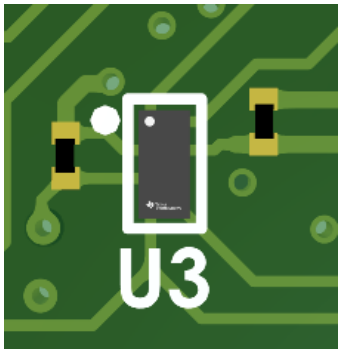


**Figure 4.51:** I²C lines and level shifter placed on the bottom layer.

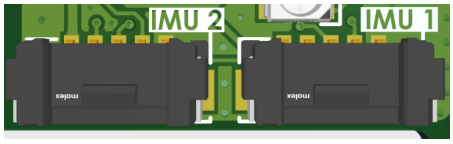


**Figure 4.52:** IMU Micro-Lock Molex connector.

**RGB LED** The RGB LED was placed in the remaining free space on the PCB, as far as possible from the sensitive RF circuit to avoid any potential interference (Fig. 4.53). The resistors controlling the LED were placed on both the top (two resistors) and the bottom layers (one resistor).

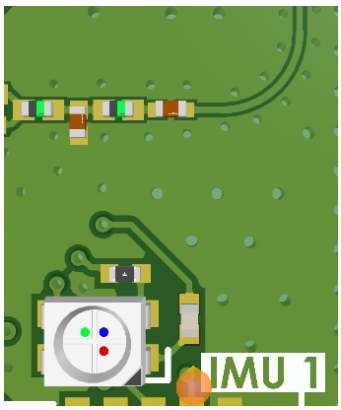


**Figure 4.53:** RGB LED placement, far from the RF circuit.

**JTAG Connector** The JTAG connector was placed near the microcontroller at the top of the PCB to ensure that the TCKC and TMSC lines remained short, minimizing the possibility of signal degradation (Fig. 4.54). The reset signal (RST) was connected to a pull-up resistor and linked to the reset pin of the microcontroller. Since there is no dedicated reset button on the PCB, the JTAG can be used to reset the device during debugging if necessary.

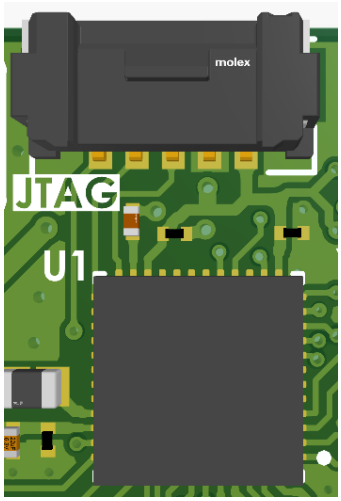


**Figure 4.54:** JTAG connector near the microcontroller to keep lines short.

**Bluetooth Activation Button** Finally, we placed a button on the PCB to activate the Bluetooth connection for parsing data. This button, along with its debouncing circuit, was placed in the remaining free space on the board (Fig. 4.55). The button allows the user to establish a Bluetooth connection when needed, making the device more user-friendly.

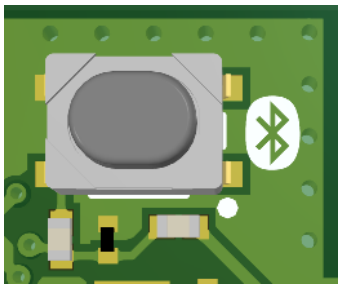

**Figure 4.55:** Bluetooth activation button with debouncing circuit.

**Final Considerations** To ensure robust signal integrity and minimize potential interference, we added a ground (GND) pour on the top layer of the PCB. This provided additional shielding for sensitive signals and helped stabilize the overall power distribution across the board.

In addition, via stitching was applied extensively throughout the PCB, particularly around the edges and near the antenna section (Fig. 4.56). This was done to prevent fringing effects near the PCB's edges and to maintain signal integrity, especially in the RF section. Given that we implemented ground planes on three different layers (layers 2, 3, and part of layer 1), the vias helped unify the ground

planes and provided a consistent low-impedance path for return signals. This stitching improves the overall electrical performance by reducing inductance and ensuring solid grounding.

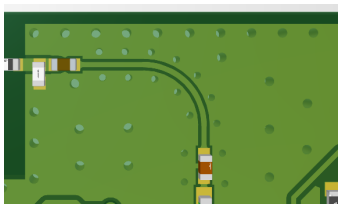

**Figure 4.56:** Extensive via stitching, especially near the PCB edge and antenna section.

Additionally, teardrops were added to the layout (Fig. 4.57) to strengthen the connection between traces and pads or vias. This helps reduce the likelihood of mechanical stress breaking the connections during manufacturing, assembly, or operation. The teardrop design improves manufacturability and reliability, particularly in areas where traces transition into smaller pads or vias.

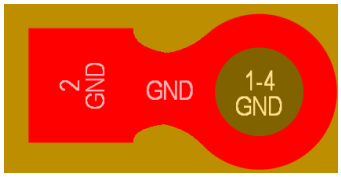


**Figure 4.57:** Teardrops added to reinforce trace-to-pad and trace-to-via connections.

To facilitate testing and debugging, we added test points for key signals. Specifically, test points were placed on the power lines, including GND, 1.8V, and 3.3V, allowing easy access to monitor the power supply levels during operation. Additionally, we added test points for the SPI signals, including MI (Master In), MO (Master Out), CS (Chip Select), and SCLK (Serial Clock) to ensure the signals can be checked during development and troubleshooting via an oscillator, touching the exposed pad of about 0.8mm in diameter(Fig. 4.58).

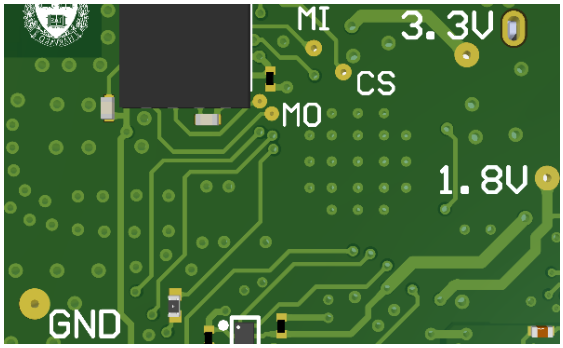


**Figure 4.58:** Test points for power lines and SPI signals

For the $I^2C$ signals, test points were not explicitly added, as we can easily access the signals directly from the connector pads on the IMU, providing a straightforward way to check the SDA (data) and SCL (clock) lines.

### IMU PCB Layout

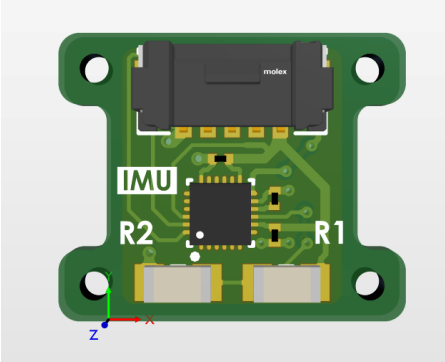


**Figure 4.59:** IMU PCB top view

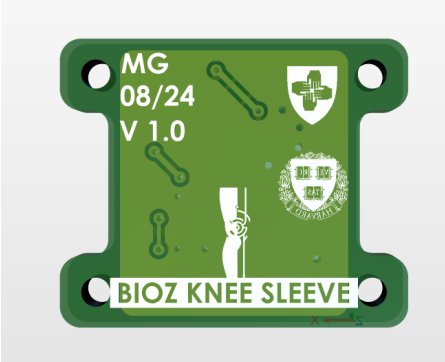


**Figure 4.60:** IMU PCB bottom view

The layout of the IMU PCB was designed with several key factors in mind to ensure optimal performance while maintaining a compact size. The final dimensions of the PCB are very small, which was crucial given the wearable nature of the device. The board has a thickness of 1.6 mm to provide sufficient mechanical stability.

The IMU itself was placed at the center of the PCB, which allowed for balanced routing of signals and ensured that the critical connections had short and direct paths.

**Capacitor Placement** Bypass capacitors and filter capacitors were placed very close to the IMU, following best practices to minimize noise and stabilize the power supply. Keeping these components close to the IMU helps to maintain the integrity of the power signals and reduces the risk of voltage fluctuations that could affect the IMU's performance.

**Connector Header Placement** The connector header, which supplies power to the IMU, was positioned on the side of the PCB that best aligned with the IMU's power pins. This strategic placement ensured that the power lines were as short as possible, reducing power losses and ensuring a stable supply to the IMU (Fig. 4.59).

On the opposite side of the PCB, we placed the resistor that connects to the $I^2C$ lines. Since the $I^2C$ lines are not critical in terms of signal integrity, their placement was not as constrained, allowing more flexibility in routing.

**Routing and Ground Plane** Routing began with the power signals, ensuring that they had clean, direct paths to the IMU. A ground pour was added on the bottom layer to provide a stable ground reference for all signals. The $I^2C$ signals were routed with care, keeping them spaced apart to avoid crosstalk between the data (SDA) and clock (SCL) lines.

A small break in the ground plane was introduced in a non-critical area of the PCB, either under the connector or along the side. This break did not affect the functionality but allowed for easier routing and improved layout flexibility.

Overall, the design of the IMU PCB successfully balanced the need for compactness with mechanical and electrical stability.

### Manufacturing settings

The manufacturing process of the printed circuit boards (PCBs) involved several key decisions that were guided by the requirements of our project.

For the main PCB, we opted for a four-layer design, which facilitated controlled impedance at 50 Ohms. This choice was made to ensure optimal signal integrity, especially for high-frequency applications, as discussed in previous sections. The surface finish selected was lead-free hot air solder leveling (HASL), which is environmentally friendly and provides a reliable surface for soldering components.

In terms of copper thickness, we chose 1 oz for the outer layers and 0.5 oz for the inner layers. This configuration balances electrical performance with mechanical strength. For vias, we specified epoxy-filled vias for the necessary via-in-pad applications, which helps to prevent solder wicking and improves reliability. The remaining vias were simply plugged to ensure proper connectivity without compromising the mechanical integrity of the PCB.

Additionally, we decided on a two-layer assembly for the main PCB, which allows for efficient space utilization while maintaining performance.

In contrast, the inertial measurement unit (IMU) PCBs were designed as two-layer boards, also using lead-free processes. The thickness of 1.6 mm was chosen for these boards to ensure mechanical stability during operation, which is critical given the IMU's role in sensing and measurement applications.

These manufacturing choices were instrumental in achieving the performance and reliability targets set for our project.

## 4.4 Firmware Development

Given the limited development time, we opted for a streamlined firmware version focused solely on BioZ measurement functionality. This bare version excluded non-essential features, prioritizing efficient development and testing. Despite its simplicity, the firmware was structured for scalability, allowing easy integration of additional threads for future functionalities within the Real-Time Operating System (RTOS) environment.

In the current implementation, the `main_tirtos.c` file initializes the system and creates a single thread dedicated to managing SPI communication with the BioZ sensor. This thread is implemented in the `spiBIOZthread.c` file, which handles sensor initialization, configuration, and data acquisition.

The thread creation process in `main_tirtos.c` involves defining the thread attributes, setting scheduling parameters, and specifying the stack size. The following code snippet demonstrates how the thread is created:

**Listing 4.1:** Thread creation in `main_tirtos.c`

```
1 pthread_create(&thread, &attrs, spiBIOZthread, NULL);
```

The `spiBIOZthread` function initializes the necessary hardware peripherals (GPIO, SPI, Timer) and configures the BioZ sensor for operation. It ensures robust SPI communication and proper data handling for the BioZ measurements.

This modular approach enables the addition of new threads for other functionalities, such as data logging or user interface management, without major changes to the existing firmware structure.

### Code Explanation

Figure 4.61 shows the flowchart representing the flow of operations in the `spiBIOZthread.c` code. Each block in the flowchart corresponds to a specific step in the SPI communication and BioZ measurement process. Below, we explain each step in detail, accompanied by the relevant code.

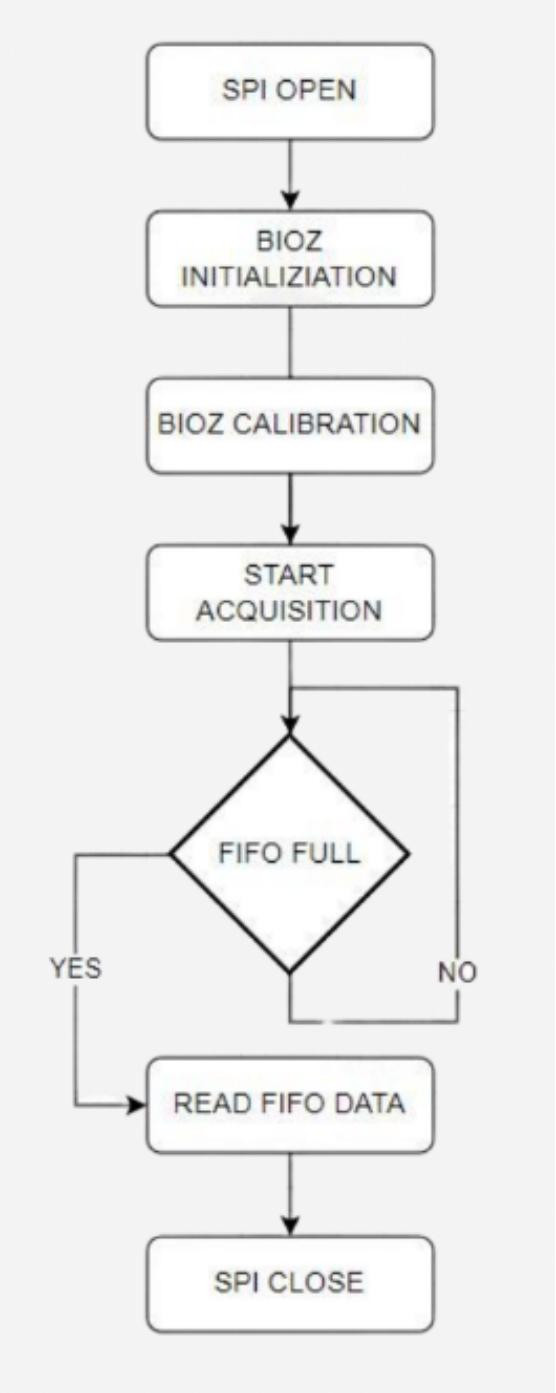


**Figure 4.61:** Flowchart of the `spiBIOZthread.c` code.

- **SPI Open**: This step initializes the SPI driver with phase 0 and polarity 0, to have the data sampled on the rising clock edge, and the clock idle value

equal to 0. Then it opens the SPI interface at 4 MHz in controller mode. If the SPI initialization fails, an error is signaled using an LED.

**Listing 4.2:** Opening the SPI interface

```
    SPI_Params_init(&spiParams);
    spiParams.frameFormat = SPI_POL0_PHA0;
    spiParams.bitRate = 4000000;
    controllerSpi = SPI_open(SPI_MAX, &spiParams);
    if (controllerSpi == NULL) {
        while (1) { LED_setOn(ledHandle[CONFIG_LED_R], 100); }
    }

```

- **BioZ Initialization**: The BioZ sensor is initialized by configuring its registers to enable basic functionality. For example, this includes resetting the sensor and setting FIFO thresholds.

**Listing 4.3:** Initializing the BioZ sensor

```
    regWrite(0x20, 1 << 2); // BIOZ_BG_EN1
    regWrite(0x11, 1);      // Reset the device
    regWrite(0x0d, FIFO_SIZE - NUM_SAMPLES_PER_INT); // Set FIFO
    A_FULL threshold

```

- **BioZ Calibration**: Calibration is performed to calculate offsets and coefficients for accurate impedance measurements. This involves writing to configuration registers and reading calibration data from the FIFO.

**Listing 4.4:** Calibrating the BioZ sensor

```
    regWrite(0x20, (3 << 6) | (4 << 3) | (1 << 2)); // Enable I &
    Q channels
    regWrite(0x25, (1 << 7) | (1 << 6));            //
    Calibration mode

```

- **Start Acquisition**: Once calibrated, the sensor is configured to start impedance data acquisition. The FIFO is monitored to ensure data readiness.

**Listing 4.5:** Starting BioZ acquisition

```
    regWrite(0x20, (3 << 6) | (4 << 3) | (1 << 2) | (1 << 1)); //
    Start acquisition

```

- **FIFO Full Check**: The program enters a loop to monitor the FIFO status register. If the FIFO is full, data is read and processed.

**Listing 4.6:** Checking FIFO status

```
    while ((fifo_full & (1 << 7)) != 0x80) {
        regRead(0x00, 1); // Read the status register
        fifo_full = rx_buffer[2]; // Status byte
    }

```

- **Read FIFO Data**: Once the FIFO is full, data is read in burst mode and processed to calculate impedance values.

**Listing 4.7:** Reading data from the FIFO

```
    regRead(0x0c, totalBytes); // Read all FIFO data in burst
    mode

```

- **SPI Close**: After all necessary data has been acquired, the SPI interface is closed to free up resources.

**Listing 4.8:** Closing the SPI interface

```
    SPI_close(controllerSpi);

```

This modular approach ensures clarity and maintainability while focusing on accurate BioZ measurements.

### Testing and Debugging

The testing and debugging phase presented several challenges, particularly with the SPI communication between the microcontroller and the BioZ sensor. Initially, we encountered an issue where the sensor always returned zeros on the SPI lines, making it impossible to verify the communication or retrieve valid data.

**Debugging SPI Communication** To identify the root cause, we used an oscilloscope to analyze the SPI lines (MOSI, MISO, SCLK, and CS) through test points placed on the PCB. Figure 4.62 shows the oscilloscope setup used during this process. Despite a thorough review of the sensor's datasheet, we were unable to resolve the issue initially.

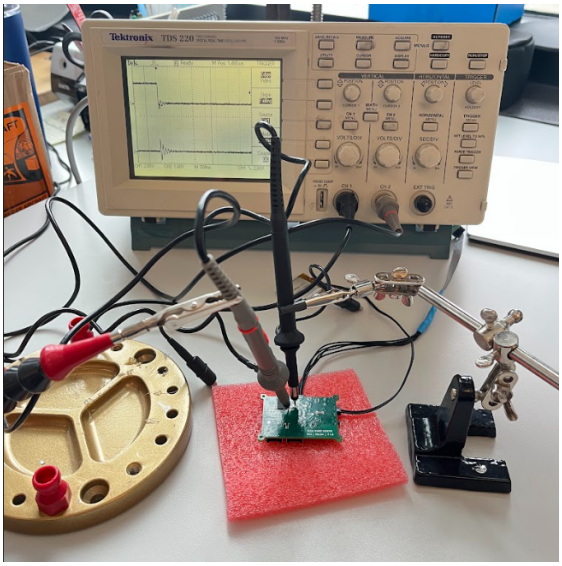


**Figure 4.62:** Oscilloscope setup for debugging SPI communication.

After extensive analysis, we decided to compare the SPI behavior of our system with a development kit that used the same sensor. By observing the SPI signals on the development kit using the oscilloscope, we discovered a critical timing detail: the chip select (CS) line must go low (active) 3.5 µs before the clock (SCLK) starts, and it must remain low for 3.5 µs after the communication ends.

This behavior was not explicitly mentioned in the datasheet but was crucial for proper communication with the sensor. To address this, we implemented manual control of the CS line in our code and introduced the required delays, as shown in the following code snippet:

**Listing 4.9:** Manual CS line control with delays

```
GPIO_write(SPI_MAX_CS, 0); // CS low (active)
usleep(3.5);               // 3.5 us delay before SCLK starts

// Perform SPI transfer
SPI_transfer(controllerSpi, &transaction);

usleep(3.5);               // 3.5 us delay after communication ends
GPIO_write(SPI_MAX_CS, 1); // CS high (inactive)
```

After implementing this change, the SPI communication began functioning correctly, allowing us to proceed with debugging the remaining parts of the code. To aid in the debugging process, we utilized LEDs as visual feedback indicators throughout the program. Different LED colors and blinking patterns were used to signal specific states or errors, such as SPI initialization failure or successful

data acquisition. This approach proved to be a simple yet effective method for monitoring program behavior and quickly identifying issues during development.

With the corrected SPI implementation and the use of visual feedback through LEDs, we successfully debugged the firmware. The BioZ sensor communication and data acquisition were verified to work as expected, enabling the final testing and integration.

## 4.5 Knee Sleeve Implementation

After successfully debugging and verifying the firmware, the next step was the physical implementation of the knee sleeve. This process involved preparing the PCB with all necessary components, integrating it into the sleeve, and making modifications to the sleeve itself to ensure functionality and usability. I took charge of this physical implementation, overseeing all aspects of the process to ensure proper integration of the electronics with the wearable.

The implementation began with soldering the remaining components onto the PCB to complete the hardware assembly. Following this, the PCB was carefully sewn onto the knee sleeve to secure it in place. Additionally, we made structural modifications to the sleeve, including cutting holes and sewing fabric tunnels to route wires and sensors efficiently while maintaining comfort and flexibility for the user.

This section provides a detailed explanation of each step in the implementation process, including the challenges faced and the solutions devised to achieve a robust and functional design.

### 4.5.1 Soldering of Components

Upon receiving the printed circuit boards (PCBs), we proceeded with the soldering of the remaining components to ensure full functionality. This process involved several critical steps:

First, we soldered the button onto the main PCB, which allows for user interaction with the device. Next, the electrodes' cables were soldered to the bioimpedance (BIOZ) pads, facilitating the necessary electrical connections for bioimpedance measurements, avoinding connectors that might degrade the signal.

For the inertial measurement unit (IMU) PCBs, we soldered resistors R1 and R2 to configure the boards with two distinct I2C addresses, as shown in 4.63 This is essential for enabling communication with the microcontroller, as previously described.

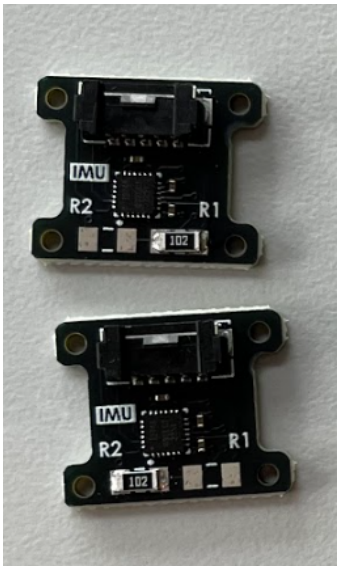


**Figure 4.63:** IMUs with R1 and R2 soldered on them

Additionally, we adapted the battery cable to connect with the Molex Microlock connector, ensuring a secure power supply to the device 4.64. Lastly, we soldered the JTAG cable from the 20-pin ribbon connector to the 5-pin Molex Microlock. This step is crucial for enabling debugging capabilities via the JTAG interface, which allows for efficient firmware development and troubleshooting.

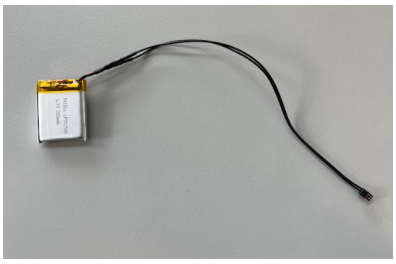

**Figure 4.64:** Battery cable soldered to the MicroLock connector

Overall, this soldering process was integral to the successful assembly and functionality of the PCBs in our project.

### 4.5.2 Knee Sleeve Integration

**Figure 4.65:** Lateral view


**Figure 4.66:** Frontal view

**Figure 4.67:** Medial view

To integrate the electronics into the knee sleeve, several modifications and adjustments were made to ensure both functionality and user comfort during activity. I began by cutting two horizontal holes on the sides of the patella (4.68 to connect the cables to the electrodes positioned under the sleeve. The edges of the holes were reinforced by sewing red wire along the borders. These holes were made slightly wider horizontally to accommodate different knee sizes and ensure a proper fit.

**Figure 4.68:** Knee sleeve openings

To manage the cables for the two IMUs and the electrodes, elastic fabric tunnels were sewn into the sleeve, as shown in 4.69. These tunnels securely encapsulated the cables, ensuring they were not obstructive or uncomfortable for the patient during movement. The use of elastic material preserved the flexibility and stretchability of the sleeve, maintaining its overall elasticity and adaptability to the user's leg.

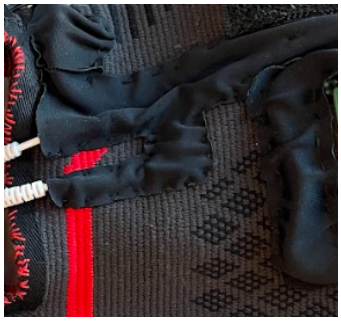

**Figure 4.69:** Tunnels for cable management

The PCBs were securely sewn onto the sleeve to provide stability, particularly for the IMU measurements. The IMUs themselves were strategically positioned to minimize artifacts caused by muscle movement, ensuring more accurate data collection.

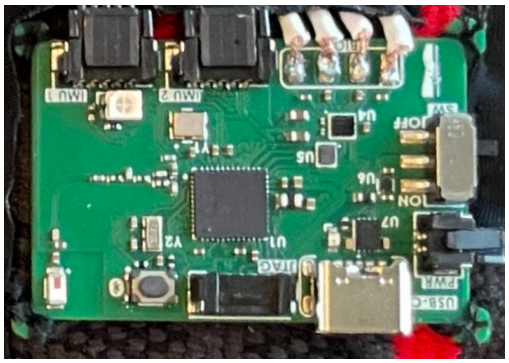


**Figure 4.70:** Main PCB sewed onto the sleeve


**Figure 4.71:** IMU PCB sewed onto the sleeve

The battery was not permanently attached to the sleeve but was instead placed in a fabric pouch equipped with a Velcro strap (4.72). This design allowed the battery to be easily removed and replaced when necessary, providing practicality and convenience for the user.

**Figure 4.72:** Pouch for the battery

All sewing was performed with the sleeve kept under tension to replicate the stretch that occurs when the sleeve is worn. This ensured that the placement of the components and cables would be correct when in use and prevented undue tension on the materials during wear, preserving both comfort and durability.

## 4.6 Results and discussion

The performance of the knee sleeve was evaluated in terms of both comfort and measurement accuracy. Below, we discuss the findings from these evaluations.

### 4.6.1 Comfort and Stability

**Figure 4.73:** Lateral view


**Figure 4.74:** Frontal view

**Figure 4.75:** Medial view

The knee sleeve demonstrated excellent comfort during our tests. We conducted walking and running tests on a treadmill with the sleeve in place. The sleeve remained comfortable to wear throughout these activities, and the electrodes stayed firmly in place, even during more vigorous movements. This ensured that the BioZ measurements were not disrupted by electrode displacement or discomfort, highlighting the practical usability of the device during physical activities.

### 4.6.2 Measurement Accuracy

To evaluate the measurement accuracy of the knee sleeve, we conducted a comparison test by measuring BioZ with both the knee sleeve and a development kit immediately afterward. Figure 4.76 shows the results, with resistance and reactance plotted on the y-axis and the samples on the x-axis, with the DevKit measurements plotted in blue and the bioz knee sleeve measurements plotted in orange.

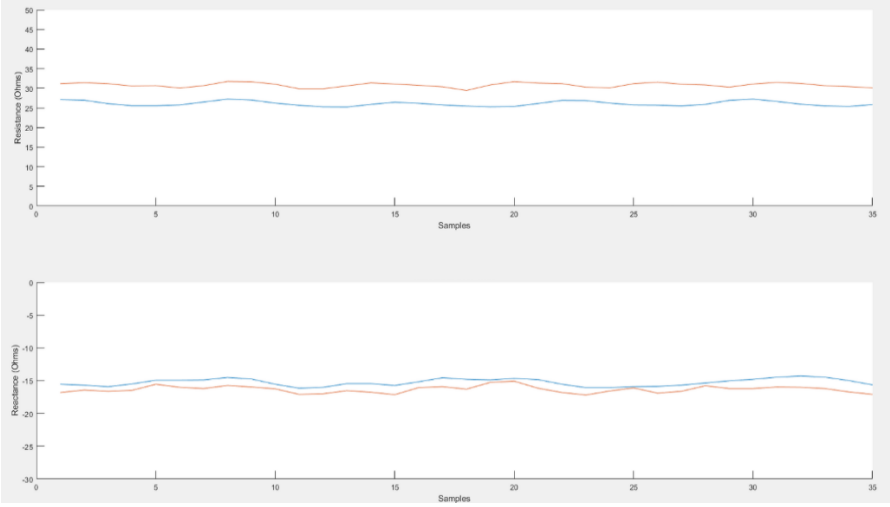


**Figure 4.76:** Comparison of BioZ measurements: Knee sleeve vs. development kit.

As shown in the graph, the measurements from the knee sleeve are very close to those from the development kit, with only a small offset of approximately 3 Ω. This offset is attributed to the different cable lengths and configurations used in the two setups. However, this difference falls well within the range of daily variations in BioZ measurements and is therefore considered negligible.

### 4.6.3 Discussion

These results confirm that the knee sleeve successfully measures the BioZ of the knee during activity. The sleeve remains in place during movement and provides accurate measurements comparable to those from a development kit, making it a reliable tool for BioZ monitoring in dynamic conditions.

#### Evaluation of the Knee Sleeve Effectiveness

The knee sleeve effectively meets its primary objective of enabling accurate and reliable BioZ measurements during physical activities. The comfortable design ensures that it can be worn for extended periods without causing discomfort, while the secure placement of the electrodes and cables prevents disruptions in signal acquisition. Additionally, the measurements obtained from the sleeve closely match those from a reference development kit, confirming its effectiveness in achieving the intended goals of precise BioZ monitoring.

### Potential Advantages and Limitations

One of the key advantages of the knee sleeve design is its seamless integration of electronic components into a wearable form factor. The use of elastic tunnels for cable management maintains the flexibility and comfort of the sleeve, while strategic placement of the IMUs minimizes artifacts caused by muscle movement.

However, the design is not without limitations. The observed offset of approximately 3 Ω in the measurements, while negligible in practical terms, highlights the potential impact of cable length and configuration on accuracy. Future iterations could focus on standardizing these factors to minimize offsets. Additionally, while the sleeve was tested on a treadmill, further validation in diverse real-world scenarios, such as outdoor running or uneven surfaces, would be beneficial to confirm its robustness under various conditions.

Overall, the knee sleeve represents a significant step forward in wearable BioZ monitoring, combining accuracy, comfort, and practicality. Nonetheless, addressing the identified limitations could further enhance its reliability and applicability for broader use cases.

# Chapter 5

# Conclusion

This thesis explored the application of bioimpedance for monitoring physiological changes and its integration into a wearable device for knee osteoarthritis management. The work can be divided into two main components: the bioimpedance analysis experiments and the development of a sensorized knee sleeve.

## 5.1 Bioimpedance Analysis

### 5.1.1 Summary of findings

The experiments conducted provided valuable experience in using the development kit and served as an initial exploration of potential trends in bioimpedance measurements. Several key observations emerged:

- The influence of sweat on bioimpedance measurements was evident, emphasizing the need for stable electrode placement and proper skin preparation to minimize measurement variability.
- Lower limb exercise had a pronounced effect on both resistance and reactance, leading to noticeable decreases during activity. This effect was less pronounced but still observable during upper limb exercises, which also contributed to a reduction in resistance and reactance.
- The gradual return of bioimpedance values to baseline after exercise highlighted the delayed recovery phase, particularly for lower limb activity.

Regarding data collection, no conclusions can be drawn at this stage, as the study is still ongoing and currently limited to healthy subjects. These participants provide normative data that will serve as a reference for future comparisons with osteoarthritis patients.

Overall, these initial experiments and observations set the foundation for refining measurement protocols and exploring bioimpedance as a potential tool for monitoring physiological changes during physical activity.

### 5.1.2 Future Work in Bioimpedance Analysis

Further studies are required to explore the full potential of bioimpedance in clinical diagnostics, particularly in the continuous monitoring of osteoarthritis treatment. The current data collection needs to be completed to establish a comprehensive dataset that allows for meaningful comparisons between healthy subjects and osteoarthritis patients.

## 5.2 Sensorized Knee Sleeve

The knee sleeve development demonstrated the feasibility of integrating bioimpedance monitoring into a wearable device. The sleeve was shown to be comfortable, reliable during physical activity, and capable of providing accurate measurements comparable to a development kit. This represents a significant step toward creating a practical tool for osteoarthritis management.

### 5.2.1 Summary of Findings

The development of the knee sleeve successfully addressed all initial requirements. The sleeve proved to be comfortable, capable of continuous BioZ monitoring, easy to use, and featured transversal electrodes and integrated IMUs for additional data collection. Extensive testing confirmed that the sleeve remained securely in place during activity, provided accurate measurements comparable to a reference development kit, and ensured practicality for real-world applications.

### 5.2.2 Future Work in Knee Sleeve Development

While the current implementation of the knee sleeve meets its intended goals, several areas for future development have been identified:

- **Completing the Firmware:** The firmware can be further enhanced by adding features such as Bluetooth connectivity for wireless data transfer, IMU data handling for detailed movement analysis, and flash memory support for offline data storage. These updates will expand the sleeve's capabilities and enable more advanced applications.
- **Developing a GUI:** A user-friendly Graphical User Interface (GUI) on a PC could significantly improve the usability of the knee sleeve. The GUI would

allow real-time data visualization, making it easier for users to monitor BioZ measurements and other metrics. This interface would also facilitate data logging and analysis, providing a seamless connection between the sleeve and the end user.

- **Additional Testing and Validation:** Further testing in varied real-world conditions, such as outdoor running or uneven surfaces, could provide additional insights into the sleeve's performance and robustness. Iterative improvements based on these tests would ensure the sleeve's reliability across a broader range of use cases.
- **Exploring Electrode Types:** Further exploration into alternative electrode types, such as dry and textile electrodes, is necessary. These electrodes could significantly improve the comfort of the sleeve for long-term wear. However, their performance in terms of measurement accuracy and consistency needs to be validated against the gel electrodes currently in use.
- **Investigating Flexible PCBs:** The use of flexible PCBs could further enhance the comfort of the knee sleeve, particularly in reducing stiffness and increasing adaptability to the knee's contours. However, this approach requires careful consideration of mechanical strength and durability to ensure the sleeve remains robust during intensive physical activities.
- **Additional Testing and Validation:** Further testing in varied real-world conditions, such as outdoor running or uneven surfaces, could provide additional insights into the sleeve's performance and robustness. Iterative improvements based on these tests would ensure the sleeve's reliability across a broader range of use cases.

By addressing these areas, the knee sleeve could evolve into a more versatile and powerful tool for BioZ monitoring, expanding its potential applications in healthcare and fitness.

## 5.3 Final conclusion

The journey of this research has been both challenging and rewarding, laying a foundation for future exploration and innovation in bioimpedance monitoring and wearable devices applications. By bridging the gap between bioimpedance research and real-world scenarios, this work aims to contribute to the development of innovative, patient-centered solutions for managing osteoarthritis.

# Acknowledgements

ACKNOWLEDGMENTS

# Appendix A

# PCB scematics

The following schematic shows the detailed layout of the PCB, including the microcontroller, sensors, power management, and IMU . It illustrates how each part is interconnected to ensure the functionality of the knee sleeve device.

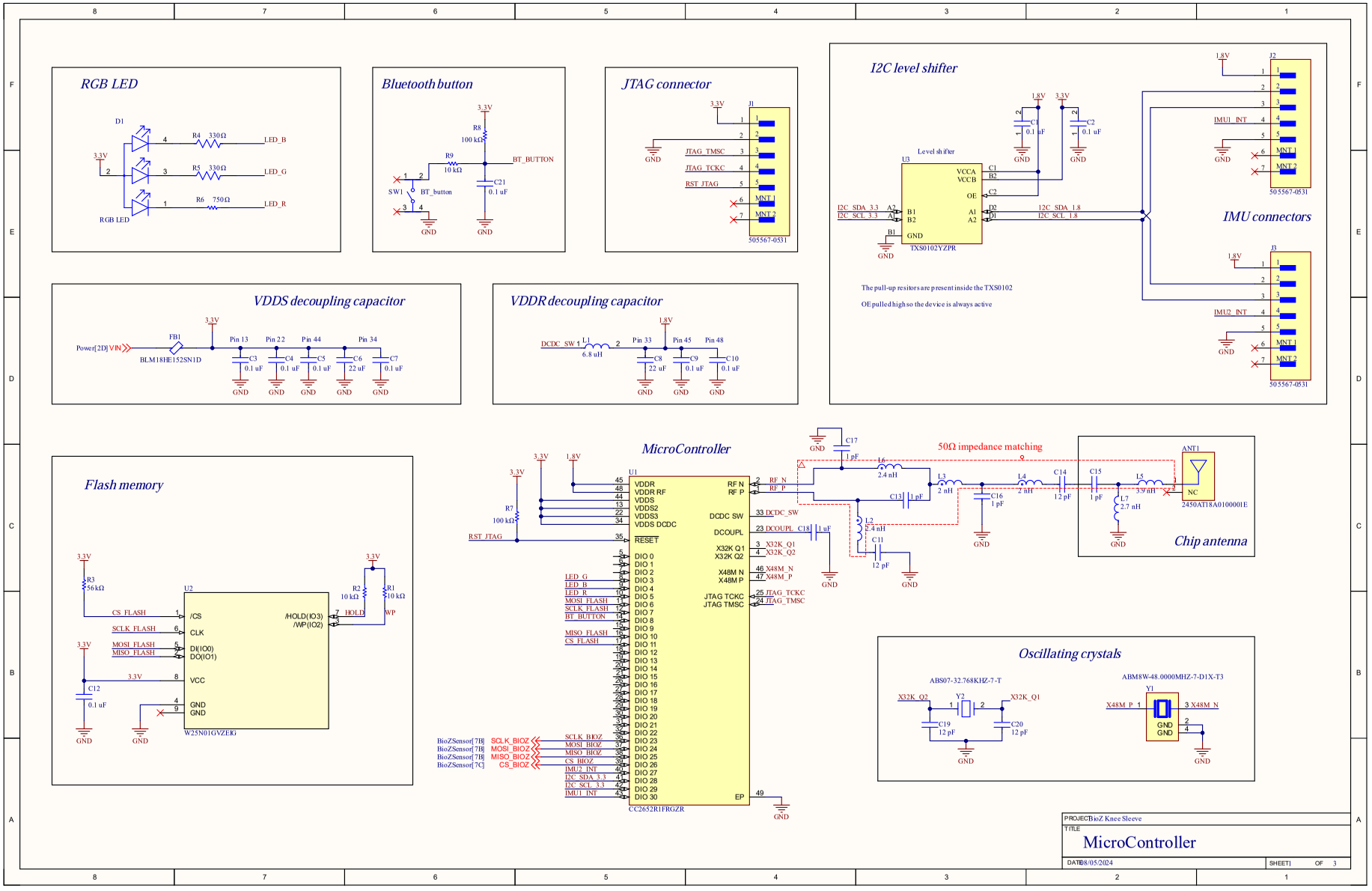
RGB LED
D1
3.3V
R4 330Ω
R5 330Ω
R6 750Ω
LED_B
LED_G
LED_R
RGB LED
Bluetooth button
3.3V
R8 100 kΩ
R9 10 kΩ
BT_BUTTON
SW1
BT_button
C21 0.1 uF
GND
JTAG connector
J1
JTAG_TMSC
JTAG_TCKC
RST_JTAG
MNT 1
MNT 2
505567-0531
I2C level shifter
1.8V
3.3V
U3
Level shifter
VCCA
VCCB
OE
GND
TXS0102YZPR
I2C_SDA_3.3
I2C_SCL_3.3
I2C_SDA_1.8
I2C_SCL_1.8
The pull-up resistors are present inside the TXS0102
OE pulled high so the device is always active
IMU connectors
J2
J3
IMU1_INT
IMU2_INT
VDDS decoupling capacitor
Power[2D]
VIN
FB1
BLM18HE152SN1D
Pin 13
Pin 22
Pin 44
Pin 34
C3 0.1 uF
C4 0.1 uF
C5 0.1 uF
C6 22 uF
C7 0.1 uF
VDDR decoupling capacitor
DCDC_SW
L1 6.8 uH
Pin 33
Pin 45
Pin 48
C8 22 uF
C9 0.1 uF
C10 0.1 uF
Flash memory
R3 56kΩ
R2 10 kΩ
R1 10 kΩ
U2
/CS
CLK
DI(IO0)
DO(IO1)
/HOLD(IO3)
/WP(IO2)
HOLD
WP
VCC
GND
C12 0.1 uF
CS_FLASH
SCLK_FLASH
MOSI_FLASH
MISO_FLASH
W25N01GVZEIG
MicroController
U1
VDDR
VDDR RF
VDDS
VDDS2
VDDS3
VDDS DCDC
RESET
RF N
RF P
DCDC SW
DCOUPL
X32K Q1
X32K Q2
X48M N
X48M P
JTAG TCKC
JTAG TMSC
EP
DIO 0
DIO 1
DIO 2
DIO 3
DIO 4
DIO 5
DIO 6
DIO 7
DIO 8
DIO 9
DIO 10
DIO 11
DIO 12
DIO 13
DIO 14
DIO 15
DIO 16
DIO 17
DIO 18
DIO 19
DIO 20
DIO 21
DIO 22
DIO 23
DIO 24
DIO 25
DIO 26
DIO 27
DIO 28
DIO 29
DIO 30
CC2652R1FRGZR
R7 100 kΩ
RST_JTAG
LED_G
LED_B
LED_R
MOSI_FLASH
SCLK_FLASH
BT_BUTTON
MISO_FLASH
CS_FLASH
IMU2_INT
I2C_SDA_3.3
I2C_SCL_3.3
IMU1_INT
BioZSensor[7B]
BioZSensor[7B]
BioZSensor[7B]
BioZSensor[7C]
SCLK_BIOZ
MOSI_BIOZ
MISO_BIOZ
CS_BIOZ
50Ω impedance matching
C17 1 pF
L6 2.4 nH
L3 2 nH
L4 2 nH
C14 1.2 pF
C15 1 pF
L5 3.9 nH
L7 2.7 nH
C13 1 pF
C16 1 pF
L2 2.4 nH
C11 12 pF
C18 1 uF
ANT1
NC
2450AT18A0100001E
Chip antenna
Oscillating crystals
ABS07-32.768KHZ-7-T
Y2
C19 12 pF
C20 12 pF
ABM8W-48.0000MHZ-7-D1X-T3
Y1
X32K_Q2
X32K_Q1
X48M_P
X48M_N
PROJECT BioZ Knee Sleeve
TITLE
MicroController
DATE 8/05/2024
SHEET 1 OF 3

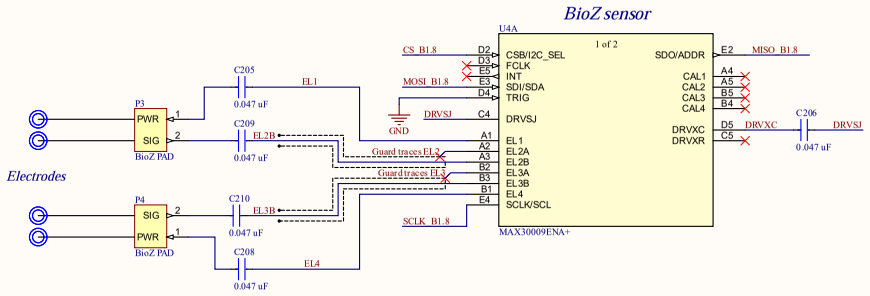


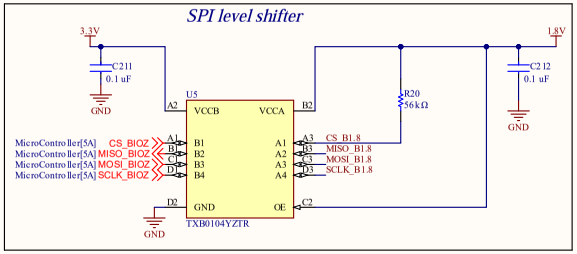


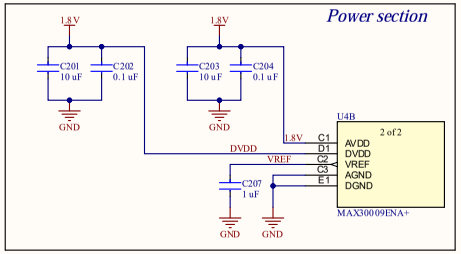


PROJECT BioZ Knee Sleeve

TITLE

# BioZSensor

DATE 08/05/2024 SHEET 2 OF 3

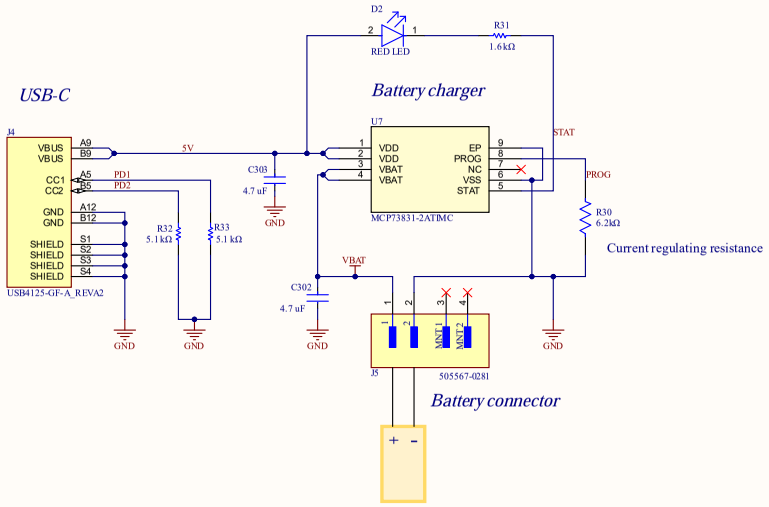


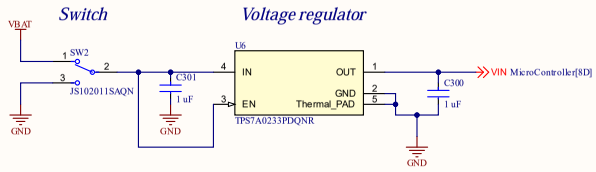


| | |
|---|---|
| PROJECT | BioZ Knee Sleeve |
| TITLE | Power |
| DATE | 08/05/2024 |
| SHEET | 3 OF 3 |

## Molex connector

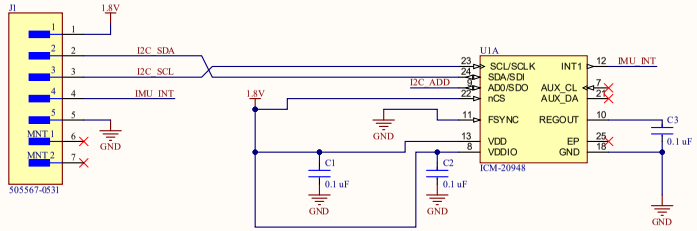


## I2C address selection

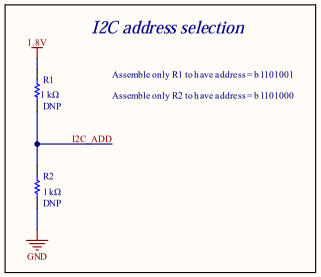


| | |
|---|---|
| PROJECT | BioZ Knee Sleeve |
| TITLE | IMU |
| DATE | 08/05/2024 |
| SHEET | 1 OF 1 |

# Appendix B

# Gerber files

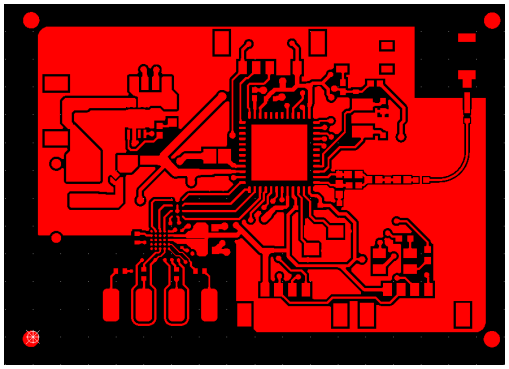

**Figure B.1:** Upper layer

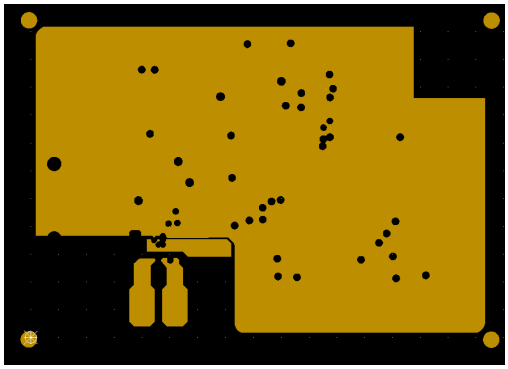

**Figure B.2:** Internal layer 1

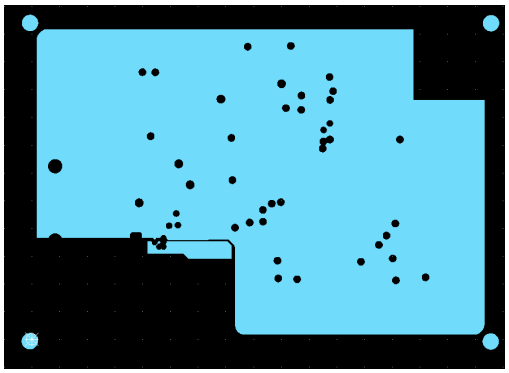

**Figure B.3:** Internal layer 2

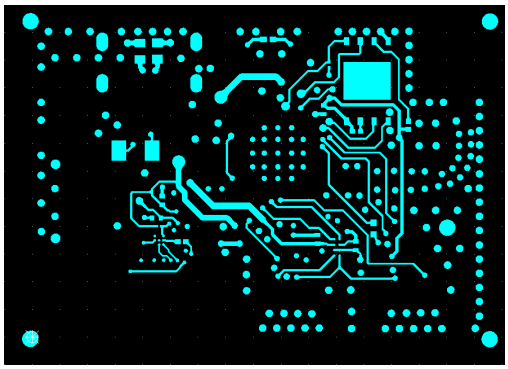

**Figure B.4:** Bottom layer

# Appendix C

# BioZKneeSleeve Concept

The following drawing illustrates the design concept of the bioimpedance knee sleeve, showcasing the placement of key components such as the bioimpedance electrodes, IMU sensors, and electronics housing within the sleeve.

Mattia Ghibaudo

# Sensorized BioZ Knee Sleeve Concept

N. 01

07/15/24

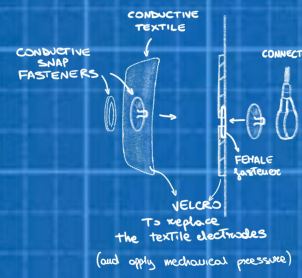


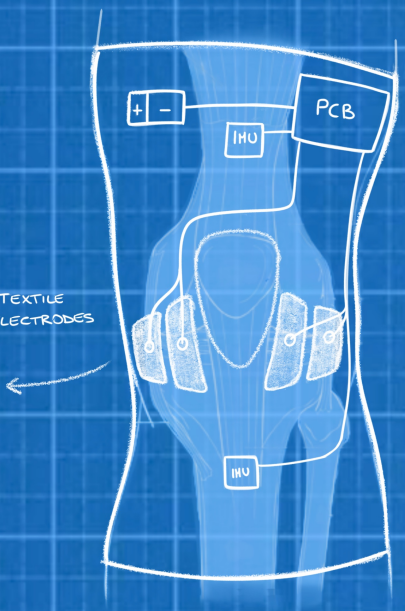


TEXTILE ELECTRODES

PCB

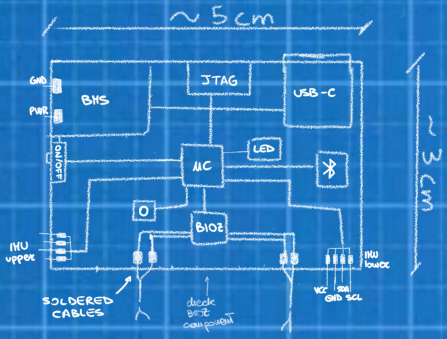


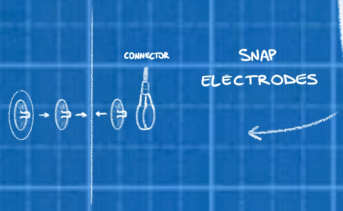


SNAP ELECTRODES

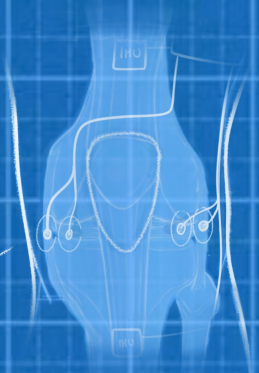


VELCRO ELECTRODES


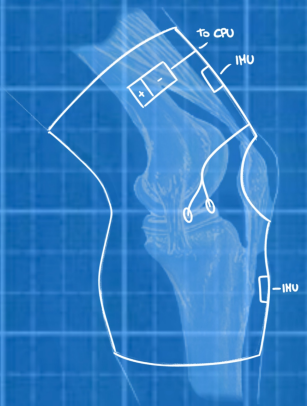


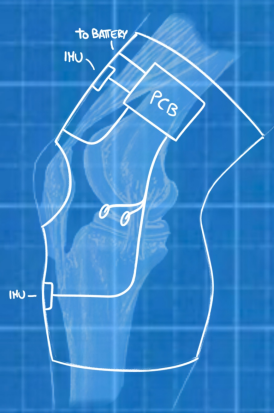

Mattia Ghibaudo

Sensorized BioZ Knee Sleeve Concept

N. 02

07/22/24

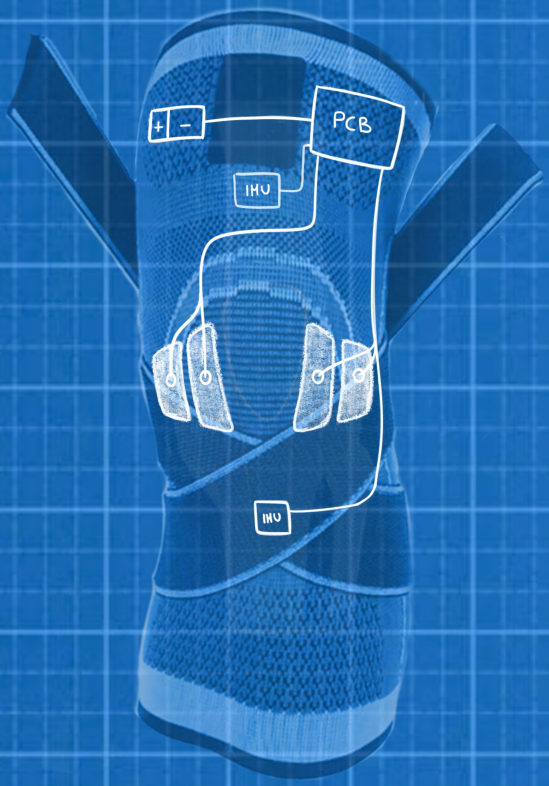


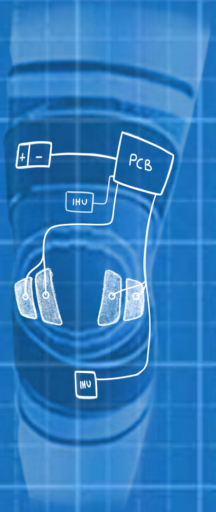


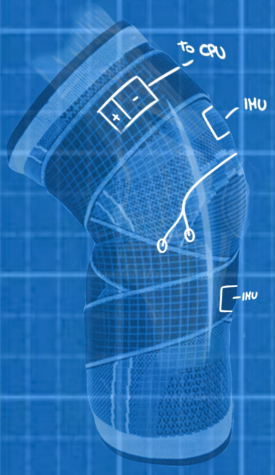


# Appendix D

# Bill Of Materials

## D.1 BioZ Knee Sleeve PCB

| | Quantity | Designator | Comment | Description |
|---|---|---|---|---|
| 2 | 1 | ANT1 | 2450AT18A0100001E | Antenna Chip 2.4GHZ |
| 3 | 12 | C1, C2, C3, C4, C5, C7, C9, C10, C12, C21, C211, C212 | 0.1 uF | Multilayer Ceramic Capacitors 0402 |
| 4 | 2 | C6, C8 | 22 uF | Multilayer Ceramic Capacitors 0402 |
| 5 | 4 | C11, C14, C19, C20 | 12 pF | Multilayer Ceramic Capacitors 0402 |
| 6 | 3 | C13, C16, C17 | 1 pF | Multilayer Ceramic Capacitors 0402 |
| 7 | 1 | C15 | 1 pF | Multilayer Ceramic Capacitors 0402 |
| 8 | 4 | C18, C207, C300, C301 | 1 uF | Multilayer Ceramic Capacitors 0402 |
| 9 | 2 | C201, C203 | 10 uF | Multilayer Ceramic Capacitors 0603 |
| 10 | 2 | C202, C204 | 0.1 uF | Multilayer Ceramic Capacitors 0402 |
| 11 | 5 | C205, C206, C208, C209, C210 | 0.047 uF | Multilayer Ceramic Capacitors 0402 |
| 12 | 2 | C302, C303 | 4.7 uF | Multilayer Ceramic Capacitors 0402 |
| 13 | 1 | D1 | AAA3528LSEEZGKQBKS | LED RGB CLEAR 4SMD |
| 14 | 1 | D2 | APT1608LSECK/J3-PRV | LED RED CLEAR 2SMD |
| 15 | 1 | FB1 | BLM18HE152SN1D | Chip Ferrite Bead, 0603 |
| 16 | 3 | J1, J2, J3 | 505567-0531 | Connector Micro-Lock 5 Position |
| 17 | 1 | J4 | USB4125-GF-A_REVA2 | USB-C connector |
| 18 | 1 | J5 | 505567-0281 | Connector Micro-Lock 2 Position |
| 19 | 1 | L1 | 6.8 uH | Shielded Multilayer Inductor 0805 |
| 20 | 2 | L2, L6 | 2.4 nH | Multilayer type RF Inductor 0402 |
| 21 | 2 | L3, L4 | 2 nH | Multilayer type RF Inductor 0402 |
| 22 | 1 | L5 | 3.9 nH | Fixed inductor 0402 |
| 23 | 1 | L7 | 2.7 nH | Fixed inductor 0402 |
| 24 | 2 | R1, R2 | 10 kO | Resistor 0402 |
| 25 | 2 | R3, R20 | 56 kO | Resistor 0402 |
| 26 | 2 | R4, R5 | 330 O | Resistor 0402 |
| 27 | 1 | R6 | 750 O | Resistor 0402 |
| 28 | 3 | R7, R8, R9 | 100 kO | Resistor 0402 |
| 29 | 1 | R30 | 6.2kO | Resistor 1206 |
| 30 | 1 | R31 | 1.6 kO | Resistor 0402 |
| 31 | 2 | R32, R33 | 5.1 kO | Resistor 0402 |
| 32 | 1 | SW2 | JS102011SAQN | SWITCH SLIDE SPDT |
| 33 | 1 | U1 | CC2652R1FRGZR | MicroController |
| 34 | 1 | U2 | W25N01GVZEIG | Flash memory SPI |
| 35 | 1 | U3 | TXS0102YZPR | Level shifter I2C |
| 36 | 1 | U4 | MAX30009ENA+ | BioZ sensor |
| 37 | 1 | U5 | TXB0104YZTR | Level shifter SPI |
| 38 | 1 | U6 | TPS7A0233PDQNR | Voltage regulator |
| 39 | 1 | U7 | MCP73831-2ATIMC | Battery charger |
| 40 | 1 | Y1 | ABM8W-48.0000MHZ-7-D1X-T3 | 48 MHz Crystal |
| 41 | 1 | Y2 | ABS07-32.768KHZ-7-T | 32.768kHz Crystal |

**Figure D.1:** Bill of Materials for BioZ Knee Sleeve PCB.

## D.2 IMU PCB

| | Quantity | Designator | Comment | Description |
|---|---|---|---|---|
| 2 | 3 | C1, C2, C3 | 0.1 uF | CAP CER 0402 |
| 3 | 1 | J1 | 505567-0531 | Connector Micro-Lock 5 Position |
| 4 | 1 | U1 | ICM-20948 | 9-Axis IMU |
| 5 | 1 | R1 | 1 kOhm | Resistor 1206 |
| 6 | 1 | R2 | 1 kOhm | Resistor 1206 |

**Figure D.2:** Bill of Materials for IMU PCB.

# Bibliography


[1] Sara Abasi, John R. Aggas, Guillermo G. Garayar-Leyva, Brandon K. Walther, and Anthony Guiseppi-Elie. «Bioelectrical Impedance Spectroscopy for Monitoring Mammalian Cells and Tissues under Different Frequency Domains: A Review». In: *ACS Measurement Science Au* 2 (2022), pp. 495–516. DOI: 10.1021/acsmeasuresciau.2c00033. URL: https://pubs.acs.org/doi/10.1021/acsmeasuresciau.2c00033 (cit. on pp. 2, 5, 6).

[2] Jane Smith and John Doe. «Fundamentals, Recent Advances, and Future Challenges in Bioimpedance». In: *Journal of Biomedical and Clinical Research* 10.1 (2022), pp. 100–120 (cit. on pp. 5, 6).

[3] Samer Mabrouk et al. «Robust Longitudinal Ankle Edema Assessment Using Wearable Bioimpedance Spectroscopy». In: *IEEE Transactions on Biomedical Engineering* 67.4 (2020), pp. 1019–1028 (cit. on pp. 6, 7, 17, 18, 52).

[4] Emily Moise. «Wearable Bioimpedance Sensing for Quantifying Knee Health in Juvenile Idiopathic Arthritis». MA thesis. Atlanta, Georgia: Georgia Institute of Technology, 2022 (cit. on pp. 6, 7, 18, 52).

[5] Sinan Hersek, Hakan Töreyin, Caitlin N. Teague, Mindy L. Millard-Stafford, Hyeon-Ki Jeong, Miheer M. Bavare, Paul Wolkoff, Michael N. Sawka, and Omer T. Inan. «Wearable Vector Electrical Bioimpedance System to Assess Knee Joint Health». In: *IEEE Transactions on Biomedical Engineering* 64 (2020), pp. 2353–2360 (cit. on pp. 8, 12, 13, 15, 19, 52, 53).

[6] Juan D Muñoz, Víctor H Mosquera, Carlos F Rengifo, and Elizabeth Roldan. «Machine learning-based bioimpedance assessment of knee osteoarthritis severity». In: *Biomedical Physics & Engineering Express* 10 (2024), p. 045013. DOI: 10.1088/2057-1976/ad43ef (cit. on p. 9).

[7] Shelby Critcher, Patricia Parmelee, and Todd J. Freeborn. «Localized Multi-Site Knee Bioimpedance as a Predictor for Knee Osteoarthritis Associated Pain Within Older Adults During Free-Living». In: *IEEE Open Journal of Engineering in Medicine and Biology* 4 (2023). DOI: 10.1109/OJEMB.2023.3256181 (cit. on pp. 9, 14, 19).

[8] Elif Pala, Tuba Denkçeken, and Türkan Turgay. «Serum RANKL levels and bioelectric impedance assessments in knee osteoarthritis patients». In: *Journal of Surgical Medicine* 4.3 (2020), pp. 222–225. DOI: 10.28982/josam.697686 (cit. on p. 9).

[9] Allison Seeley, Seerut Dhillon, Patrick Atkinson, Ajay Srivastava, and Theresa Atkinson. «Difference in Bioimpedance Across the Knee in Un-injured Young Adults». In: *The Iowa Orthopedic Journal* 43.1 (2023), pp. 123–129 (cit. on pp. 10–12, 15).

[10] Bo Fu and Todd J Freeborn. «Biceps tissue bioimpedance changes from isotonic exercise-induced fatigue at different intensities». In: *Biomedical Physics & Engineering Express* 4 (2018), p. 025037. DOI: 10.1088/2057-1976/aaabed (cit. on p. 11).

[11] Todd J. Freeborn, Gabriella Regard, and Bo Fu. «Localized Bicep Tissue Bioimpedance Alterations Following Eccentric Exercise in Healthy Young Adults». In: *IEEE Access* 8 (2020), p. 2970314. DOI: 10.1109/ACCESS.2020.2970314 (cit. on p. 11).

[12] Xuanjie Ye, Lexi Wu, Kaining Mao, Yiwei Feng, Jiajun Li, Lei Ning, and Jie Chen. «Bioimpedance Measurement of Knee Injuries Using Bipolar Electrode Configuration». In: *IEEE Transactions on Biomedical Circuits and Systems* 16.5 (2022), pp. 962–970 (cit. on p. 15).

[13] Antonio Scandurra, Carmelo Militello, and Francesco Cappello. «Portable Knee Health Monitoring System by Impedance». In: *Journal of Biomechanical Engineering* 144.6 (2022) (cit. on pp. 15, 16).

[14] Kristine L. Richardson et al. «Quantifying Rheumatoid Arthritis Disease Activity Using a Multimodal Sensing Knee Brace». In: *IEEE Transactions on Biomedical Engineering* 69.12 (2022), pp. 3772–3781 (cit. on p. 20).

[15] Omer T. Goktug et al. «An Integrated Multimodal Knee Brace Enabling Mid-Activity Tracking for Joint Health Assessment». In: *IEEE Engineering in Medicine Biology Society* 43 (2021) (cit. on p. 21).

[16] J. Ferreira et al. «A Handheld and Textile-Enabled Bioimpedance System for Ubiquitous Body Composition Analysis. An Initial Functional Validation». In: *IEEE Journal of Biomedical and Health Informatics* 21.5 (2017), pp. 1224–1232. DOI: 10.1109/JBHI.2016.2628766 (cit. on p. 21).

[17] Shelby Critcher and Todd J. Freeborn. «Localized Bioimpedance Measurements with the MAX3000x Integrated Circuit: Characterization and Demonstration». In: *Sensors* 21.3013 (2021). DOI: 10.3390/s21093013. URL: https://doi.org/10.3390/s21093013 (cit. on p. 54).